Metal Species and Surfactant Impact on Bacterial Populations and Community Behavior

Submitted in partial fulfillment of the requirements for

the degree of

Doctor of Philosophy

In

Chemical Engineering

Alex J. Bertuccio

M.S., Chemical Engineering, Manhattan College

B.S., Chemical Engineering, Manhattan College

Carnegie Mellon University
Pittsburgh, PA

August, 2017

Acknowledgements

This journey has been no easy battle and there are a number of people I need to thank for helping me get to where I am. I owe many my deepest gratitude for their support.

First, I cannot stress enough that my family has been nothing but amazing and supportive the whole way. They are the best and I love them dearly. Mom, Aunt Carmela, Rebecca and Dad thank you for always being there and sending so much positivity my way.

I would also like to thank my fellow graduate students. In these four years, I have been fortunate enough to meet so many wonderful and special people. I think I would have gone nuts if I did not have such great friendships and a strong support group. I have so many fond memories in Pittsburgh and I will certainly miss everyone!

Some people I would especially like to acknowledge are:

Kal Hajj, thank you. I am so fortunate to have met you and I am glad that we have become best friends. Our coffee breaks, Middle Eastern food excursions and lifting sessions have been some of my favorite memories in Pittsburgh. I could spend a full day documenting all our adventures so I will leave it at this.

Blake Bleier, I have enjoyed so many conversations we have had about shows, audiobooks and most recently MMA! You have always been a fantastic friend, great listener, and extremely caring person. I greatly appreciate you sitting in to watch me give a practice lecture before I interviewed at Rutgers. That practice helped tremendously and I might not have gotten my job without your help.

Chris Hanselman (Handsome), thank you for being such a dedicated gym buddy. I would have skipped quite a few workouts if I knew you weren't going to be there. I think our gym

with both of you. I am glad that over these four years we managed to finally get some collaborations that produced some good results.

Ron Ripper, thank you for all your help with getting me acquainted with the lab and dealing with my baffling first year self. I have enjoyed all those conversations we have had in your office especially when you went on a tirade about the current events.

Michael Patrick, thank you for helping me find (or at least start to pursue) a work/life balance. You have helped me stay grounded and embrace the obstacles that come my way.

Tom, my barber, for always giving me the "freshest cuts". Tom, you will be truly missed and I am certain I will never look forward to seeing a barber as much as you. You are a truly caring, down-to-earth person and I appreciated that you always checked in to see how my job search was going.

Jackline, the nightly custodian who cleaned the bio office, thank you for your positive energy and for all the late night conversations we had. You helped keep me sane all the nights I was in the office late at night.

Allyson Danley, Heather DePasquale, Shirley Pavlischak, Larry Hayhurst, and Janet Latini thank you for your support. I've enjoyed getting to know you these past few years and greatly appreciated the conversational breaks you have provided when I needed to get away from my thesis. I would also like to thank Cindy Vicker, Julie Tilton, and Justin Dawber for their helpfulness. I will miss all of you.

Dr. Lynn Yanyo, thank you for your constant support and for taking a chance on me.

Jake Boes, thank you for recommending and strongly hinting at me taking Evidence Based Teaching in STEM. It was a fantastic course and I do not think I would have the job I

have if I did not take the course. Thank you for all the stimulating teaching conversations, it was great to have these conversations with another person who is so passionate about teaching.

Stephanie Kirby for always being so helpful and answering any questions I had both as a symposium chair and for grad school.

Additional folks from the chemical engineering department (or honorary ChemEs) that I need to thank are: Christopher Knapp, Nick Austin, Nicholas Lamson, Melissa Lamson, Rebecca Ball, Bruce Yan, Randy Gamball, Kathy Fein, Justin Weinberg, Charles Sharkey, Michael Davidson, Irem Sen, Qin Gu, Dana McGuffin, Naser Mahfouz, Anirudh Subramanyam, Nikos Lappas, Zach Wilson, Tory Ivey, Yuan Chen, Nick Golio, Andrew Fox, Sarah Robb, Ken Riordan, Stefanie Baker, Tom Brubaker, Jonathan Goldman, Stephen Spagnol, Patrick Boyer, Sarah Feicht, Todd Moyle, Nichole Asermeley, Thank you all for your support and the wonderful adventures.

From the Environmental Engineering Department:

Clint Noack, thank you for all your help with the ICP-MS with all the times I have encountered issues. Nizette Consolazio, Eleanor Spielman-Sun, Stephanie Laughton, Jonathan Callura, Aniela Burant, Daniel Ross, Megan Leitch, Lauren Burgman, Ke Gai, Kai Chucherdwatanasak, Astrid Avellan, Adam Cadwallader, and Will Gao thanks for all your support and discussions when I popped into the lab.

I would also like to thank the undergraduates I had the opportunity to mentor: Victor Accacio, Stephanie Kong, Brigid McGovern, Tamara Amin, Justin Peruzzi, and Michelle Karabin. Thank you for your interest in research. You have given me a chance to develop as a mentor and refine my mentoring style.

From my former life at Manhattan College I need to thank:

Dr. Ann Marie Flynn, thank you for being such an enthusiastic instructor. It is because of your energy and passion for teaching that I too want to become just like you. A professor that students love and respect.

Brother Robert Berger, thank you for always knowing the right thing to say. You have been an immense help at points where the path was not clear. Thank you for being an amazing friend and providing so much positive support my way.

Brother Augustine Nicoletti, thank you for sharing some of the parts for being a teacher and continuously threatening to knock some sense into me if I did not get my dissertation written. I am happy to tell you there will not be any sense knocking that needs to be done.

Andrew Weingarten, Amanda Rodela, AJ Goodman, Elizabeth Gibbons and Gabrielle Occhiogrosso, thanks guys. I had wonderful times as a Resident Director and I appreciated all your support for me while I was applying to graduate school and for the brief times we had a chance to catch up.

Adam Schmalz, Karen Tschinkel, Justin Sierpinski, Vincent DeVita, Kerry Hynes, and Eric Weintraub, thank you for continuing to put the effort in to keep our friendships going even with the distance. Your friendships mean the world to me.

I would like to thank my committee for agreeing to serve on my committee. I want to thank Greg Lowry for all his input over the years with the direction of my research and suggestions of experiments to pursue. I would also like to thank Steve Garoff and Dennis Prieve for general life discussions and glimpses of the academic life.

I must especially thank Bob Tilton. None of this would have happened without him. I am the lecturer/presenter, researcher, and person I am because of him. Bob, thank you for always

being technical and pointing out every detail. The devil is in the details. You have pushed me to think critically and be precise with the way I phrase everything. These are skills I will continue using for the rest of my life.

Abstract

This work is motivated by the need to understand the environmental risks posed by antimicrobial silver and copper nanoparticles, from consumer products and pesticides, and surfactants, used for oil remediation. Silver and copper nanoparticles have biocidal properties, and surfactants have similar chemical structures as autoinducers, molecules bacteria use to communicate (known as quorum sensing), which may alter bacterial communication. The introduction of both classes of chemicals may pose different threats to bacterial populations to affect normal ecosystem functions.

The dissertation addresses the role natural organic matter and bacterial concentrations play to serve as silver and copper sinks to mitigate toxicity and probes the effects that surfactants have on bacterial quorum sensing.

Pseudomonas fluorescens was used as a model biofilm forming bacterium to understand the role natural organic matter (NOM) and bacterial concentration play on bacterial survival and colonization of AgNP-decorated surfaces. It was seen that both NOM and *P. fluorescens* serve as silver sinks and the critical amount of bacteria-bound silver necessary to inhibit growth was on the same order of magnitude for each initial bacterial concentration. An increased silver sensitivity was observed when NOM was present.

Escherichia coli was used as a model Gram-negative bacterium to study Cu^{2+} toxicity in the presence of NOM. NOM increased bacterial tolerance to Cu^{2+} over ten-fold. Copper responsive genes were measured with and without NOM at the same initial bacterial concentration and it was observed that copper sensitive gene expression was lowered with NOM.

Vibrio harveyi was used as a model quorum sensing bacterium to study the effect of Tween 80 surfactant on quorum sensing. Bioluminescence is one form of quorum sensing

response for *V. harveyi*, and the addition of Tween 80 caused a decrease in luminescence for similar bacterial concentrations. Liquid chromatography-mass spectrometry was used to study interactions between Tween 80 and N-butyryl homoserine lactone (AI-2). A decrease in autoinducer AI-2 signal was observed with Tween 80 suggesting that there is some interaction between the surfactant and AI-2 that may result in a decrease of available signal. These results indicate that further studies should be performed to better understand these observations.

Table of Contents

xiii

List of Tables

List of Figures

Chapter 1. Introduction

1.1 Motivation

1.1.1 Metal nanoparticle presence in the environment

A nanoparticle is a particle with at least one dimension less than 100 nm.[1] Nanoparticles have gained interest for their different properties compared to their bulk counterparts[2] and have applications in a wide range of areas. Titania nanoparticles are used in sunscreens and paints, silver and copper nanoparticles are used as pesticides, iron nanoparticles are used for groundwater remediation, fullerene particles are used in cosmetics.[1,3] In the past two decades there has been a large increase in the use and production of nanoparticles for consumer products.[4] The difference in properties and reactivity between nanoparticles and bulk materials of the same composition is one main reason for the surge in nanoparticle usage.[5–10] In 2006, only 200 products were reported to contain nanoparticles and this number has jumped to almost 2000 products in 2015.[3,11] The volume of nanoparticles produced has also risen from hundreds to thousands of tons per year.[12] Nanoparticle production has exponentially increased and it is predicted to continue to rise for the next few years.[13,14] With rising nanoparticle production it is expected that environmental exposure will also increase.[15]

In 2010, between 260,000 and 309,000 tons of nanoparticles were disposed in landfills; this accounted for 63 to 91% of the nanoparticles released and the remainder entered the environment.[14] With the large production of nanoparticles and their potential for release into the environment, there is a growing concern for the impact this can have in the environment especially on the organisms.[16–19] Although there have been studies on nanoparticle toxicity there are still uncertainties for the impact nanoparticles have on the environment especially with the changing amounts and types of nanoparticles produced.[1,20–22]

Two nanoparticles of concern are silver nanoparticles (AgNPs) and copper oxide nanoparticles (CuONPs). Products including fabrics, personal care products, catheters and pesticides incorporate these nanoparticles primarily for their antimicrobial properties.[3,23–36] Extensive usage of these products leads to increased nanoparticles in wastewater runoff. Wastewater treatment sludge is typically used as fertilizer, providing another potentially significant route for nanoparticle entry into ecosystems in agricultural regions.[24,37–40] It is believed that the main mode of toxicity, for each type nanoparticle, is the release of their ions.[35,41–47]

Several models have indicated the possibility of nanoparticles and their ions accumulating in soils.[48–52] Garner and coworkers estimate that some nanoparticles and their ions could reach concentrations above the minimum toxicity threshold.[53] In the environment bacteria are essential for nutrient recycling,[4,19,54] and the potential for biocidal nanoparticles entering the environment via waste streams represents an environmental risk.[24,39,40] It is therefore important to study factors that affect metal ion and nanoparticle toxicity on bacteria in environmentally relevant conditions to better understand the potential risk nanoparticles pose to microbial communities.

1.1.2 Artificial surfactants released into the environment

In 2010, 1.8 million gallons of dispersants were released in response to the BP Deepwater Horizon spill.[55] The dispersants used were Corexit 9527 and 9500A which are blends of several synthetic surfactants including Tween 80, Tween 85, dioctyl sodium sulfoccinate (DOSS) and Span 80.[56] These dispersants are used as a quick response to oil spills so oil is finely dispersed in water and larger surface areas of oil are available for bioremediation.[57] However, studies have

shown that these surfactants when released into the environment can persist for long periods of time up to 4 years.[58–60]

The presence of surfactants for periods longer than needed could pose a threat on aquatic life,[57,61] especially with studies showing that Corexit is toxic to some aquatic life.[62,63] It is also possible that these long-lasting surfactants could interfere with the regular functions of bacteria.

Quorum sensing, a means by which bacteria chemically communicate to each other to identify the population density, could be affected by the addition of surfactants to the environment. The chemicals produced for quorum sensing are called autoinducers and are usually amphiphilic.[64] With the addition of surfactants it is possible that these autoinducers could be solubilized by micelles and alter the communication amongst one or more bacterial populations.[65] Several studies have shown that Corexit can have stimulating or inhibitory effects on bacterial populations.[66–70] Evidently, there is an uncertainty on the impact dispersants can have on bacterial populations in areas of oil spill remediation, and there is a need to investigate the effects these surfactants have on bacterial populations and quorum sensing.[61]

1.2 Background

1.2.1 Bacterial Lifecycle and Quorum Sensing
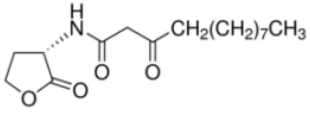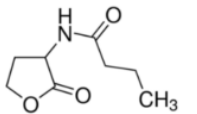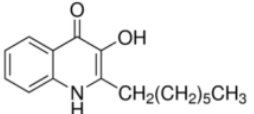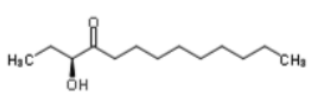
Bacteria are ubiquitous in any ecosystem[71,72] and are essential for recycling nutrients such as carbon, nitrogen and phosphorous. [4,19,54] Bacteria will transform compounds with these elements into forms that can be metabolized by other organisms such as plants and other bacteria.[4] Microbial communities are diverse to allow a division of functions amongst the different species of bacteria.[73,74]

There are three stages in the lifecycle of bacteria which are: the planktonic state (in suspension), surface colonization and biofilm formation.[75,76] A biofilm is a network of bacteria

3

that are surrounded by organic material produced by bacteria called extracellular polymeric substance (EPS).[77,78] The EPS serves as a protective barrier between bacteria and toxic agents.[79] Biofilms are reported to increase the tolerance of bacteria, in a biofilm, to external agents up to 1000 times as much as bacteria are in the planktonic state. [76,80,81]

As a part of the bacterial lifecycle, bacteria release hormone-like molecules called autoinducers that serve as chemical signals for communicating amongst each other to determine the cell population. This process is called quorum sensing[82–84] and representative molecules are shown in Table 1.1. The more bacteria that are present the higher the autoinducer concentration is, and when there is a sufficient autoinducer concentration bacteria will change their gene expression to perform a different function.[83,84] Quorum-sensing is a way bacteria can function like a multi-cellular organism by expressing a gene in unison with other bacteria of its species at an appropriate time. Some products from bacterial quorum sensing include biofilm formation, virulence and bioluminescence. [82–84]

Table 1.1 Representative autoinducer molecules found in *V. harveyi*[83,241]

AI-1 N-(3-oxododecanoyl) homoserine lactone	**AI-2** N-butyryl homoserine lactone	**PQS** 2-heptyl-3-hydroxy-4-quinolone	**CAI-1** (*S*)-3-hydroxytridecan-4-one

1.2.2 Silver-Bacteria Interactions

Silver is toxic to microorganisms in both the forms Ag^+ and AgNP.[23,47,85–93] Previous research has thoroughly investigated AgNP toxicity to planktonic bacteria [85,87,94–96] as well as to bacteria in biofilms.[97–100] Silver can significantly damage a bacterium through a variety of mechanisms including Ag^+ binding to DNA and proteins in the cell, formation of cell wall pits or

other cell wall damage that degrades its performance as a transport barrier, and production of reactive oxygen species (ROS).[85,86,101–107] Although bacteria in biofilms are still vulnerable to Ag^+ and AgNP toxicity, bacteria in biofilms have significantly higher resistances to antimicrobials in general compared to their planktonic counterparts,[76,80,81] and this includes increased tolerance of AgNP exposure.[99,108]

In addition to studies of pre-established biofilm susceptibility to AgNPs, bacterial colonization on AgNP-decorated surfaces has also been investigated by a number of groups.[25,26,109–116] Using glass[113,114,116] and a variety of other types of surfaces, such as TiO_2 or AgNP-impregnated plastics,[25,26,109–112,115] these investigations address the question of whether or not bacteria are capable of colonizing a surface in the presence of nanoparticles, but they do not indicate particular factors that promote or inhibit colonization. The effects of humic acid on bacterial colonization in the presence of AgNPs were not considered. Wirth and coworkers[116] showed that *Pseudomonas fluorescens* freely colonize directly on AgNP-decorated surfaces. Surface colonization was shown to depend significantly on planktonic bacterial inoculum concentrations. This inoculum effect was attributed to the decreased availability of silver ion bound to cells at sublethal levels. In addition to bacterial cells serving as silver sinks, in the environment there are numerous materials such as natural organic matter (NOM) that can bind silver and reduce the amount that is free to interact with bacteria. Several forms of organic matter have been observed to increase bacterial tolerance of silver nanoparticles in the planktonic state.[96,99,117,118] Natural organic may serve as a silver sink to promote bacterial colonization on nanoparticle coated surfaces. The critical aspect of a silver sink effect is how silver binding to that sink decreases the concentration of silver ions that are free to bind to bacteria and could provide insight to evaluating toxicity.

1.2.3 Copper-Bacteria Interactions

Copper has well-known antimicrobial effects and copper-based pesticides have had known uses for centuries or even millennia. [27–32,119] Copper-based pesticides are attractive because of low development of resistance and they are accepted for "organic agriculture" applications.[29] Commercial scale pesticides typically contain copper salts such as $Cu(OH)_2$ or $CuSO_4$ and more recently copper based nanomaterials such as CuO nanoparticles (CuONPs)[120].

There is strong evidence that the main source of toxicity for $CuSO_4$, $Cu(OH)_2$, CuO and CuONPs is the cupric ion.[35,41–45,121,122] Although copper-based products applied to crops are effective at reducing plant disease[27–31] studies demonstrating that they can affect the microbial communities have raised concerns for potentially harmful impacts.[45,74,121,123–125]

The presence of NOM and other compounds in the environment that are capable of binding metals will decrease the bioavailable copper concentration. Previous investigations have established that NOM decreases silver and copper toxicity to bacteria [96,117,118,124,126,127] and that microbial communities are affected to different extents by metals when exposed in soils or media with large amounts of organic material than when they are exposed under more pristine laboratory media conditions.[11,74,125,128,129] It has also been demonstrated that both silver and copper toxicity can depend on initial microbial inoculum concentrations.[116,126,130] Quantitative tracking of copper ion partitioning among the aqueous solution, cells and NOM has not been performed and thus the possible physicochemical origins of the NOM and inoculum effects on Cu^{2+} microbial toxicity have not been established.

Some mechanisms that have been identified for copper toxicity to bacteria include Fe-S cluster enzyme inactivation[131], DNA damage[42], membrane damage[124,132], inhibition of nucleotide synthesis[133], mismetallation of enzymes[134,135], and differential protein expressions.[136] While the

role of reactive oxygen species (ROS) in copper toxicity to bacteria remains a subject of debate,[131,137,138] several publications suggest that elevated ROS contributes to copper toxicity, and ROS production is still commonly monitored. [42,132,138,139]

The bacterial response to metal ion stress agents includes characteristic alterations in gene expression.[140–142] Moore and co-workers observed significant increases in *E. coli* gene expression for *copA*, *cueO*, *cusC* and *cpxP* after 30 minutes of Cu^{2+} and CuONP exposure.[143] The copper-responsive genes (*copA*, *cueO*, and *cusC*) code for copper-regulating proteins: *copA* for a transporter that shuttles cystoplasmic Cu^+ to the periplasm[144], *cueO* for a protein that oxidizes Cu^+ to Cu^{2+}, its less toxic form[145], and *cusC* codes for part of an efflux pump that transports Cu^+ from the periplasm to outside the bacterium.[146] *copA* and *cueO* are on the same operon while *cusC* resides on a separate operon.[147] *cpxP* is also induced by elevated levels of copper. This particular gene targets misfolded periplasmic proteins.[148] A study of gene responses when bacteria are exposed to different copper sinks could provide a better mechanistic understanding of copper toxicity to bacteria.

1.2.4 Corexit Toxicity to Bacteria

After the Deepwater Horizon Spill there was a surge in the amount of research surrounding the toxicity of the dispersant Corexit to aquatic life, particularly for microorganisms. Previous research has shown a variety of effects surfactants can have on marine bacteria.[61,63,66,70,149–153] Some groups such as Hamdan and Fulmer have seen Corexit is toxic to various levels for different species of marine bacteria and some species of bacteria such as *Marinobacter* have high sensitivities to Corexit and experienced nearly 100% reduction in viability.[150] Others like Overholt et al. have seen differing responses between bacterial speciesfor where some such as *Acinobacter* are inhibited by Corexit while other species like *Alcanivorax*

7

experienced enhanced growth with the presence of Corexit.[66] All of this work reveals a variety of inhibitory and stimulatory effects that Corexit has on bacterial growth. However, to our knowledge no prior work has investigated the impact that dispersants such as Corexit may have on quorum sensing for different bacterial species. Quorum sensing is a tool that some species of bacteria use to communicate. If dispersants interfere with this chemical signaling it may affect microbial populations. There is therefore a need to assess in addition to toxic effects of Corexit but also effects on quorum sensing to better understand the impact this can have on marine bacteria.

1.3 Dissertation Objectives

The overall objective of this work is to investigate the impacts of metal species and surfactants on bacterial populations and community behavior. *Pseudomonas fluorescens,* a model biofilm forming bacterium commonly found in soils, was used to assess AgNP and Ag^+ toxicity. *Escherichia coli*, a model bacterium with a well characterized genome, was used to study Cu^{2+} toxicity. Lastly, *Vibrio harveyi* was used to identify potential effects of Tween 80, a component of Corexit, on bacterial growth and quorum sensing. Specific aims and hypotheses are described in more detail below.

1.3.1 Determine silver toxicity in "environmentally" relevant systems and how this impacts bacterial colonization on surfaces coated with silver nanoparticles

The prevalence of AgNPs in the environment leads to a concern for disrupting the lifecycle of bacteria especially during the colonization process which has been studied to a lesser extent than the other parts of the bacterial lifecycle.[154] The first objective for this dissertation is to identify factors that affect AgNPs and Ag^+ toxicity to bacteria especially during the colonization process. We hypothesize that AgNP and Ag^+ toxicity will be dependent on the

initial inoculum concentration, and that natural organic matter such as humic acid could considerably reduce bioavailable silver and mitigate silver toxicity.

Prior literature concerning organic compound effects on silver tolerance does not quantitatively evaluate silver ion partitioning between solution, bacteria-bound and organic matter-bound states, and as a result it is not known whether there is a critical lethal threshold of silver binding to bacteria. One of the goals of this work is to develop silver binding isotherms for *P. fluorescens* and humic acid and perform a material balance around the system to identify silver partitioning. We also plan to use minimal inhibitory concentrations and minimal bactericidal concentrations to supplement the binding isotherms and determine toxic amounts of silver.

1.3.2 Determine how initial inoculum concentration and the presence of humic acid affect copper toxicity and identify potential mechanisms for mitigation

Similar to AgNPs in the environment there is a large amount of copper in both the nanoparticle and salt forms added to the environment both intentionally and unintentionally. [27–32,119] Since copper, like silver, is an antimicrobial agent, the applications of copper, especially in agricultural soils, could affect the microbial communities. Thus, the second objective for this dissertation is to investigate copper toxicity on bacteria with environmentally relevant compounds and the effects copper sinks have to mitigate toxicity.

The goal of this work is to quantify copper bioavailability and identify how the initial inoculum concentration and the presence of humic acid affect copper toxicity. We hypothesize that, similar to silver, the initial inoculum concentration and the presence of humic acid will considerably increase bacterial tolerance to copper. Copper binding isotherms to *E. coli* and humic acid will be obtained to estimate copper partitioning to each component. Minimal

inhibitory and bactericidal concentrations will be measured to provide additional information about the copper partitioning. Furthermore, gene expressions and oxidative stress levels will be measured to identify changes induced due to increases and decreases in bioavailable copper.

1.3.3 Determine the impact that surfactants in commercial dispersants used for bioremediation can have on bacterial growth and quorum sensing

The third objective is to investigate how surfactants, especially ones used for oil spill remediation, can affect bacterial populations. *V. harveyi* is a model quorum sensing organism and will be used to probe the effects Tween 80 has on bacterial growth and quorum sensing. Luminescence will be measured to indirectly assess potential effects on quorum sensing since bioluminescence is a gene expression induced by quorum sensing for *V. harevyi*. Since most autoinducers are surfactant-like[64] we hypothesize that surfactants in commercial dispersants will interact with autoinducers to disrupt quorum sensing.

There is a major concern for the impact that these surfactants can have on microbial populations especially in light of the current studies revealing that these surfactants may persist for years in the ocean. [58–60] If these surfactants are toxic to bacteria or interfere with quorum sensing that could severely affect aquatic communities and the bacterial diversity.

1.4 Outline of this dissertation

Chapter 2 will include detailed materials and experimental procedures used in this work. Detailed characterization of AgNPs will be included. The culturing procedures for the different species of bacteria along with protocols to determine the minimal inhibitory and minimum bactericidal concentrations will also be included.

Chapter 3 addresses parts of objective 1.3.1. This chapter identifies the dependence of AgNP toxicity on the initial inoculum concentration. It briefly discusses *P. fluorescens* binding

silver to reduce its bioavailability. The material presented was published in the Journal of Colloids and Interface Sciencs under the title "Inhibition of bacterial surface colonization by immobilized silver nanoparticles depends critically on the planktonic bacterial concentration," written by Stacy M. Wirth and co-authored by Alex J. Bertuccio, Feng Cao, Gregory V. Lowry, and Robert D. Tilton.[116]

Chapter 4 further addresses objective 1.3.1 by providing a mechanistic understanding to explain inoculum effect present for silver and the role the inoculum effect plays on bacterial colonization on AgNP-decorated surfaces. This chapter also identifies the role humic acid serves in mitigating silver toxicity and how it affects bacterial colonization on glass surfaces. The material presented in Chapter 4 was published in Environmental Science and Technology under the title "Silver Sink Effect of Humic Acid on Bacterial Surface Colonization in the Presence of Silver Ions and Nanoparticles," written by Alex J. Bertuccio and co-authored by Robert D. Tilton.[126]

Chapter 5 addresses objective 1.3.2 by investigating the role that initial inoculum concentrations and the presence of humic acid play on copper toxicity. This chapter explores the contributions of humic acid and *E. coli* towards removing free copper. It also delves deeper into a mechanistic understanding to explain how humic acid and initial bacterial concentration mitigate copper toxicity by measuring gene expressions and oxidative stress levels.

Chapter 6 addresses objective 1.3.3 by probing *V. harvyi* growth and luminescence when exposed to Tween 80, a component of Corexit. Growth and luminescence are measured for a range of Tween 80 concentrations. A proposed mechanism to explain how Tween 80 affects quorum sensing is also provided.

A summary of conclusions for this work and future directions are discussed in Chapter 7.

Chapter 2. Materials and Methods

2.1 AgNP –PVP 55K Synthesis

The AgNPs used in these studies were sterically stabilized with poly(vinylpyrrolidone) (PVP) of a molecular mass of 55 kDa. These particles were synthesized by Stella Marinakos in the Department of Civil and Environmental Engineering at Duke University. The detailed synthesis was reported by Ma et al.[155] Briefly, 1.5 g of PVP (MW 55, 000) was dissolved in 280 mL of water. 9 mL of 0.1 M silver nitrate was added. The solution was stirred for 5 minutes and then 11 mL of 0.08 M ice-cold sodium borohydride was added. The PVP-stabilized nanoparticles were centrifuged 3 times for 1 h at 112,000 g (Beckman Optima L-100XP equipped with a Type 45 Ti rotor) and resuspended in water. As part of their synthesis AgNPs were washed so no further washing was performed. The reported diameter of these particles was 9.3 ± 2 nm based on TEM (Figure 2.1). Particles were obtained as an aqueous suspension and stored in the dark at 4°C. All experiments using AgNPs were diluted from stock suspensions of 750 ppm AgNPs and 182 ppm PVP.
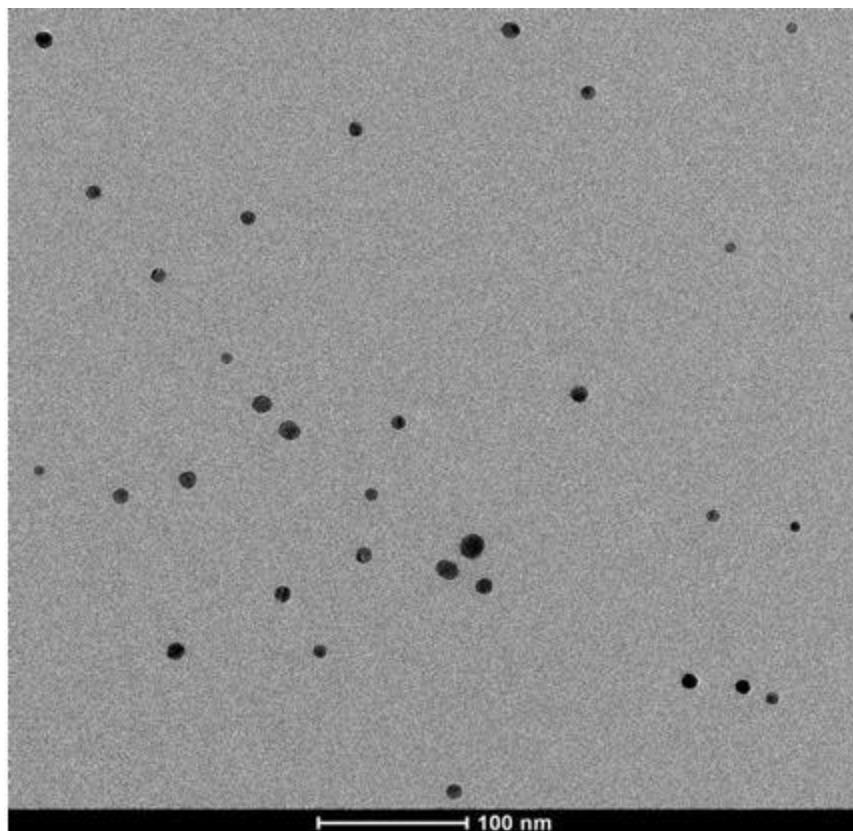
Figure 2.1. TEM micrograph of AgNP-55KPVP. Scale bar is 100 nm. Particles are 9.3 $\pm$ 2 nm. Image is courtesy of Stella Marinakos

2.2 Nanoparticle Characterization Techniques

2.2.1 Dyanmic Light Scattering

A Malvern Zetasizer Nano ZS equipped with a He-Ne 633 nm laser was used to perform dynamic light scattering (DLS) measurements. DLS is generally used for particles that range in size between 10 nm and 10 µm. DLS relies on the constant, random movements of Brownian motion for suspended particles. A light is shined on the suspension and the fluctuations in light

scattering from the suspended particles are measured and applied to an autocorrelation function which is then fit to a group of exponential decay functions using a NNLS (Non-Negative Least Squares) algorithm. The diffusion coefficient is proportional to the lifetime of the exponential decay, so multiple exponential functions are employed in order to obtain the particle diffusion coefficients for each particle size in the sample.[156–158] The smaller the particle is the higher the diffusion coefficient will be.[159] After a diffusion coefficient is obtained, the particle is assumed to be spherical and the Stokes-Einstein relationship is used to determine the corresponding hydrodynamic diameter. The hydrodynamic diameter accounts for an additional water layer that forms around the surface of particles and is higher than a diameter obtained through TEM imaging.[157]

Intensity distributions will favor larger particles[158] due to the fact that light scattering is proportional to the radius of the particle raised to the sixth power.[160] Thus, to more accurately represent the particle size population, intensity distributions can be converted to number intensities. In order to make this conversion, the real/imaginary parts of the refractive index for the particle are used. For AgNPs these values are 0.135/3.99 (real/imaginary).[161] The number intensity for the sizes of the AgNPs is shown in Figure 2.2. These numbers are meant for AgNPs and do not account for the adsorbed layer of polymer. However, it has been found that this relationship is empirically weak.
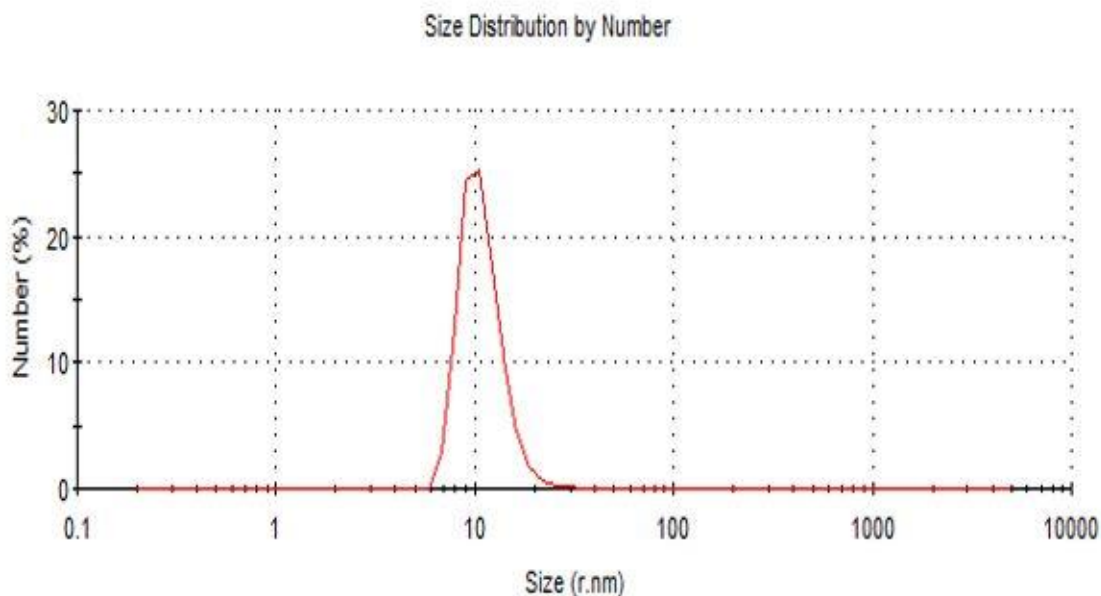
Figure 2.2 DLS hydrodynamic diameter number distribution for AgNP-55KPVP in minimal Davis media (described in section 2.5).

2.2.2 UV-VIS absorbance Spectroscopy

The small size of metal nanoparticles gives them different properties compared to their bulk counterparts. For example, AgNPs in suspension have a yellow-brown hue while bulk silver is gray. The difference in color is attributed to the different electronic properties of the two forms of silver. The small size of AgNPs (the radius of the nanoparticle is less than 10% of the incident light), has a large contribution from the surface electrons. Oscillations in electrons from incident light are enhanced by the small size and cause a change in the absorption and scattering patterns of the nanoparticle. This is known as localized surface plasmon resonance (LSPR) and can be observed with noble metals such as silver and gold in nanoparticle in the visible light range.[2,162,163]

15

The UV-VIS spectrum was recorded with a microplate reader (Spectramax M2) at $23\pm$ $2°$ C. The 4.5 mL macro cuvette (VWR) with a pathlength of 10 mm was filled with 2 mL of a 10 ppm AgNP dispersion in DI H_2O and minimal Davis media (described in section 2.5). The characteristic LSPR peak of AgNPs used in these studies from UV-VIS spectroscopy is expected at 392 nm[164,165] and was observed with the AgNPs used in this research (Figure 2.3). Shifts in the absorption peak are signs that the nanoparticles are aggregating. When AgNPs are dispersed in MDM (ionic strength of ~50 mM), there are no shifts in absorption peak wavelengths indicating these nanoparticles are stable in MDM.
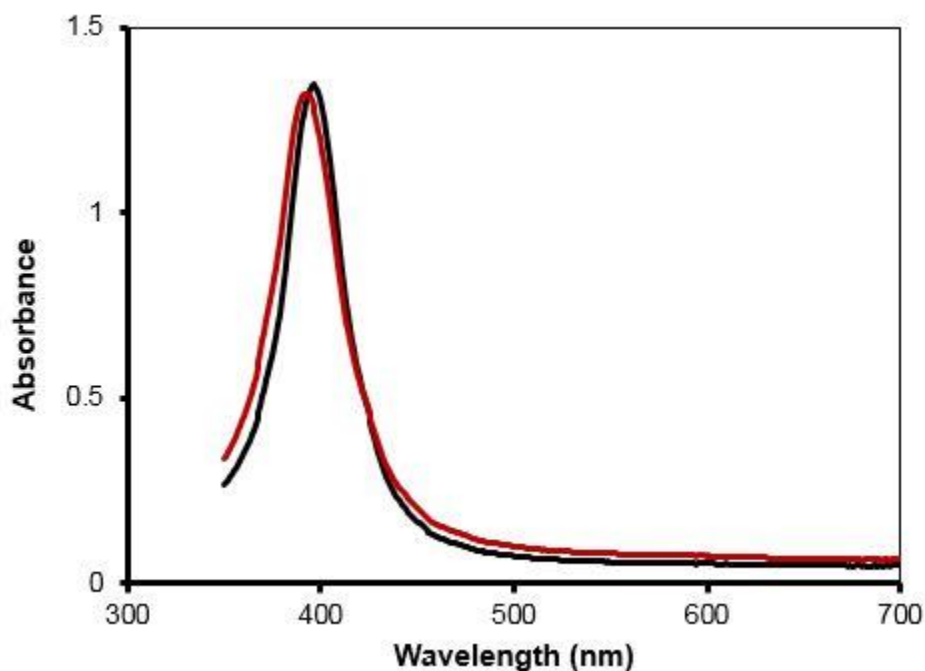
Figure 2.3 AgNP-55KPVP ultraviolet-visible spectrophotometry spectrum in DI H_2O (black line) and minimal Davis media (red line).

2.2.3. Darkfield Microscopy

Darkfield microscopy is an optical technique used to image opaque materials. With this technique, a patch stop is used to prevent any light from being directly shined onto the sample being imaged. Oblique rays of light are condensed through a condenser lens and shined onto the sample. Any light that is scattered by the sample enters an objective lens to form an image.[166,167]

Representative darkfield images of AgNPs on glass coverslips are shown in Figure 2.5. These images were taken with a ZeissAxioobserver Z1 inverted microscope equipped with a HAL 100 halogen illuminator and a 0.8 NA dark-field condenser. Darkfield images were collected using either a $40 \times$ LD Plan-NEOFLUAR objective (Zeiss) with an NA of 0.6 or a $20 \times$ LD Plan-NEOFLUAR objective (Zeiss) with NA 0.4, with images collected at 1 s (AxioCam MRm). The images are not representative of the AgNP size, they are only scattered light. (Particles are below the diffraction limit). AgNPs can be imaged because the LSPR and small size make AgNPs extremely efficient at scattering light.[168,169] The software used for analysis was the Fiji tool developed for ImageJ (National Institute of Health) by Schindelin and coworkers.[170] (http://fiji.sc/). Images were analyzed using the "analyze particles" function under the "analyze" tab.
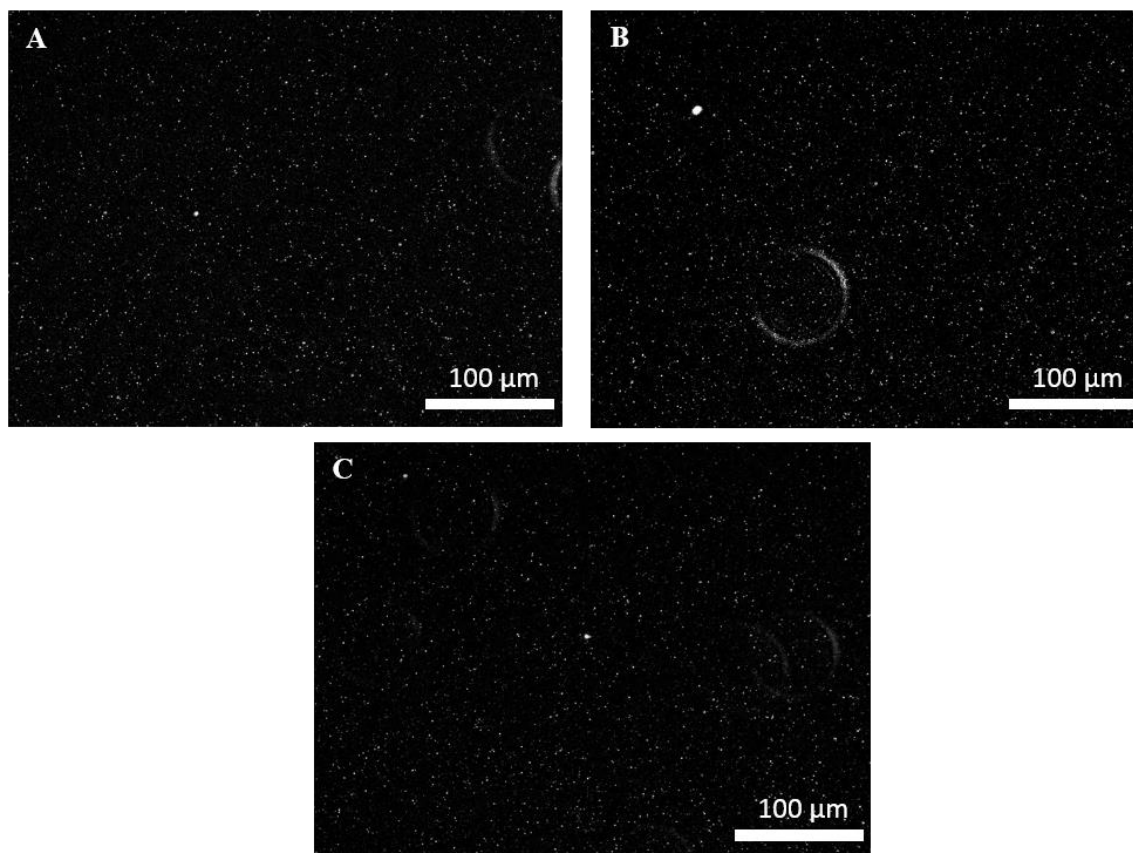
Figure 2.4. Representative darkfield microscopy images of AgNP-decorated coverslips. AgNPs appear as bright spots due to resonance Rayleigh scattering associated with the localized surface plasmon resonance. The AgNP area densities on these images are 3.34 (A), 4.01 (B) and 3.39 (C) $\times 10^5$ particles/mm^2. Circular features are out of focus objects.

2.2.3.1. Coverslip cleaning

Glass coverslips (22×22 mm, No. 1.5, Fisher Scientific) were used as substrates for AgNP imaging and bacterial colonization. However, one of the disadvantages to using darkfield microscopy is that any dust or dirt that is present on the surface of the glass coverslip will also be diffracted and cannot be differentiated from the desired sample. Thus, an intensive glass cleaning procedure is implemented to remove any dust or dirt present on the glass coverslips. Coverslips

18

were thoroughly cleaned before each experiment. Coverslips were cleaned by 30 min of bath sonication (Branson 1200 Ultrasonics Corp.) in a 10% solution of RBS 35 detergent concentrate (Thermo Scientific) in water, 20 min in Nochromix (Sigma-Aldrich) dissolved in sulfuric acid (technical grade, 93-98% , Fisher Scientific), 20 min in 6 N HCl (BDH chemicals), and 30 min in 10 mM NaOH ($\geq$ 98%, Fisher Scientific). Between each step and after the NaOH step the coverslips were washed with copious amounts of ultrapure water (Barnstead Nanopure, > 18 MΩ cm resistivity) and then dried with a nitrogen stream. Coverslips were sterilized under UV light (Spectroline Model EN-180L, 365 nm, 0.2 A) for 15 minutes prior to use.

2.3 Inductively Coupled Plasma – Mass Spectrometry (ICP-MS)

An Agilent 7700X ICP-MS was used to measure silver and copper concentrations in samples. All samples were prepared by adding concentrated HNO_3 (67% purity, Aristar Plus trace metal grade BDH chemicals) and 30% H_2O_2 (Fisher Scientific). For a 5 mL sample 300 µL of HNO_3 and 150 µL of H_2O_2 were added. After adding these oxidants samples are heated at 100° C for 15 minutes (VWR International).[171] Nitric acid and hydrogen peroxide are used to digest metal samples because they are excellent oxidants and will convert metals into their ionic forms so they can be detected through ICP-MS.[172]

For analysis the ICP-MS nebulizes and ionizes samples with an argon plasma. Ions are passed through a vacuum chamber at room temperature to reduce collisions with gas molecules. Afterwards the quadripole mass filter uses oscillating radio frequencies to control the mass to charge ratio (m/z) and selects the desired value for the element being measured. The desired isotope will strike a dynode electron multiplier that will release electrons. Electrons from the first multiplier will strike another dynode detector and the process continues until a measurable

electrical pulse is produced.[173] Representative calibration curves for copper and silver can be found in Figure 2.5.
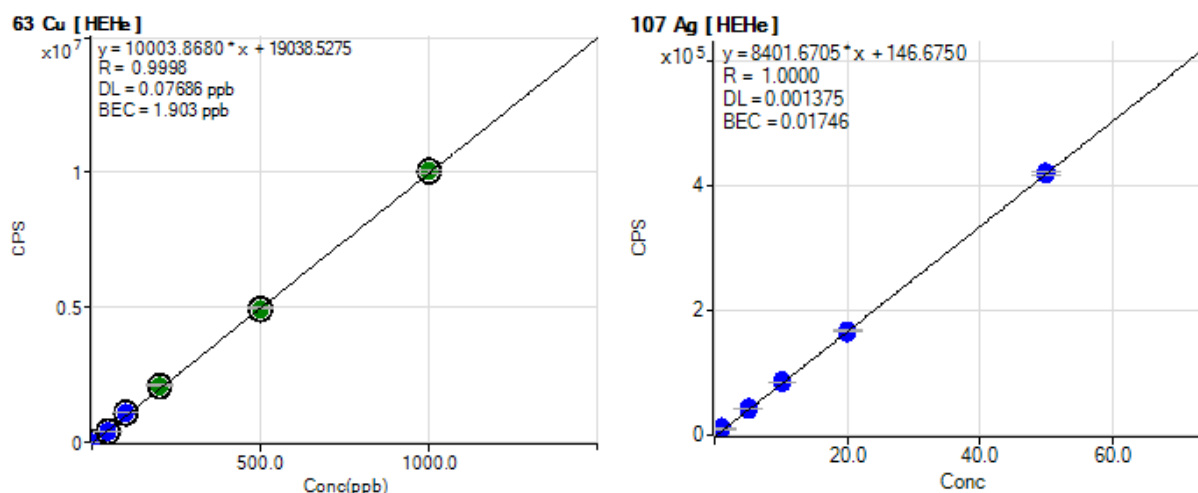
Figure 2.5. Representative ICP-MS calibration curves for copper-63 (A) and silver-107 (B). Calibration curves relate the counts per second measured by the detector and convert those to the appropriate concentrations.

2.4 Humic Acid

Humic acid (HA) is one type of natural organic matter that is commonly found in the environment that originate from decayed organic matter and thus encompasses a large family of organic molecules instead of only one chemical. Humic acids are characterized as the substances that precipitate out of solution when the pH is decreased below 2 and are known to have carboxyl, phenol and aromatic moieties.[174]

A stock of ~200 mg C/L of Pahokee Peat humic acid (International Humic Substances Society, St. Paul, MN) was prepared in ultrapure water and the pH of the solution was adjusted

to 7.1 with 0.1 M KOH (Fisher Scientific) and magnetically stirred overnight at $23 \pm 2°C$. The

pH was again adjusted with 0.1 M KOH to a pH of 7.1 the following day. The solution was then

aseptically filtered with a 0.22 µm cellulose acetate filter (VWR) to achieve sterility and to

remove undissolved material. The concentration of the resulting stock HA solution was

determined as total organic carbon using a Sievers Innovox Laboratory TOC analyzer (General

Electric Analytical Instruments) (Section 2.4.1.). HA concentrations are therefore reported as

milligrams of organic carbon per liter (mg C/L). Rivers and lakes have 2 -10 mg C/L while bog,

swamps and marshes have 10 – 60 mg C/L.[175] Experimental samples contained environmentally

relevant HA concentrations of 20 or 60 mg C/L HA.

Table 2.1 Elemental Composition (%w/w) in a dry, ash free sample of Pahokee Peat humic acid[176]

Element	C	H	O	N	S	P
% Composition	56.84	3.60	36.62	3.74	0.70	0.03

2.4.1. TOC analyzer

A total organic carbon (TOC) analyzer measures the amount of dissolved organic carbon

present in water samples. Samples are first acidified with a 10% w/w phosphoric acid (100 g/L

H_3PO_4) to remove the inorganic carbon in the forms of carbonate and bicarbonate. A heated

sodium persulfate solution with a concentration of 100 g/L is then added to oxidize organic

carbon in samples. The temperature is elevated to increase the reactions of the sodium persulfate

to form sulfate radicals that allows macromolecules to be oxidized to form carbon dioxide

molecules.[177] All CO_2 formed is then detected using a non-dispersive infrared detector found

within the analyzer. Since each different type of gas molecule has its own signature absorption wavelength in the infrared region it is easy to measure the amount of CO_2 present. Several infrared absorption wavelengths for CO_2 a are 2.7 µm, 4.26 µm, and 13 µm.[178] Light is transmitted through the gas sample at one of the absorption wavelengths for CO_2 and then a detector, with a filter to block all but one wavelength, will measure the final light intensity that passed through the sample. The lower the final light intensity is the higher the CO_2 concentration since there are more gas molecules that absorb the light and reduce the amount that passes.

When running this analyzer it is essential to run calibration standards in order to properly determine the CO_2 concentration. Potassium hydrogen phthalate (KHP, $C_8H_5KO_4$) is commonly used as the standard.[177] KHP is comprised of 47% carbon and concentrations of KHP are in units of mg C/L. A stock solution of 1000 mg C/L KHP in ultrapure DI water was prepared by dissolving 0.532 g KHP in 250 mL DI water. This was then diluted to 100 mg C/L KHP. Standard concentrations of 2, 5, 10, 20 and 50 mg C/L KHP were directly made from the 100 mg C/L KHP standard. No serial dilutions were performed as those can propagate any errors made from diluting. The blank calibration was ultrapure deionized water.

A calibration curve between the measured values and the expected KHP external calibration standards was created (see Figure 2.6). The measured values provided by the Sievers Innovox TOC for HA samples were converted to mg C/L.
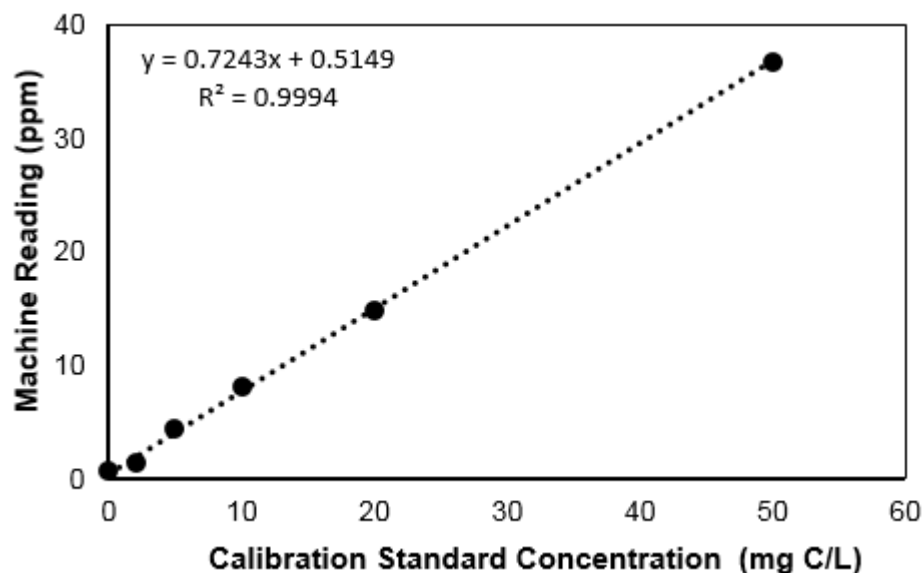
Figure 2.6. A calibration curve generated from Sievers Innovox TOC Analyzer using prepared KHP calibration standards at concentrations of 0, 2, 5, 10, 20, and 50 mg C/L KHP.

2.5 Bacterial Strains and Culture Conditions

2.5.1. *Pseudomonas fluorescens*

Pseudomonas fluorescens is a model Gram-negative, biofilm forming, bacterium that is an obligate aerobe and has the least hazardous rating of BSL-1. *P. fluorescens* is commonly found in both water and soil environments[179] and is known to form biofilms on a variety of surfaces.[180]

P. fluorescens (ATCC 13525) was received in a freeze-dried pellet from ATCC. An autoclaved solution of 8 g/L of nutrient broth (BD Difco) dissolved in ultrapure DI H_2O was used to revive bacteria. 0.5 mL of nutrient broth was added to rehydrate the pellet. The liquid was withdrawn and added to 6 mL of nutrient broth in a UV sterilized polypropylene culture tube

(Evergreen Scientific). Cells were orbitally shaken for 24-48 hours, until the media became turbid.

100% glycerol (BDH chemicals) was diluted to 30% (v/v) with ultrapure water and autoclaved with microcentrifuge tubes. 750 µL of 30% glycerol and 750 µL of revived cells were added to microcentrifuge tubes and stored at -80 °C. Cells are stored at a 15% glycerol solution to reduce ice crystal formation and protect the integrity of the bacterial cell wall when cells are frozen.[181,182]

A frozen stock of *P. fluorescens* stored at -80°C was inoculated in 100 mL of minimal Davis media (MDM) in a 250 mL Erlenmeyer flask and orbitally shaken overnight at 160 rpm until the bacteria reached the early log-growth phase. MDM contains 0.7 g/L K_2HPO_4 ($\geq$ 99%, Acros Organics), 0.2 KH_2PO_4 ($\geq$ 99%, J.T. Baker), 0.5 g/L sodium citrate dihydrate ($\geq$ 99%, BDH chemicals), 1 g/L $(NH_4)_2SO_4$ ($\geq$ 99%, Sigma-Aldrich), 0.1 g/L $MgSO_4 \cdot 7H_2O$ (Acros Organics), and 1 g/L glucose ($\geq$ 99.5%, Amresco) as the primary carbon source. The pH was adjusted to 7.2 $\pm$ 0.02 by adding 0.1 M H_2SO_4 (Acros Organics) and 0.1 M KOH (Fisher Scientific).

For MDM, when sterilizing media using an autoclave, it is essential that a solution of $MgSO_4 \cdot 7H_2O$ and a solution of glucose be separate from all other components of MDM. After autoclaving, mix these ingredients when the media has cooled to room temperature. The temperatures achieved through autoclaving are high enough that the $MgSO_4 \cdot 7H_2O$ and glucose solutions will undergo Maillard reactions with other nutrients in MDM to form undesired compounds that are metabolized differently than the original nutrients. [183,184]

This media was used in previous studies for AgNP toxicity.[51,96–99,116] The potassium phosphates serve as a buffer to help maintain the pH at 7.2 and a source for phosphorous, the

$(NH_4)_2SO_4$ serves as the nitrogen source, the glucose is the primary carbon source but the citrate is another carbon source metabolized by *P. fluorescens*. This media has been used in previous studies and shown minimal nanoparticle aggregation.[51,96,99] MDM does not represent any ecologically relevant media and is solely used to identify critical parameters affecting silver toxicity to *P. fluorescens*.

2.5.1.1 Determining bacterial concentration

A spectrophotometer (Spectramax M2, Molecular Devices) was used to monitor the growth of bacterial suspensions. Aliquots were measured for their optical density at a wavelength of 600 nm (OD_{600}) to determine the amount of light scattered by the bacteria in suspension. The wavelength of 600 nm was chosen because it is a wavelength well past interfering with AgNP absorbance and it is a wavelength that bacteria absorb minimally so all changes in light intensity are from bacteria scattering light. Previous studies have seen that there is a linear relationship between bacterial concentration and optical density up to an $OD_{600} = 0.4$.[185] With *P. fluorescens* the relationship between OD_{600} and bacterial concentration is:

$$C = 10^9 \times OD_{600} \tag{2.1}$$

Where C is the bacterial concentration (CFU/mL).

2.5.1.2 Spread plate method

8 g of nutrient broth (BD Difco) and 15 g of agar (BD Difco) were dissolved in ultrapure DI H_2O and then autoclaved. The autoclaved solution cooled at room temperature for $20 - 30$ minutes and then aseptically poured into petri dishes (VWR). Once plates solidified they were stored at 4 °C until needed.

The conversion factor was determined by the spread plate method. The OD_{600} was measured and then bacterial samples were serially diluted in ten-fold increments until the number of bacteria on the petri dish would be 30 – 300.[186] A 100 µL aliquot was spread on a plate of agar and this was done in triplicate. After spreading, petri dishes were incubated at room temperature for 24 – 48 hours until individual colonies were visible to the naked eye. When colonies are visible the colonies are counted. An individual colony is assumed to have originated from one colony forming unit

2.5.2 *Escherichia coli*

E. coli is a facultative anaerobe that is a model Gram-negative bacterium. This is another species of bacteria with a BSL-1 rating. *E. coli* (ATCC 11775) was grown and tested to assess factors affecting copper toxicity on bacteria. *E. coli* was selected because its genome has been well characterized and has several known copper-responsive genes.

E. coli were received in a freeze-dried pellet and were revived using the same steps used for *P. fluorescens* (section 2.5.1). For experiments, *E. coli* was grown in a modified vitamin supplemented minimal Davis media (VDMD) deficient of sodium citrate because the citrate greatly reduces the solubility of the cupric ions. VDMD consists of 1.58 g/L K_2HPO_4 ($\geq$ 99%, Acros Organics), 2.50 g/L KH_2PO_4 ($\geq$ 99%, J.T. Baker), 1 g/L $(NH_4)_2SO_4$ ($\geq$ 99%, Sigma-Aldrich), 0.1 g/L $MgSO_4{\cdot}7H_2O$ (Acros Organics), and 4 g/L glucose ($\geq$ 99.5%, Amresco) as the primary carbon source. The pH was adjusted to 6.5 $\pm$ 0.02 with the addition of 0.1 M H_2SO_4 (Acros Organics) and 0.1 M KOH (Fisher Scientific). The potassium phosphates serve as a buffer to help maintain the pH at 6.5 $\pm$ 0.02 and a source for phosphorous, the $(NH_4)_2SO_4$ serves as the nitrogen source, the glucose is the primary carbon source but the citrate is another carbon

source. 5 mL of modified Wolfe's vitamin and Wolfe's mineral solutions were added to 500 mL

of media. The modified Wolfe's mineral and vitamin solutions are $100 \times$ concentrations. Tables

2.1 and 2.2 show the compositions for these solutions. These solutions were mixed in ultrapure

DI water and filter sterilized using a 0.22 µm cellulose acetate filter. These supplemental

minerals and vitamins enable *E. coli* to grow to higher concentrations due to the extra nutrients

present.

Table 2.2 Modified Wolfe's media mineral solution recipe (concentration is 100× the concentration to be used)[187]		
Chemical	**Concentration**	**Supplier**
$MgSO_4 \cdot 7 H_2O$	3.0 g/L	Acros Organics
$MnSO_4 \cdot H_2O$	0.50 g/L	Fisher Scientific
NaCl	1.0 g/L	Amresco
$Co(NO_3)_2 \cdot 6 H_2O$	0.1 g/L	Alfa Aesar
$ZnSO_4 \cdot 7 H_2O$	0.178 g/L	Aldrich Chemical
$AlK(SO_4)$ anhydrous	0.01 g/L	Fisher Scientific
H_3BO_3	0.01 g/L	Fisher Scientific
$Na_2MoO_4 \cdot 2 H_2O$	0.01 g/L	MP Biomedical
Na_2SeO_3	0.001 g/L	Acros Organics
$Na_2WO_4 \cdot 2 H_2O$	0.001 g/L	Sigma Aldrich
$NiCl_2 \cdot 2 H_2O$	0.020 g/L	Fisher Scientific
$FeSO_4 \cdot 7 H_2O$	0.1 g/L	Fisher Scientific

This is a modified version of Wolfe's mineral solution. EDTA and copper were removed so

copper toxicity could be better understood since EDTA chelates copper ions and it was desirable

to not expose control samples of *E. coli* to any copper.

Table 2.3 Modified Wolfe's media vitamin solution recipe (concentration is 100× the concentration to be used)[188]

Chemical	Concentration	Supplier
Folic Acid	0.002 g/L	Fisher Bioreagents
Pyridoxide hydrochloride	0.010 g/L	Fisher Bioreagents
Riboflavin	0.050 g/L	Fisher Scientific
Biotin	0.020 g/L	VWR
Thiamine	0.005 g/L	Fisher Scientific
Nicotinic acid	0.005 g/L	Acros Organics
Calcium Pantothenate	0.005 g/L	ICN biomedicals
Vitamin B12	0.0001 g/L	VWR
P-aminobenzoic acid	0.005 g/L	ICN biomedicals
Thiotic acid	0.005 g/L	Fisher Bioreagents
Monopotassium phosphate	0.9 g/L	Fisher Scientific

The OD_{600} was measured to monitor bacterial growth. The same techniques described in sections 2.5.1.1 and 2.5.1.2 were employed, and it was determined that the conversion between OD_{600} and bacterial concentration for *E. coli* was:

$$C = 10^9 \times OD_{600} \tag{2.2}$$

Where: C is the bacterial concentration (CFU/mL).

2.5.3 *Vibrio harveyi*

V. harveyi (ATCC BAA-1116) is a model Gram-negative bacterium used for quorum sensing.[189] It is a marine organism that is non-pathogenic towards humans and is BSL-1. *V. harveyi* are also a facultative anaerobe and when they reach a quorum they luminesce to produce a vibrant turquoise-blue hue.

V. harveyi were received in a freeze dried pellet. A solution of marine broth was prepared by dissolving 37.4 g of marine broth (MB, BD Difco) in DI water and then autoclaved. 0.5 mL of MB were deposited on the freeze-dried pellet. Once the pellet was fully hydrated it was withdrawn and added to 5.5 mL of MB in a culture tube. The culture tube was then orbitally

shaken at 30°C at 200 rpm for 24 hours. Afterwards, 750 µL of *V. harveyi* is added to 750 µL of

30% glycerol in a microcentrifuge and then stored at -80°C.

For experiments *V. harveyi* was grown in autoinducer bioassay medium (AIM). When

making AIM, 17.5 g NaCl (Amresco), 12.3 g $MgSO_4$ (Sigma Aldrich), and 2.0 g Casamino acids

(BD Bacto) were dissolved in 960 mL of ultrapure water, and the pH was adjusted to 7.5 ± 0.02

by adding 3 M NaOH (Fisher Scientific). Separately, solutions of potassium phosphate, L-

arginine and glycerol were prepared. A 1 M potassium phosphate solution at a pH of 7.0 was

prepared by mixing 24.6 mL of 1 M K_2HPO_4 ($\geq$ 99%, Acros Organics), and 15.4 mL KH_2PO_4 ($\geq$

99%, J.T. Baker). The pH was adjusted by adding 0.1 M NaOH (Fisher Scientific) or 0.1 M

H_2SO_4 (Acros Organics). 0.1 M L-arginine (Alfa Aesar) was prepared by adding 0.348 g L-

arginine in 20 mL ultrapure water. A 50% (v/v) glycerol (BDH chemicals) solution was prepared

by mixing 15 mL of glycerol with 15 mL ultrapure water. All solutions described were then

autoclaved and allowed to cool to room temperature. Once solutions are cooled 10 mL of 1 M

potassium phosphate, 10 mL L-arginine and 20 mL of 50% glycerol to the stock solution.

A white polystyrene opaque-bottomed polystyrene 96 well-plate and a black polystyrene

clear-bottomed well plate were used to monitor luminescence and bacterial growth, respectively,

when *V. harveyi* were exposed to a range of Tween 80 concentrations. Both plates were sterilized

for 15 minutes under a UV light (Spectroline EN-180L, 365 nm, 0.2 A). The white well plates

were used to measure luminescence while the black plates were used to measure optical density.

Luminescence and optical density are measured differently and therefore require different plates

in order to obtain the correct measurements.

For Tween 80 exposure experiments a frozen stock of *V. harveyi* were inoculated and

grown overnight at 30°C and rotating at 200 rpm. This culture was diluted from an $OD_{600} = 0.4$

to 0.5 down to a final $OD_{600} = 0.001$ when added to wells. An 80 mM stock solution of Tween 80 (Sigma Aldrich) was prepared by dissolving Tween 80 in AIM. This solution was then filter sterilized with a 0.22 µm cellulose acetate filter. Tween 80 concentrations ranged from 0.08 mM to 40 mM. Two-fold serial dilutions from 20 mM down to 0.08 mM were performed. One column was used as a surfactant control with a 0.08 mM Tween 80 and no bacteria to ensure there was no contamination and one column was a surfactant-free control to monitor normal *V. harveyi* growth. Plates were then shaken at 200 rpm for 10 hours at 30°C.

Additional experiments were performed to monitor where, the autoinducer N-butyryl homoserine lactone (AI-2, ≥97%, Cayman chemicals) was used to probe *V. harveyi* response to autoinducers in media with surfactants. A stock solution of 8 mM AI-2 was prepared immediately before testing and then was diluted to a final concentration of 0.4 µM for the experiment. The AI concentration was diluted by performing adding AI-2 to the suspension of bacteria right before adding them to the well-plates. For these experiments half of the plate was a control and bacteria were not exposed to additional AI-2 and the other half of the bacteria did receive additional AI-2 so the final concentration in the well was 0.4 µM.

2.6 Minimum Inhibitory Concentration and Minimum Bactericidal Concentration

A black polystyrene clear-bottomed well plate (Corning Costar) was sterilized under a UV light (Spectroline EN-180L, 365 nm, 0.2 A) for 15 minutes. Well-plate lids were rinsed, prior to sterilization, with 70% ethanol and DI water and dried under a pre-pure nitrogen stream.

For both copper and silver toxicity, one column was used a cell free control to monitor contamination and another was a metal free control to monitor normal bacterial growth. The

other ten columns were dosed with different concentrations of silver or copper. Those concentrations were adjusted by performing two-fold serial dilutions. For both of these experiments the final bacterial concentrations were $OD_{600} = 0.0001$, 0.001 and 0.01 which are approximately bacterial concentrations of 10^5, 10^6, 10^7 CFU/mL respectively. These concentrations were checked by the spread plate method. The specific concentrations of silver and copper can be found in the appropriate section (for silver Chapters 3 and 4 and for copper Chapter 5). Once media, metal agent and bacteria were added to all wells, the initial optical density was measured with a plate reader. Plates were orbitally shaken for 160 rpm at 25 ± 2 °C and the minimal inhibitory concentration was determined to be the lowest concentration where there was no significant change in optical density after the allotted time of 24 hours for silver and 48 hours for copper.

To determine the MBC, agar plates were prepared with an autoclaved mixture of 4 g Difco Nutrient broth (BD Diagnostics) and 7.5 g Bacto Agar (BD Diagnostics) in 500 mL of ultrapure water. 100 µL samples were taken from wells of the MIC experiments, corresponding to the highest concentration below the MIC and all higher concentrations, and plated. The plates were observed for growth over 24 h. The MBC was determined as the minimal concentration yielding no colonies on agar after 24 h.

2.7 Microscopic Analysis of Bacterial Surface Colonization

A Zeiss Axio Observer Z1 inverted microscope equipped with HBO 100 illuminating system was used to image bacteria adhered on the coverslips. LIVE/DEAD® *Bac*Light™ Bacterial Viability staining (Life Technologies) was used to aid visualization and assess adherent bacteria viability based on membrane integrity. Previous work has demonstrated that *Bac*Light

staining intensities and percentage viability determinations are not affected by the presence of AgNPs.[99] The field of view was 37,300 µm^2.

To prepare the coverslips for imaging they were gently rinsed of non-adherent bacteria by immersing in two separate centrifuge tubes containing 40 mL of 1 mM NaCl and then stained with 300 µL of a LIVE/DEAD *BacLight* solution containing 10 µM SYTO-9 and 60 µM PI in 1 mM NaCl. Coverslips were then stored in the dark for 20 min and then gently rinsed by immersion in a centrifuge tube containing 40 mL of 1 mM NaCl. The underside of the coverslip was then gently blotted dry with a laboratory tissue (Kimwipe). Coverslips were wetted with 100 µL of 1 mM NaCl and imaged using the Zeiss Axio Observer Z1 microscope with a 40 X LD plan-NEOFLUAR objective (Zeiss). Images were collected at a 400 ms exposure (AxioCam MRm) and gain of 2. At least ten randomly selected locations on each AgNP-coated coverslip were imaged and analyzed to determine viability and the number of adherent bacteria per unit area. Four images, at 5 second intervals, were recorded at each location alternating between the AF488 and AO Filter.

Discrete bacterial cells were identified and counted using the Fiji tool developed for ImageJ (National Institute of Health) by Schindelin and coworkers.[170] (http://fiji.sc/). The four images taken for each location were processed in the following way: The first pair of AF488 and AO filter images were added together and thresholded. The second pair of images were treated the same. The first image was analyzed with the "Analyze particles" function and the size setting was 10 to infinity pixel units. The regions of interest (ROIs) created were superimposed on the added product of the second pair of images. If the location of a bacterium shifted by more than one cell length between successive images, it was deemed non-adherent and not counted.[116] Next, the background was subtracted from the first pair of images with a rolling ball radius of 50

pixels and smoothing was disabled. The pixel intensity for each ROI under the AF488 and AO filters were obtained by performing an image analysis and redirecting ROIs to the original images. The intensity ratio between the AF488 and AO filter was calculated and each ROI with an intensity ratio of 1.73 or greater was deemed a viable bacterium based on prior work by Wirth et al.[116] Figure 4.3 shows four representative Live/Dead Images.
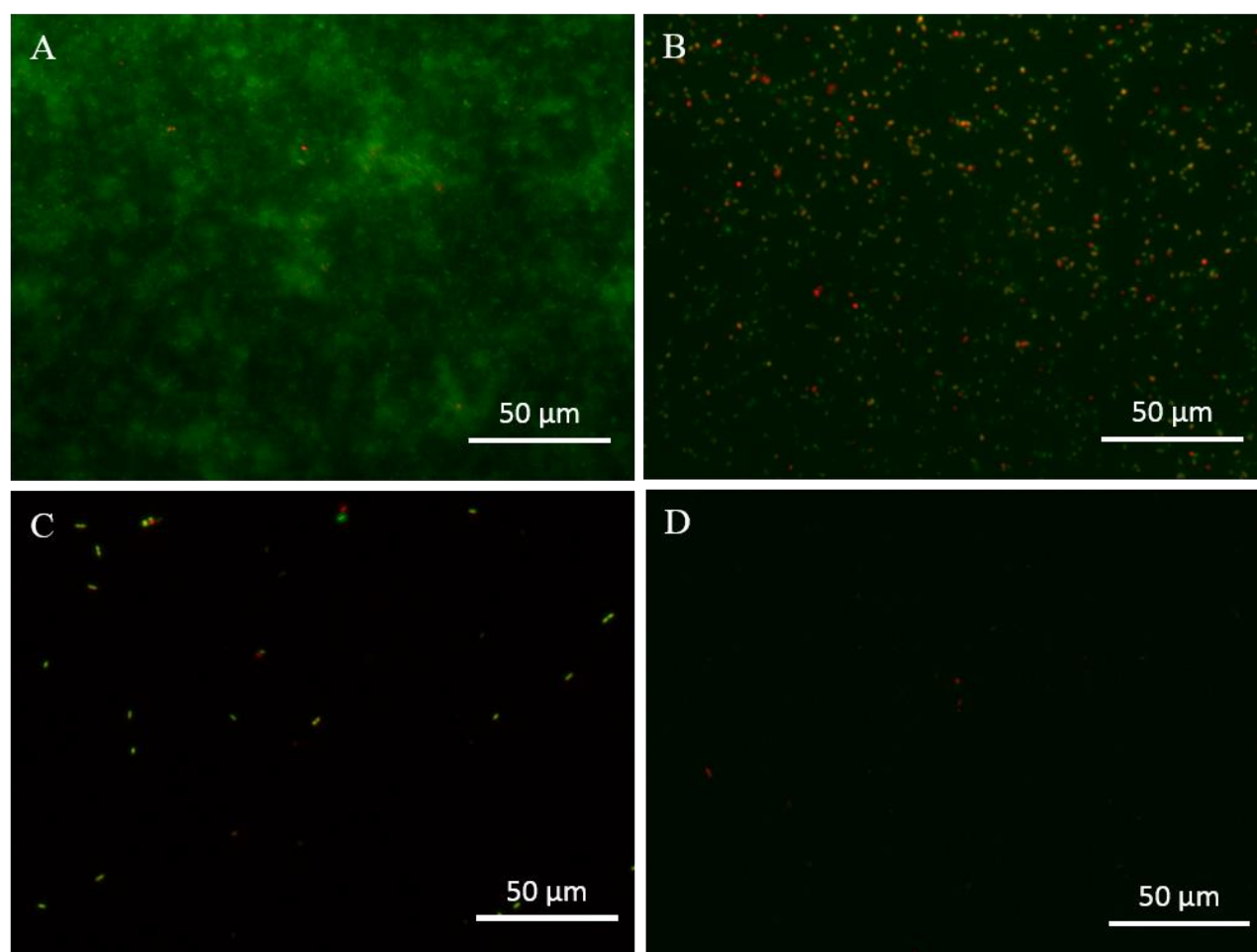
Figure 2.7. Representative Live/Dead Images of *P. fluorescens* on AgNP-decorated coverslips for 10^7 CFU/mL in MDM (A) and MDM with 60 mg C/L HA (B), 10^6 CFU/mL in MDM with 60 mg C/L HA (C) and 10^6 CFU/mL in MDM (D)

2.8 Reactive Oxygen Species Assay

Reactive oxygen species (ROS) are chemically reactive molecules and radicals containing oxygen. When bacteria experience elevated levels of ROS they are in a state of oxidative stress. The fluoroprobe 2',7' dichlorofluorescein acetate (H$_2$DCFDA) is a non-fluorescent molecule that freely enters a bacterium and is hydrolyzed by esterases to remove the DA group and further reacts with ROS groups to form the fluorescent molecule dichlorofluorescein (DCF).[190,191] The higher concentrations of ROS should react with more H$_2$DCF molecules to form more DCF molecules resulting in higher amounts of fluorescence.

2.8.1 H$_2$DCFDA Probe

Methods modified from ones previously described were used to monitor ROS.[192,193] *E. coli* suspensions in the early log-growth phase were diluted to OD$_{600}$ = 0.10 and 0.01, and 1 mL samples were centrifuged for 10 minutes at 8000g (Eppendorf Centrifuge 5415 D) and the supernatant was decanted. A phosphate buffered saline solution (PBS) was prepared and contains 8 g/L NaCl (Amresco), 2 g/L KCl (Fisher Scientific), 2.68 g/L NaHPO$_4$·7H$_2$O (Fisher Scientific), 0.24 g/L KH$_2$PO$_4$ (JT Baker). The pH of PBS was adjusted with 0.2 N HCl (Fisher Scientific) to pH 7.4.

A stock 2 mM of 2',7'-dichlorofluorescin diacetate (H$_2$DCFDA, Sigma Aldrich) probe solution was prepared in 200 proof ethanol (Pharmco-AAPER) and diluted down to a concentration of 10 µM with phosphate buffered solution (PBS) at a pH of 7.4; 1 mL of 10 µM H$_2$DCFDA was added to the decanted *E. coli* samples. The samples were briefly vortexed, wrapped in aluminum foil to protect from light and then orbitally shaken at 160 rpm for one hour at room temperature. Bacteria were then centrifuged for ten minutes at 8000g and the supernatant

was removed. [87,190,192] 1 mL samples of media, either MDM or MDM with 60 mg C/L HA were added to centrifuge tubes that contain bacteria. Cu^{2+} stock solution aliquots or H_2O_2 were added to the samples to yield concentrations of 300 ppb Cu^{2+} or 2 mM H_2O_2, respectively. The samples with H_2O_2 serve as a positive control to verify that the probe is responsive to ROS under these media conditions. Negative control samples containing neither Cu^{2+} nor H_2O_2 were slightly diluted with additional media to match the sample volumes for the positive control and Cu^{2+} exposure samples. Samples were orbitally shaken for 20 h and three 200 L aliquots per sample were collected per condition for fluorescence analysis (Spectramax M2, Molecular Devices) with an excitation wavelength of 493 nm and an emission wavelength of 527 nm with a 515 nm wavelength cutoff filter. Triplicate measurements were made at numerous time points over the course of 24 h (Figure 2.8). Increasing fluorescence intensity indicates increasing ROS levels. [192,193]
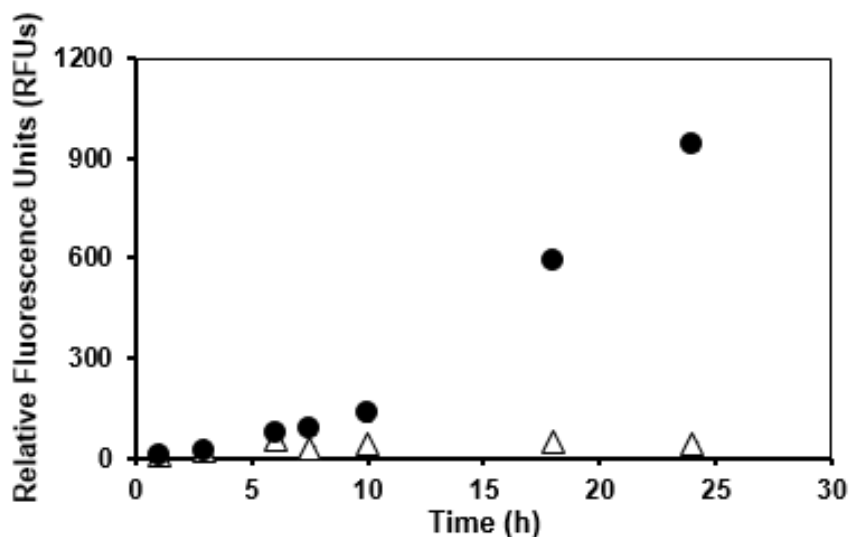
Figure 2.8. ROS generation from *E. coli* after being exposed to 300 ppb Cu^{2+} (black circles) and in the absence of copper (white triangles) over 24 h. Symbols are from triplicate experiments and error bars are smaller than symbols.

Chapter 3. Effects of Initial Bacterial Concentration on Colonizing AgNP-Decorated Surfaces

The material in Chapter 3 has been reformatted and reprinted with the permission of S. M. Wirth, A. J. Bertuccio, F. C. Cao, G. V. Lowry and R.D Tilton from the publication, "Inhibition of Bacterial Surface Colonization by Immobilized Silver Nanoparticles Depends Critically on the Planktonic Bacterial Concentration." *Journal of Colloid and Interface Science,* 2016, 467, 17-27.[116]

Sections 3.1 through 3.4 was work performed by Dr. Stacy M. Wirth, a former graduate student at Carnegie Mellon University. These sections investigate bacterial colonization on AgNP-coated coverslips and factors that can influence the colonization process of bacteria. Section 3.5 through 3.7 was research conducted by Alex Bertuccio to further explore the results observed by Dr. Wirth and to identify a potential mechanism to explain the factors affecting bacterial colonization on AgNP-coated surfaces.

3.1 Introduction

The objectives of this work were to determine the influence of bacterial inoculum concentrations on the degree to which AgNPs adsorbed on a solid surface prevent surface colonization by a model biofilm-forming bacterium, *Pseudomonas fluorescens* (ATCC13525) and to isolate the effects of direct bacterial interaction with AgNP-laden surfaces from the effects of dissolved silver released from the nanoparticles. Gram negative bacteria tend to be more vulnerable to silver ion and AgNP toxicity than Gram positive bacteria that have thicker cell walls that appear to hinder silver uptake.[194–197] Thus, this study focuses on a more vulnerable class of microorganism that one might expect to be less likely to tolerate an AgNP-based

antifouling system. The importance of the initial inoculum concentration was assessed for both short-term (< 24 h) and long-term (up to 96 h) resistance to colonization and, in some cases, progression to biofilm formation, on both AgNP-coated and uncoated surface regions. Results were compared to control experiments with no silver present anywhere in the system.

These experiments indicated that colonization inhibition by AgNP-coated surfaces was controlled by the bioavailable dissolved silver in the system, with a strong dependence on the starting inoculum concentration. In conditions where the dissolved silver was insufficient to cause 100% killing of the initial inoculum, the planktonic population eventually recovered and colonization occurred, regardless of the presence of AgNPs on the surface. This was consistent with measurements of the effect of bacterial concentration on silver binding to suspended bacteria. This has implications for the suitability of AgNP coatings to produce biofilm-resistant materials and for the environmental implications of AgNPs adhered to environmental surfaces.

3.2 Materials and Methods

3.2.1 Surface immobilized AgNPs.

Silver nanoparticles used in this study are described in sections 2.1 and 2.2 and are described previously.[155] The particular particles, denoted as Ag PVP 8 in the prior publication, were stabilized by polyvinylpyrrolidone (PVP) (MW 55,000) and had a 7.8±4.6 nm diameter based on TEM.[155] Particles were obtained as a concentrated (> 500 ppm) aqueous dispersion and stored in the dark at 4˚C.

Glass coverslips (22×22 mm, No. 1.5, Fisher Scientific) were used as colonization substrates. Coverslips were cleaned by 30 min bath sonication (Branson 1200, Branson

Ultrasonics Corp.) in a 10% solution of RBS 35 detergent concentrate (Thermo Scientific), 20 min treatment with Nochromix (Sigma-Aldrich) dissolved in sulfuric acid (technical grade, 93-98%, Fisher Scientific), 20 min treatment in 6 N HCl (BDH Chemicals), and 30 min in 10 mM NaOH. Coverslips were rinsed thoroughly with ultrapure water after each step. Finally, they were dried under a pure nitrogen jet and sterilized by UV irradiation for 15 minutes (Spectroline Model EN-180, 365 nm, 4 W). Coverslips were used immediately after preparation.

The stock AgNP dispersion was diluted in autoclave sterilized ultrapure water (Barnstead Nanopure, >18 MΩcm resistivity) to a 10ppm final concentration, and the dispersed particle size distribution was characterized by dynamic light scattering (DLS) (Zetasizer Nano ZS, Malvern Instruments). 5 mL aliquots of this dispersion were then dispensed into sterile 50 mL polypropylene centrifuge tubes (Beckman Coulter). One cleaned, UV-sterilized glass coverslip was placed in each tube so that it was half submerged in the AgNP dispersion. The other half remained dry, thereby depositing AgNPs on half of the surface. Coverslips were handled using flame-sterilized forceps in all steps. Freshly prepared 10 ppm AgNP dispersion was used for each coverslip.

Coverslips half submerged in AgNP dispersions were incubated in the dark at room temperature (23±2°C) for 1 h without shaking. Each coverslip was then rinsed by slowly pouring 800 mL autoclave-sterilized, ultrapure water over it. Rinsed coverslips were immediately transferred to new 50 mL centrifuge tubes containing 15 mL sterile minimal Davis media (MDM, described below) for use in bacteria adhesion experiments. Coverslips were rotated 90º during the transfer so that the boundary between the AgNP-coated and uncoated portions was vertical (avoiding differences in colonization on coated and uncoated regions resulting from submersion depth), and the entire coverslip was submerged in MDM. This setup makes it

possible to easily distinguish effects from bulk dissolved silver and from direct interaction with adsorbed AgNPs, since the same liquid (with the exact same composition in all regards, including dissolved silver concentration) bathes both the uncoated and AgNP-coated surface regions.

Some of the rinsed coverslips were transferred to tubes containing ultrapure water for darkfield microscopy examination. Strong light scattering associated with localized surface plasmon resonance allows AgNPs to be identified in this way.[169] This was done with a Zeiss AxioObserver Z1 inverted microscope equipped with a HAL100 halogen illuminator. Coverslips were imaged wet using a 40× LD Plan-NEOFLUAR objective (Zeiss). Images were collected at a 1s exposure (AxioCam MRm) to count the AgNPs adhered to the coated surface region. Images from the uncoated region were also acquired to estimate the contribution of extraneous dust particles or microscopic glass defects to the total counts. Particle counting was performed with ImageJ 1.45s image analysis software.

3.2.2 Bacterial strain and culture conditions

The bacterial strain was *Pseudomonas fluorescens* ATCC 13525. All cell culture and AgNP exposure work was performed in minimal Davis media (MDM) containing 0.7 g/L K_2HPO_4 (≥99%, J.T. Baker), 0.2 g/L KH_2PO_4 (≥99%, J.T. Baker), 1 g/L $(NH_4)_2SO_4$ (≥99%, Sigma-Aldrich), 0.5 g/L sodium citrate (≥99%, Sigma-Aldrich), 0.1 g/L $MgSO_4 \cdot 7H_2O$ (≥98%, Sigma-Aldrich), and 1 g/L glucose (Sigma-Aldrich) as carbon source at pH 7.2±0.1. This media was chosen for its comparatively low ionic strength (~50 mM) and absence of chloride. For each experiment, a starting culture was prepared by inoculating autoclave-sterilized MDM with a *P. fluorescens* frozen stock (-80ºC), then growing aerobically overnight at 23 ± 2ºC with 160 rpm

orbital mixing. Growth was monitored via optical density at 600 nm (OD_{600}) in 1 cm pathlength polystyrene cuvettes (SpectraMax M2, Molecular Devices).

3.2.3 Bacterial surface colonization

Appropriate volumes of the overnight bacterial cultures were added to the centrifuge tubes containing AgNP half-coated coverslips in MDM to give either $OD_{600} = 0.01$ (~1×10^7 CFU/mL) or 0.001 (~1×10^6 CFU/mL) in a total 25 mL volume. Silver-free controls contained clean, UV-sterilized coverslips without AgNPs. Control samples containing AgNP half-coated coverslips but no bacteria were also examined. Tubes were shaken at 200 rpm on an orbital shaker, with loose caps to maintain aerobic conditions, in the dark, at room temperature (23±2°C).

After 1 h incubation, the bulk liquid in the tubes was serially diluted and plated onto nutrient agar. Colonies were counted after 48 h growth at room temperature (23 ± 2°C) to calculate the total culture sample viability. If no growth was observed, it indicated greater than 99.99% ("4 log") killing of the ~1×10^6 CFU/mL culture or 99.999% ("5 log") killing of the ~1×10^7 CFU/mL culture.

Further planktonic growth in the cultures suspended above coverslips was monitored by periodic OD_{600} and plate count measurements. In some cases noted below, after 24 h incubation in the original media, coverslips were gently rinsed with sterile MDM and transferred to tubes containing 25 mL fresh MDM to replenish depleted nutrients and test the role of nutrient depletion on growth and surface colonization.

3.2.4 Dissolved silver analysis

The dissolved silver concentration (consisting of free ionic silver and any other dissolved silver species, *i.e.*, excluding nanoparticulate Ag) in the media bathing the AgNP-coated coverslips from the cell-free tubes was measured by inductively coupled plasma mass spectrometry (ICP-MS, Agilent 7700x) at different time points. Small samples for ICP-MS analysis were taken from the bulk liquid in the tubes and diluted in HNO_3 (Aristar plus grade, BDH Chemicals) to finish with 5 vol% HNO_3. For tubes containing bacteria, the dissolved silver concentration was measured just prior to addition of the cells to determine the starting silver concentration at the time of inoculation. Then, after 1 h incubation with cells, new samples of the bulk liquid were collected and filtered using Amicon® Ultra-4 centrifugal filter units with 3 kDa molecular weight cutoffs (Millipore) to remove cells and macromolecular cell products plus any silver to which they may have been complexed. Filtrates were acidified to a concentration of 5 vol% HNO_3 and analyzed by ICP-MS to determine the amount of "free silver" in the liquid. The difference between the filtrates and the pre-inoculation (cell-free) samples provides the amount of silver that had bound to cells (or macromolecular cell products retained by the filter). This process was repeated after 48 h and 72 h incubation. As a negative control, samples from cell-free tubes were also filtered and analyzed by ICP-MS to determine the extent to which dissolved silver might be removed by binding to the filter.

3.2.5 Microscopic analysis of bacterial surface colonization

The number and viability of bacteria adhered on coverslips were measured at various time points using LIVE/DEAD® *Bac*Light™ bacterial viability staining (Invitrogen Corp.) and epifluorescence microscopy. Cell counting was only performed when bacteria were present in a monolayer or less; otherwise, three dimensional biofilm formation was simply noted when it

occurred. The *Bac*Light kit contains propidium iodide (PI) and SYTO9 fluorescent dyes that differentially stain bacteria based on membrane integrity. This difference correlates with viability,[196] and we use that association here.

To prepare coverslips for imaging, they were removed from the tubes, transferred to 40 mL of a 1 mM NaCl rinse solution and gently swirled by hand for 10 seconds. After two such rinses, the surface was covered with 300 µL *Bac*Light staining mixture (60 µM PI and 10 µM SYTO9 in 1 mM NaCl) and incubated in the dark for 20 minutes. Afterwards, coverslips were rinsed again in 40 mL 1 mM NaCl. The unstained (bottom) side of the coverslip was carefully dried with laboratory tissue (Kimwipe) and the coverslip was transferred to the microscope stage. The stained (top) side of the coverslip did not dry during any of these steps.

*Bac*Light stained cells were observed using a Zeiss Axio Observer Z1 epifluorescence microscope equipped with an HBO 100 illuminating system. Appropriate dichromatic filter sets were selected to fit the excitation/emission spectra of the *Bac*Light fluorophores. The filter sets used for SYTO9 and PI were filter set AF488 (Zeiss Filterset 10) and filter set AO (Chroma 31011 acridine orange filter set), respectively. Images were collected with an AxioCam MRm camera. The total cell counts and viability of cells in the images were quantified by the method described and validated in section 3.2.7. Bacterial calibration standards analyzed using this method showed excellent correlation between the expected and the measured viabilities. Experiments verified that AgNPs do not interfere with this assay (section 3.2.7).

3.2.6 Quantitative viability analysis by fluorescence microscopy

Quantitative analysis of viability for the adherent bacteria was based on fluorescence intensity integrated across entire fields of view. The viability analysis is developed in this section. It uses ImageJ digital image analysis software from the National Institutes of Health. It

is based on a calibration that uses countable numbers of viable and non-viable cells deposited on a substrate from planktonic suspensions containing known fractions of viable and non-viable cells, as described in the next section below.

The viability analysis is complicated by the fact that both viable and non-viable stained cells contribute to the total fluorescence intensity of images collected with both the AF488 filter set that is selective for SYTO9 and the AO filter set that is selective for PI. Because the tail of the SYTO9 emission spectrum is detected by the AO filter set, SYTO9 stained cells are visible in both images. This prevents each filter set image from being used independently to determine the number of viable cells based simply on the total intensity of the AF488 image and the number of non-viable cells based simply on total intensity of the AO image. Correction for imperfect filter selectivity should be performed for any quantitative dual staining procedure, for any type of microscopy platform.

The total intensity of the dual stained bacterial sample in each filter channel is the sum of the contributions of both viable and non-viable cells. That is,

$$I_{T,AF} = i_{L,AF}N_L + i_{D,AF}N_D \qquad (3.1)$$

$$I_{T,AO} = i_{L,AO}N_L + i_{D,AO}N_D \qquad (3.2)$$

where $I_{T,AF}$ and $I_{T,AO}$ are the total intensities of images captured with the AF488 and AO filter sets, respectively, N_L and N_D are the number of viable, or "live", and non-viable, or "dead" cells, respectively, $i_{L,AF}$ is the intensity of a single viable cell imaged with the AF488 filter set, $i_{D,AF}$ is the intensity of a single non-viable cell imaged with the AF488 filter set, and $i_{L,AO}$ and $i_{D,AO}$ are the intensities in images captured with the AO filter set of a single viable and a single non-viable cell, respectively. The single cell intensities, i, are assumed to be constants and are defined for each set of images as described below.

43

Solving for N_L and N_D allows calculation of these cell numbers as a function of the total intensities.

$$N_D = \frac{I_{T,AO} i_{L,AF} - i_{L,AO} I_{T,AF}}{i_{D,AO} i_{L,AF} - i_{L,AO} i_{D,AF}} \qquad (3.3)$$

$$N_L = \frac{I_{T,AF} - i_{D,AF} N_D}{i_{L,AF}} \qquad (3.4)$$

Two sets of AF488 and AO images were acquired for each field of view at an interval of 10 seconds. The AF488 and AO images from the first set were thresholded and combined to select all the cells in the field of view. Although all cells were visible in both images, the process of thresholding and adding the images together was necessary due to the widely different intensities of the viable and non-viable cells, as illustrated in Figure 3.1.
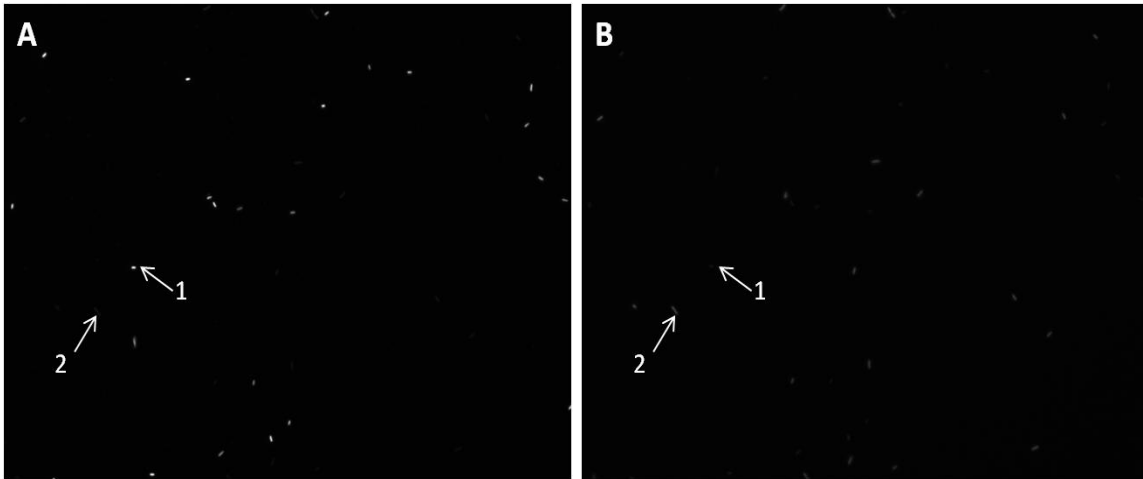
Figure 3.1. Images of a 50% viable planktonic calibration collected with the A) AF488 and B) AO filter sets. Viable cells, such as cell 1, and non-viable cells, such as cell 2, appear in both images but with varying intensities.

The thresholded objects (cells) were then added to the region of interest (ROI) manager using the "Analyze Particles" function of the ImageJ. Particles with areas smaller than 10 pixels^2 (0.26 µm^2) were excluded from the analysis as this is too small to be an intact cell.

The second set of images, collected at the same position, but 10 seconds later, was used to eliminate mobile cells from the analysis. When analyzing bacterial colonization images, it is important to distinguish cells that are adherent and immobile from cells that are only in the vicinity of or loosely associated with the surface and are mobile. The AF488 and AO images from the second set of images were also thresholded and combined. Regions of interest (ROIs) from the first set of images that did not also appear in the second set were removed. This eliminated cells that were moving, and therefore not part of the adherent population, from the analysis. The intensities of the remaining ROIs, which contain all the adherent cells in the field of view, were then measured in both the AF488 and AO background subtracted images from the first image set. The sum of these intensities for all the ROIs (cells) in a given field of view gave the values for $I_{T,AF}$ and $I_{T,AO}$.

For each set of images, the single cell intensities, i, were determined by finding ROIs that corresponded to individual viable or non-viable cells. These single cells were defined as "viable" or "non-viable" based on their individual intensity ratios, as described below in "Viability calibration using planktonic cultures". These values, along with $I_{T,AF}$ and $I_{T,AO}$, were then used in equations (A3) and (A4) to calculate the total numbers of viable, or "live", cells (N_L) and non-viable, or "dead" cells (N_D) in each image.

3.2.7 Viability Calibration using Planktonic Cultures

Planktonic calibrations were used to define the intensity ratio values that correspond to viable and non-viable cells. Different ratios of "viable" (untreated) cells and "non-viable" cells

(killed by incubation in 70% isopropanol) were mixed, stained with BacLight and incubated 20 minutes in the dark. 10 µL of each stained cell culture was then placed on a glass microscope slide, covered with a glass No. 1.5 coverslip (Fisher Scientific) and imaged through each filter set (AF488 and AO) with a 40×/0.6 NA Plan-NEOFLUAR objective (Zeiss). Images were collected with an AxioCam MRm camera at an exposure of 400 ms. For each field of view, a total of four images was collected in the following order: AF488, AO, AF488, AO. The first set of images was used to assess viability. The second set of AF488 and AO images was collected so that cells that were moving could be eliminated from the analysis, as described above.

Image analysis was carried out using ImageJ. For each field of view, the thresholded AF488 and AO images were added together so that all cells that appeared in either image were selected. The selected regions (cells) were added to the ROI (region of interest) manager, again excluding objects with areas smaller than 10 pixels^2 (0.26 µm^2). Moving cells were eliminated using the method described in Section 3.2.6, "Quantitative Biofilm Viability Analysis by Fluorescence Microscopy". The intensities of the remaining cells were measured in both the AF488 and AO background subtracted images. The ratio of these intensities for *each cell* was calculated.

Table 3.1 summarizes the image analysis results for the 0% and 100% viable calibrations. Using these values, cells were defined as "viable" if the AF488/AO intensity ratio was greater than 1.74 (which is the mean intensity ratio of the 100% viable culture minus two standard deviations). Cells with intensity ratios lower than 1.74 were defined as "non-viable" or "dead". Using this definition, the number of viable and non-viable cells in each frame was counted and the percent viability was calculated. The results are shown in Figure 3.2 (closed diamonds). There is a good correlation between viabilities measured in this way and the actual viabilities

(slope of 0.96) of samples prepared by mixing known amounts of isopropanol-killed cells and living cells to obtain various intermediate viability levels. A cutoff intensity ratio of 1.74 was therefore used to distinguish "viable" from "non-viable" individual cells in subsequent image analyses.

The possibility was considered that the presence of silver nanoparticles may alter the response of cells to the viability assay, for example, appearing as more "viable" by virtue of their AF488/AO intensity ratio due to some AgNP interference with the staining or imaging. To test this possibility, planktonic bacteria killed by incubation in 70% isopropanol were stained and imaged as described above using both silver-free and AgNP-coated coverslips. There was no statistical difference in the AF488 to AO filter intensity ratio of isopropanol-killed cells attached to the two different surfaces. Therefore, the presence of silver did not interfere with the viability assessment.

Table 3.1. AF488/AO intensity ratios for *Bac*Light stained calibration standards (0% and 100% viable).

Viability (%)	mean intensity ratio (AF488/AO)	standard deviation (σ)	mean+2σ	mean-2σ
0	0.24	0.14	0.53	-0.04
100	8.87	3.57	16.01	1.74
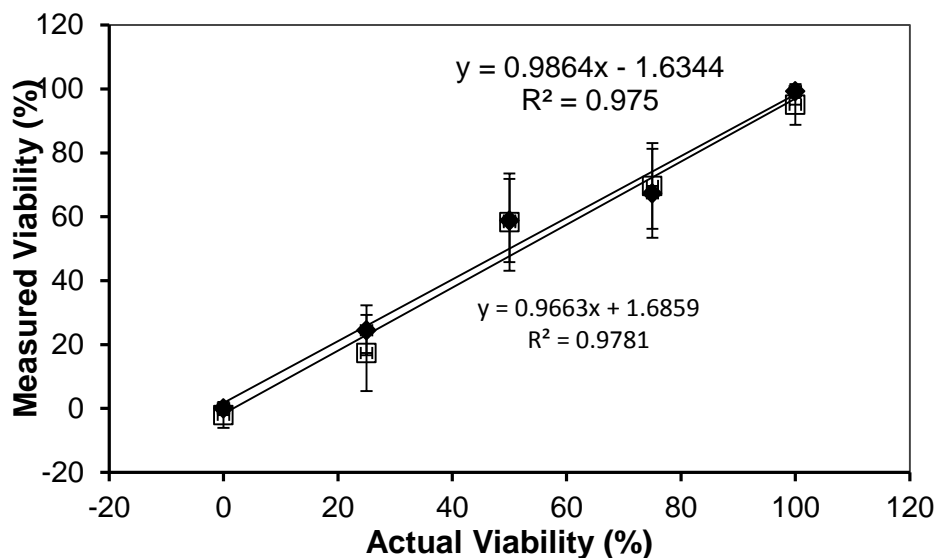
Figure 3.2. *Bac*Light calibration based on microscope images of planktonic cultures of *P. fluorescens* containing different mixtures of viable (untreated) and non-viable (isopropanol-killed) cells. Two methods were used assess to assess viability in the images: 1) Counts of individual viable and non-viable bacteria based on each cell's intensity ratio (closed diamonds) 2) Calculation of the number of viable and non-viable bacteria in each image based on total intensities (equations 3.3 and 3.4) (open squares). Both methods gave good correlation with the actual viability (slope of 0.96 for the counting method and 0.99 for the total intensity method). Error bars represent one standard deviation based on measurements from at least 10 different fields of view.

3.3 Results and Discussion

3.3.1 Surfaces with Adsorbed AgNPs

The intensity-weighted hydrodynamic diameter distribution of the AgNPs dispersed in purified water, as determined by DLS, indicates that the dispersion consisted mainly of primary particles with some aggregates (Figure 3.3). The number-weighted diameter distribution shows one peak near 10 nm, corresponding to primary particles, consistent with the 7.8 ± 4.6 nm diameter reported by TEM.
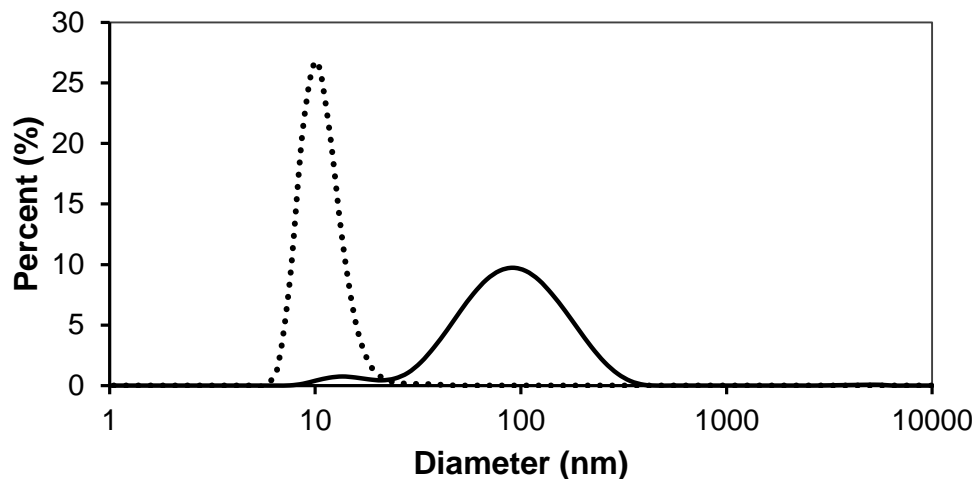
Figure 3.3. Intensity-weighted (solid line) and number-weighted (dotted line) hydrodynamic diameter distributions of AgNPs dispersed in ultrapure water as determined by dynamic light scattering.

The average particle number density on the AgNP coated coverslip regions was $(3.0\pm0.43) \times10^5$ particles/mm^2 (mean $\pm$ standard deviation), as determined by darkfield imaging (Figure 3.4). Counts from uncoated regions were 580 ± 350 particles/mm^2 indicating a negligible contribution from extraneous dust or coverslip defects to the total particle counts. Comparing particle counts between multiple coverslips prepared on different days, by one way ANOVA, showed no statistical difference (P=0.4) indicating the reproducibility of the particle adsorption procedure. After 24 h incubation in cell-free MDM, there was no significant decrease in particle counts based on average counts from three different coverslips (P=0.10). Thus, AgNP desorption is not significant over the timescale of the bacterial incubation experiments.
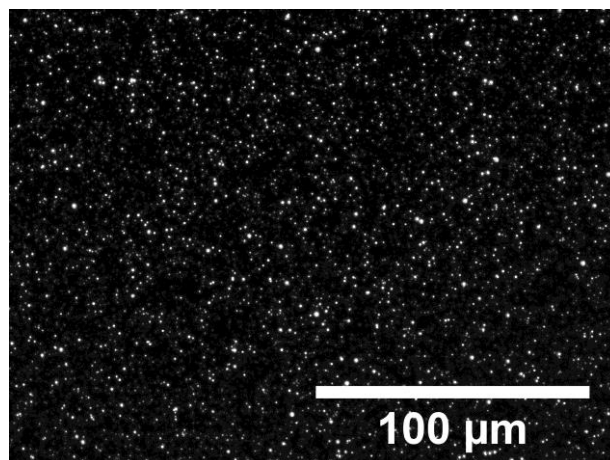
Figure 3.4. A representative darkfield microscopy image of glass coverslip with adsorbed AgNPs. This image displays 3.4×10^5 particles/mm^2.

3.3.2 Growth and Viability of Planktonic Bacteria

The effect that AgNPs, adsorbed on glass coverslips, have on the growth and viability of planktonic bacteria in the media bathing such coverslips will be discussed below. It will be shown that the planktonic population dynamics controls whether adsorbed AgNPs are able to prevent surface colonization on the AgNP-coated surfaces.

The viable cell concentration (determined by plate counts on nutrient agar) of a planktonic culture with an initial $OD_{600} = 0.001$ inoculum, after 1 h incubation in the presence of the AgNP half-coated coverslip, was 143.5 ± 135.7 CFU/mL. This was $99.97 \pm 0.3\%$ less than the viable concentration measured after 1 h incubation with silver-free coverslips, $(5.4 \pm 2.8) \times 10^5$ CFU/mL. Silver-free coverslips served as the negative controls for all experiments. With a higher inoculum concentration, corresponding to $OD_{600} = 0.01$, no statistical difference (P = 0.56) was observed between planktonic cell counts from the cultures with silver-free or AgNP

half-coated coverslips after 1 h incubation, $(4.3 \pm 1.9) \times 10^6$ and $(3.7 \pm 3.0) \times 10^6$ CFU/mL, respectively.

Planktonic growth curves (Figure 3.5) also showed a minimal effect from the AgNP half-coated coverslips for the higher concentration $OD_{600} = 0.01$ culture, in contrast to the significant effect that adsorbed AgNPs had on the $OD_{600} = 0.001$ culture. In the presence of the AgNP half-coated coverslip, the higher concentration culture had a slight lag in growth compared to the silver-free control, indicating a transient inhibitory effect from the dissolved silver. However, once these cultures entered log growth, there was no significant difference between the growth constants for the silver-free and silver-exposed cultures, 0.55 ± 0.09 h^{-1} and 0.59 ± 0.05 h^{-1}, respectively.
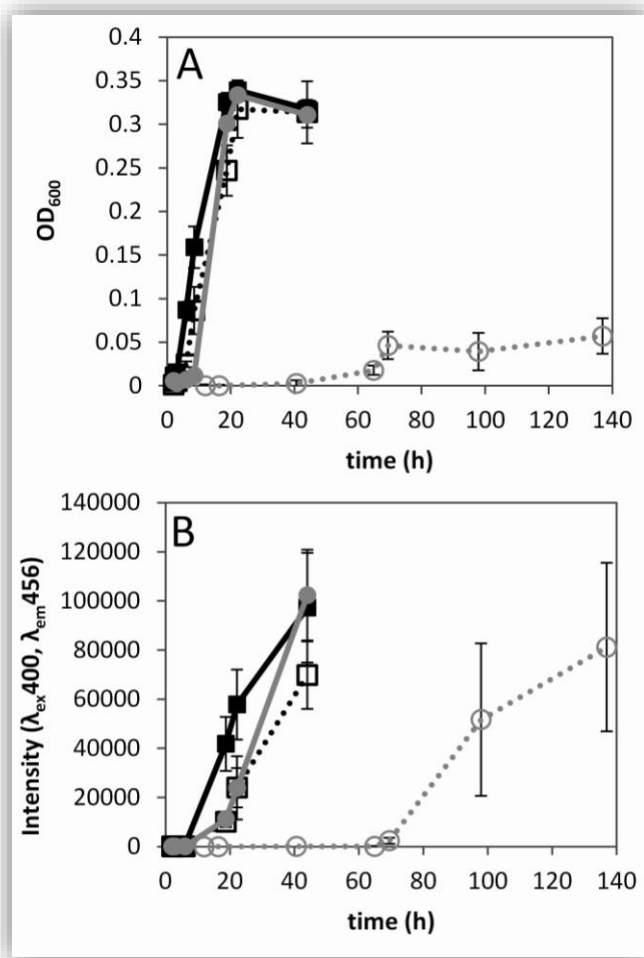
Figure 3.5. Planktonic cell growth indicated by OD_{600} (A) and fluorescence emission at 456 nm with excitation wavelength of 400 nm (B) in the bulk liquid bathing coverslips. Except for a slight lag, growth in the $OD_{600} = 0.01$ cultures exposed to the AgNP coated coverslips (open black squares) was similar to growth in the silver-free control cultures (closed black squares). When an initial $OD_{600} = 0.001$ culture was used, growth was significantly delayed in the culture that was incubated with AgNP half-coated coverslips (open grey circles) compared to the case with silver-free coverslips (closed grey circles). Fluorescence (B) produced by the bacteria in AgNP exposed cultures eventually recovered to values similar to the silver-free control. Error bars represent standard deviations based on measurements from three separate experiments.

In the more dilute $OD_{600} = 0.001$ starting culture, growth in the presence of the AgNP half-coated coverslip was greatly delayed compared to the silver-free control (Figure 3.5, open gray circles). However, at long times (> 48 h) growth was evident, indicating silver had not

52

killed 100% of the starting cell population and that remaining viable cells were capable of reproducing in the presence of silver. In these dilute culture experiments with AgNPs, OD_{600} measurements are not accurate representations of cell concentration, since these cells were observed to be growing in macroscopic, suspended flocs. These do not contribute to the OD measurements as individually dispersed cells would. These flocs were consistently observed in the low cell concentration cultures incubated with AgNP half-coated coverslips, but not in any other conditions. They were also never observed in cell-free controls, eliminating the possibility that they were contaminant organisms. Since the flocs are problematic in OD measurements, fluorescence measurements were also made to give some indication of cell activity in flocculating cultures. *P. fluorescens* produces a soluble, fluorescent siderophore (Figures 3.6 and 3.7)[198]. Although total siderophore production is not necessarily proportional to cell density, production indicates cell activity. Fluorescence production in silver-treated cultures reached similar values to those in silver-free cultures (Figure 3.5 B) at long times, suggesting that the cell cultures recovered significant activity at longer times.
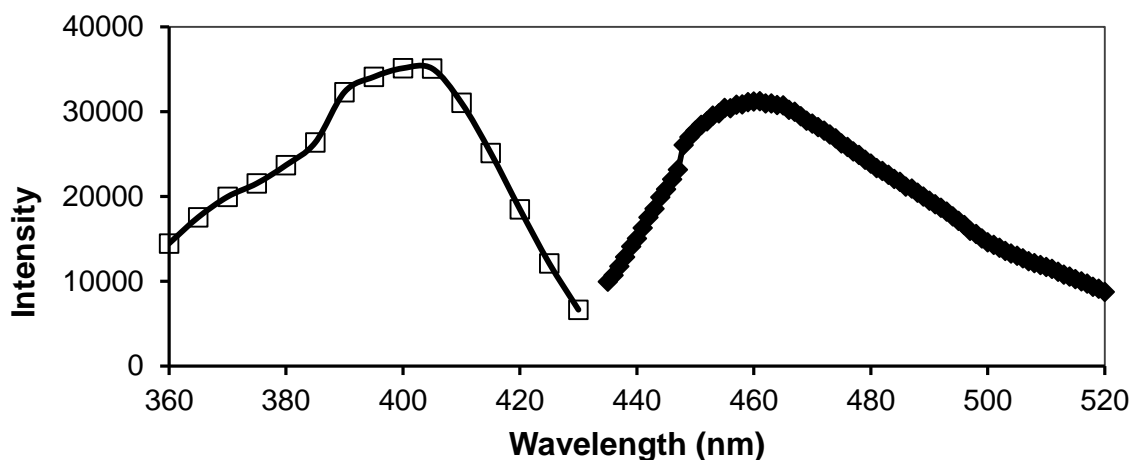
Figure 3.6. Excitation (open squares) and emission (solid diamonds) spectra of the soluble fluorophore produced by *Pseudomonas fluorescens* grown in MDM. Cells were removed by centrifugation and fluorescence measurements were made on the cell-free supernatant at pH 7. Excitation spectra were measured for a fixed emission wavelength of 460 nm. Emission spectra were measured with excitation at 400 nm.
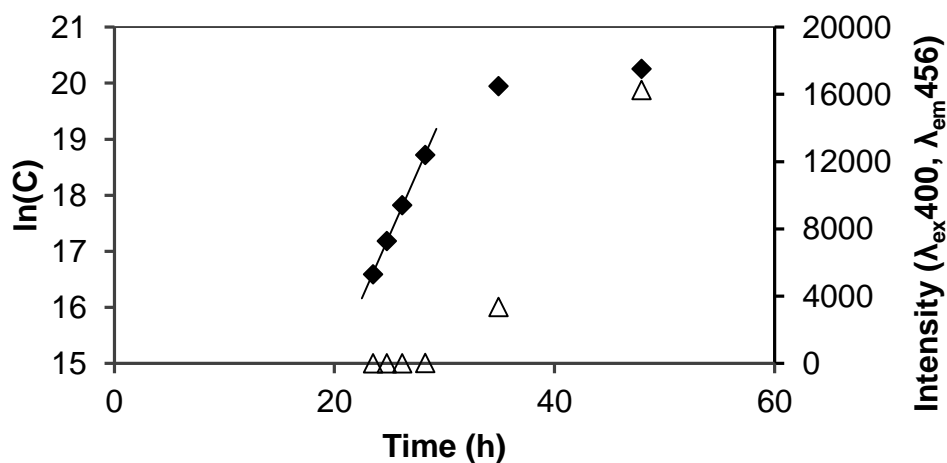
Figure 3.7. Cell concentration (CFU/mL, solid diamonds) and fluorescence increase (open triangles) as a function of time for *P. fluorescens* in MDM. The increase in the fluorescence emission at 456 nm (excitation wavelength of 400 nm) does not begin until the culture is exiting logarithmic growth (designated by linear trendline), after which the intensity increases dramatically.

54

When the initial inoculum concentration was decreased by dilution to an expected OD_{600}

of 0.0001 ("expected" because an OD of 0.0001 is below the spectrophotometer resolution), no

growth or viability was detectable in the presence of an AgNP half-coated coverslip up to 96 h of

incubation, nor was any colonization observed. In silver-free control experiments at this low

initial OD_{600}, planktonic growth and surface colonization were both significant after 72 h (Figure

3.8). This indicates that adherent AgNPs were sufficient to kill 100% of the planktonic bacteria

in the $OD_{600} = 0.0001$ inoculum, and only in such circumstances could surface colonization be

prevented.
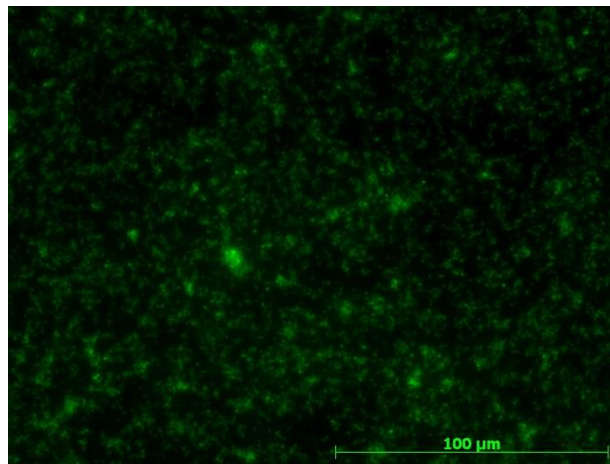
Figure 3.8. Representative image of *Bac*light stained *P. fluorescens* adhered to glass coverslip after 72 hours in Minimal Davis Media, in the absence of AgNPs. The initial inoculum had a nominal $OD_{600} = 0.0001$. Cell count was 2600 ± 360 per frame (frame size is 37300 μm^2). The planktonic suspension above the coverslip had grown to $OD_{600} = 0.32$ at this time in two replicate experiments.

Decreased efficacy with increased bacterial concentration for conventional antibiotics has been observed previously and is known as the inoculum effect.[199,200] The hypothesis for the difference in planktonic viability loss between the different initial inoculum concentrations is that the free dissolved silver concentration decreased due to silver binding to the cells themselves and/or to their byproducts. The fraction of total silver in the bound form would increase with cell concentration, with cells and byproducts serving as a silver sink. To test this, silver concentrations in the bulk liquid bathing the coverslips were measured before and after removal of cell-bound silver by centrifugal ultrafiltration. The silver in the filtrate is defined as "free silver."

The results in Figure 3.9 show that a significant fraction of the dissolved silver was removed by filtration for both starting cell concentrations. Filtration of cell-free controls did not significantly reduce the silver concentration (P=0.3), indicating that neither the possible presence of desorbed AgNPs in the bulk liquid (which would be removed by the 3 kDa filter) nor dissolved silver binding to the filter itself was significant. The cell-free control data indicate that the amount of dissolved silver released by the AgNP-coated coverslips increases over at least 72 h. The free silver concentration in the $OD_{600} = 0.001$ starting culture filtrate after 1 h was $49\pm12\%$ of that in the filtrate from the cell-free control. Silver removal was far more extensive in the $OD_{600} = 0.01$ starting culture, with no free silver detected in the filtrate after 1 h incubation with the cells, or at any later time up to 72 h. Some free silver was detected in the $OD_{600} = 0.001$ culture after 1 and 45 h incubations, but unlike the cell-free case, the concentration did not increase between 1 and 45 h. At 72 h, the cell concentration in that culture had increased due to cell growth (based on OD_{600}) and the free silver concentration had decreased to a very low level. This is attributable to more extensive silver binding by the growing bacterial population.

56
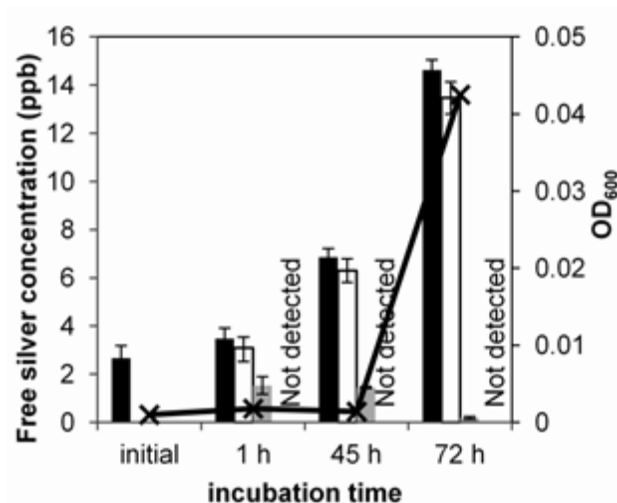
Figure 3.9. Dissolved silver concentration in the bulk liquid bathing AgNP half-coated coverslips showed an increase in dissolved silver with time in the cell-free controls (black bars). When these samples were filtered on 3 kDa ultrafiltration devices, silver concentration was not significantly affected (P=0.3) (open bars). Large decreases in dissolved silver concentrations were observed when the bulk liquid from tubes containing cells from initial inocula corresponding to $OD_{600} = 0.001$ (grey bars) or $OD_{600}=0.01$ (not detected) were filtered. No silver was detected in any of the $OD_{600} = 0.01$ filtrates. The black line ($\times$) shows the OD_{600} of the $OD_{600} = 0.001$ starting culture at the various time points.

3.3.3 Bacterial Colonization on AgNP-Coated Surfaces

When the dissolved silver concentration was insufficient to cause 100% planktonic bacterial killing, long term recovery of the planktonic population occurred, even when 99.97% of the starting culture was killed during the first hour of incubation ($OD_{600} = 0.001$ inoculum). However, bacterial surface colonization could possibly still have been impeded by direct interactions with AgNPs on the surface even after the planktonic population recovered. Surface colonization was therefore measured on three different surfaces: clean coverslips in silver-free media ("silver free"), the AgNP-coated regions of half-coated coverslips ("AgNP-coated"), and the uncoated regions of half-coated coverslips ("uncoated"). In the latter two cases, the AgNP-coated and uncoated surface regions were bathed by the same liquid.

For the higher starting bacterial concentration (OD_{600}=0.01, ~1×10^7 CFU/mL), surface colonization was measured at 20 h. Representative images of *Bac*Light stained coverslips, as well as the results of viability and attached cell count analyses are shown in Figure 3.10. Cells were observed to attach to all surfaces, and the overall viability of the attached bacteria was high (> 90%) in all cases, including the cells attached to the AgNP-coated and to uncoated regions of half-coated coverslips. A one-way ANOVA analysis showed no statistical difference for either viability ($P = 0.79$) or cell counts ($P = 0.25$) on the silver-free, uncoated or AgNP-coated surfaces.

Figure 3.10 also shows that colonization at 20 h did not produce a complete bacterial monolayer, even though the planktonic cell concentration was very high at the time of measurement (3.3×10^8 CFU/mL). Total growth in these cultures was dominated by planktonic growth, likely limiting the ability for adherent bacteria to grow into a mature biofilm. At 20 h, planktonic growth had reached stationary phase (Figure 3.5) indicating nutrient depletion in these cultures.
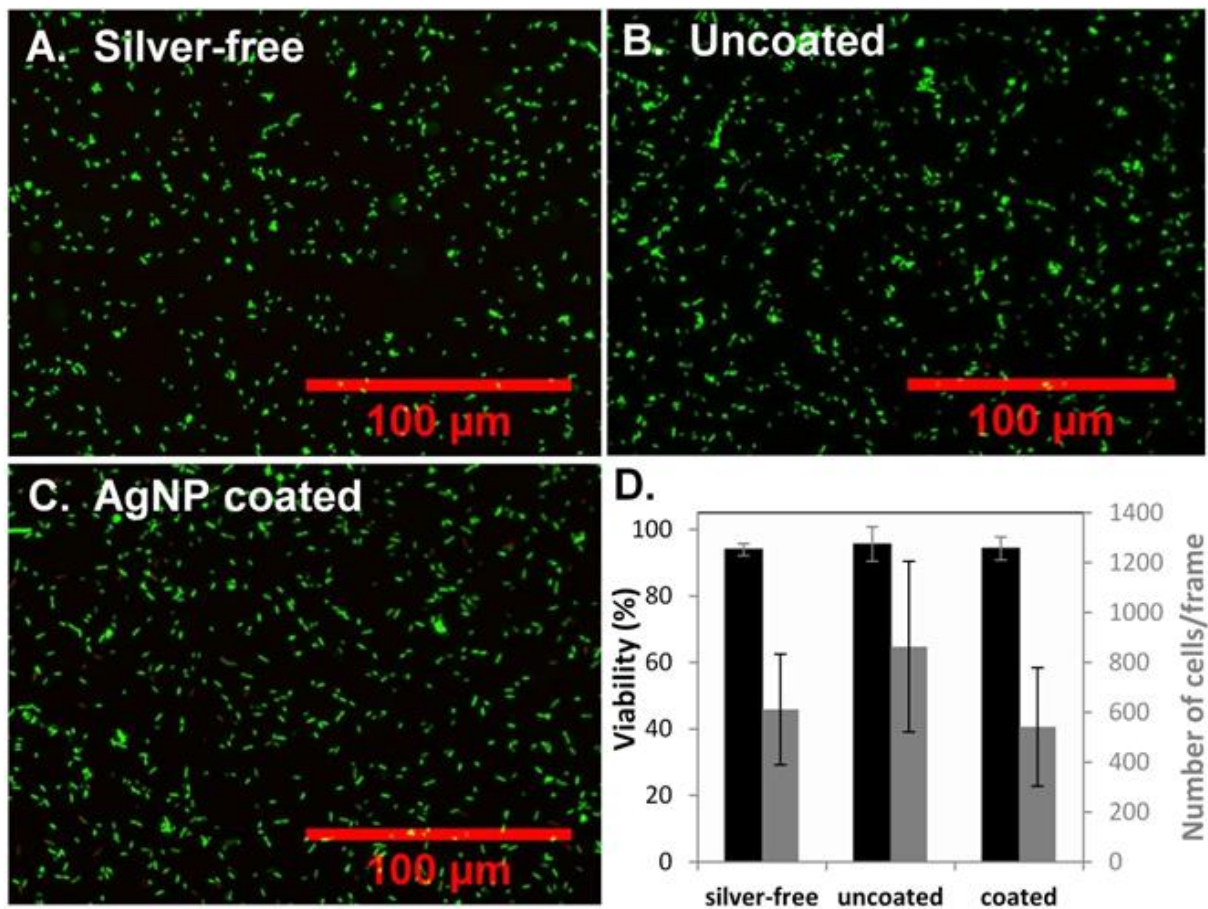
Figure 3.10. Representative images of *Bac*Light stained bacteria adhered to a silver-free control coverslip (A), the uncoated region of a coverslip half-coated with AgNPs (B), and the AgNP coated region of the half-coated coverslip (C) after 20 h incubation with the OD_{600}=0.01 (~1x10^7 CFU/mL) inoculum *P. fluorescens* culture. These are false color overlays of images collected with the AF488 (green) and AO (red) filter sets. The average viability (black bars) and cell count per image (frame size is 37300 μm^2) (grey bars) are plotted in (D). Error bars represent one standard deviation based on 4, 3, and 6 replicates for the silver-free, uncoated, and AgNP coated conditions, respectively. For each replicate experiment, at least five different, randomly selected images from each of the surface regions were analyzed.

To test whether the adherent bacterial layer could progress to a three-dimensional biofilm if the nutrient limitation were lifted, coverslips incubated for 20 h in the initial cell culture were gently rinsed in MDM to remove planktonic cells and transferred to fresh, cell-free MDM. After 24 h in the new media, this process was repeated and an additional 24 h of growth was allowed before imaging. A visible biofilm was observed by eye on both the silver-free control and the AgNP-coated coverslips. Microscopy confirmed that significant biofilm formation had occurred on all surfaces (Figure 3.11), indicating that a mature biofilm could form on the AgNP-coated coverslip if provided with sufficient nutrients.
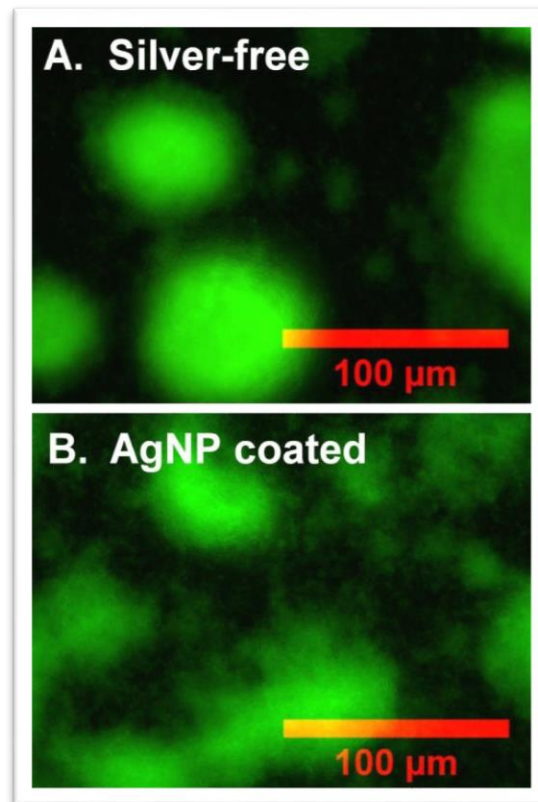
Figure 3.11. *Bac*Light stained bacterial biofilms adhered to a silver-free control coverslip (A) and an AgNP-coated coverslip (B) after a total of 68 h growth (from $OD_{600} = 0.01$ starting culture, transferred to new MDM after 20 h, second transfer after an additional 24 h). Large clusters indicate significant biofilm formation, even on the AgNP-coated surface.

Surface colonization from an $OD_{600} = 0.001$ inoculum was also measured. Recall that dissolved silver affected planktonic growth from the $OD_{600} = 0.001$ (~1×10^6 CFU/mL) inoculum to a much greater extent than the $OD_{600} = 0.01$ (~1×10^7 CFU/mL) inoculum. A similar effect of the bacterial inoculum concentration on bacterial surface colonization and subsequent biofilm formation on AgNP-coated surfaces might be expected. After 20 h incubation with the $OD_{600} = 0.001$ inoculum, significant differences were observed between the silver-free coverslips and the AgNP-coated and uncoated coverslip regions (Figures 3.12 and 3.13).
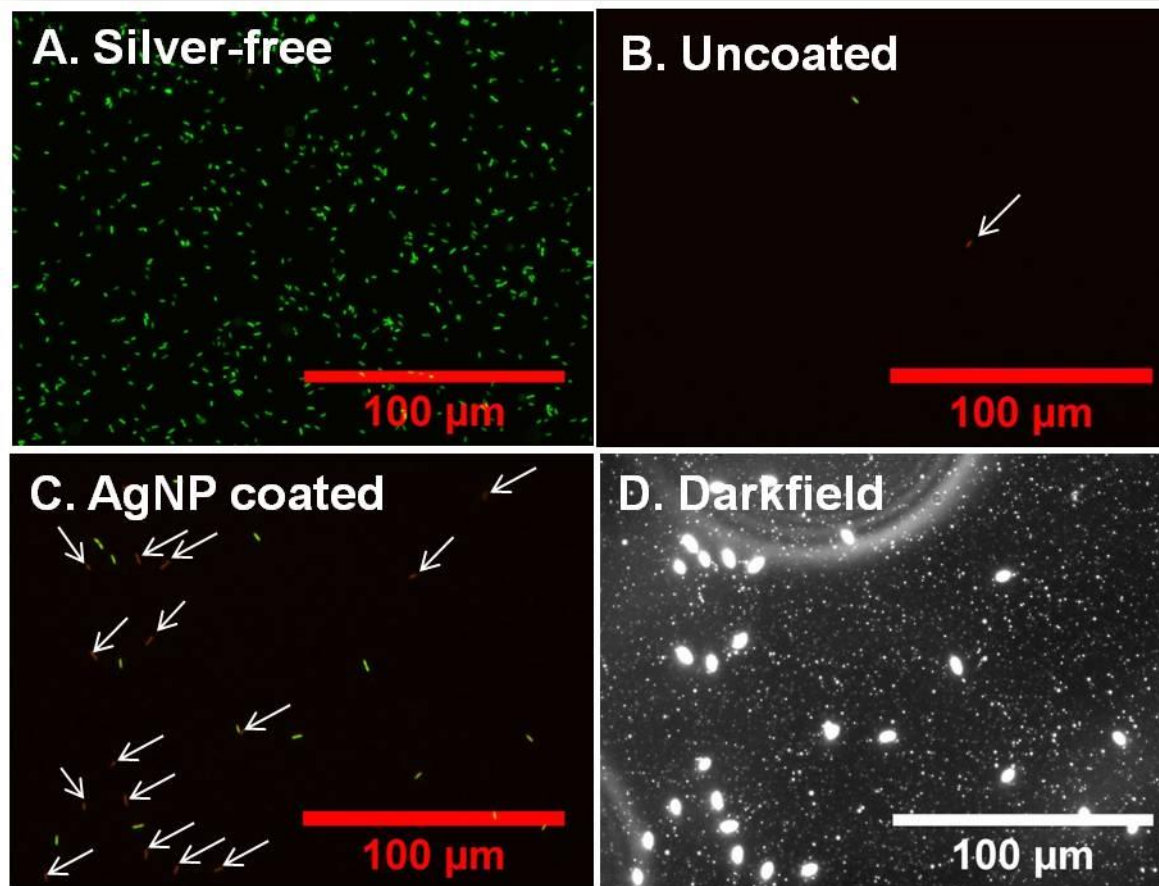
Figure 3.12. Representative images of *Bac*Light stained bacteria adhered to a silver-free control coverslip (A), the uncoated region of a coverslip half-coated with AgNPs (B), and the AgNP-coated region of the half-coated coverslip (C) after 20 h incubation with the $OD_{600} = 0.001$ (~$1x10^6$ CFU/mL) inoculum *P. fluorescens* culture. These are false color overlays of images collected with the AF488 (green) and AO (red) filter sets. "Viable" cells in these images appear as bright green, while "non-viable" cells appear as very faint red (marked with arrows). The same field of view from (C) was also imaged in darkfield (D) to show that AgNPs remain adhered to the coverslip. Large bright objects in (D) are cells, both viable and non-viable, while small dots show light scattered from adherent AgNPs. Every cell observed in (C) appears in (D).
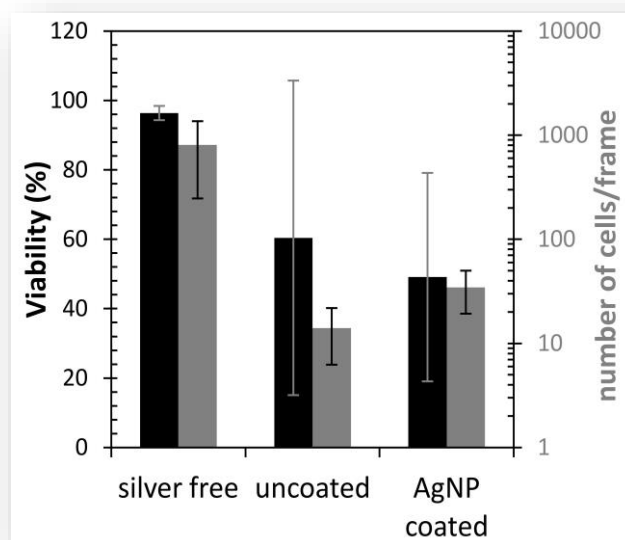
Figure 3.13. Average viability (black) and number of adherent cells per image (frame size is 37300 μm^2) (grey) on silver-free control coverslips and the uncoated and AgNP-coated regions of half-coated coverslips after 20 h incubation with the OD_{600}=0.001 (~1x10^6 CFU/mL) inoculum *P. fluorescens* culture. Error bars for the viability results represent standard deviations based on 5, 3, and 5 replicates in the silver-free, uncoated, and AgNP-coated cases, respectively. For the cell counts, there were 7, 9, and 11 replicates. For each replicate experiment, at least five different images from each of the different surface regions were analyzed.

The number of bacteria adhered to coated or uncoated regions of the AgNP half-coated coverslips after 20 h was significantly lower than the number adhered to the silver-free control coverslips in these OD600 = 0.001 experiments. This was consistent with the large difference in the planktonic populations present at this time in the presence or absence of silver (Figure 3.5). However, even though the planktonic population was exactly the same for the uncoated and AgNP-coated regions of each half-coated coverslip, the number of bacteria adhered in the AgNP-coated region was significantly greater than it was in the uncoated region (P=0.001). Greater adherent cell numbers on the AgNP-coated surface were observed by direct comparison of the coated and uncoated regions of the same coverslip in each replicate experiment. Darkfield

63

microscopy (Figure 3.12 D) confirmed that AgNPs remained adsorbed on the coated coverslips during the incubation with bacteria.

It was hypothesized that enhanced colonization of the AgNP-coated surface was due to a physical interaction between the adsorbed AgNPs and the bacteria. In other words, perhaps the presence of AgNPs simply increased the adhesion energy of bacteria behaving merely as colloidal particles, in a purely physical process without a biological basis. To test this, an OD_{600}=0.001 culture was killed by DNA-damaging ultraviolet radiation (G30T8 UV lamp, 30 W, 254 nm) before being exposed to the surfaces. At this wavelength, UV light causes DNA damage and bacterial inactivation, with minimal damage to other cellular components.[201] Therefore, it is expected that the bacterial surface chemical properties will not be altered significantly, except for the presence of membrane proteins whose expression is under active cellular control. Plate counts of UV-treated cultures confirmed at least 6 log killing of the bacteria in planktonic suspension before the start of these adhesion experiments.

The number of bacteria adhering to AgNP-coated surfaces from the UV-killed cultures (4±2 cells/frame) was very small compared to the number adhering from viable cultures with the same OD_{600} (65±38 cells). Even increasing the UV-killed culture OD_{600} to 0.01 did not result in the amount of adhesion observed in the viable cell case, giving only 19±6 cells/frame. In fact, at this higher concentration of killed cells, significantly more cells were adhered to the *uncoated* region than to the AgNP-coated region of the coverslips (P = 4.9×10^{-5}), the opposite of what was observed for the viable cultures.

A significant fraction of the adherent bacteria on the AgNP-coated surface were shown to be viable by *Bac*Light staining in the OD_{600} = 0.001 inoculum experiments, even though the surface was coated with biocidal AgNPs (Figure 3.13). In a study of bacterial growth on glasses

doped with silver ion, Valappil and colleagues[202] noted that a layer of dead bacteria could provide a protective layer that enables additional bacterial proliferation. The observation that a significant fraction of bacteria were observed to be viable with less than a full bacterial monolayer in the present study suggests that such a sacrificial layer is not a necessary condition for bacterial colonization on AgNP-coated surfaces. Biofilm formation on the AgNP-coated coverslips from the $OD_{600} = 0.001$ starting culture was also assessed at longer times (48, 72, and 96 h). Coverslips were kept in the same media for the entire time period; no media switch was performed. At these longer times, planktonic growth was evident (Figure 3.5). Figure 3.14 shows that significant biofilm formation did occur at these longer times on both uncoated and the AgNP-coated regions. By 96 h, significant formation of thick biofilms (observable by eye) with large cell clusters had occurred on the AgNP-coated coverslips for triplicate runs of the experiments, indicating the lack of any significant long-term anti-biofilm effect of the AgNP-coated surfaces at these inoculum concentrations.
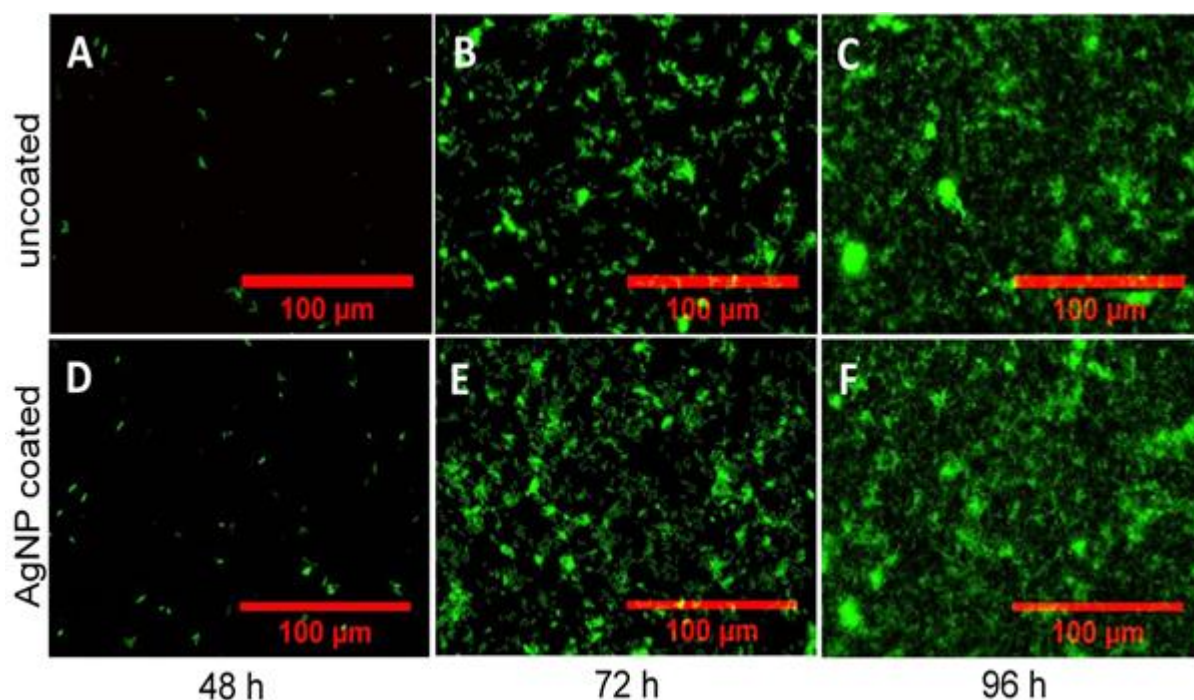
Figure 3.14. Representative images of *Bac*Light stained bacteria adhered to the uncoated (A,B,C) and AgNP-coated (D,E,F) regions of half-coated coverslips after 48 h (A,D), 72 h (B,E) and 96 h (C,F) of growth from $OD_{600} = 0.001$ (~1×10^6 CFU/mL) inoculum culture with no media switch. These images are false color overlays of the images collected with the AF488 (green) and AO (red) filter sets.

The amount of biofilm observed after 96 h on the uncoated and AgNP-coated regions of the half-coated coverslips was greater than was achieved for the silver-free control coverslips at any of the sampled time points up to 96 hours (Figure 3.15). This was the case for triplicate runs of the experiment. This suggests that *P. fluorescens* bacteria respond to the silver stress by forming biofilms, even though in the current situation the source of the stress is the silver ion released from the AgNPs that are adsorbed on the substrate. This supports the recent report that exposure to sublethal concentrations of suspended AgNPs stimulates biofilm development.[203] Since this high biofilm coverage is observed on both the uncoated and coated regions of the same coverslip, it must result from dissolved silver effects. This is consistent with the observations that growth in the bulk in the presence of silver occurred as macroscopic flocs rather than as

individually dispersed bacteria. Microbial flocs have many of the same characteristics as

biofilms[204] and planktonic growth as flocs was also induced by the silver stress.
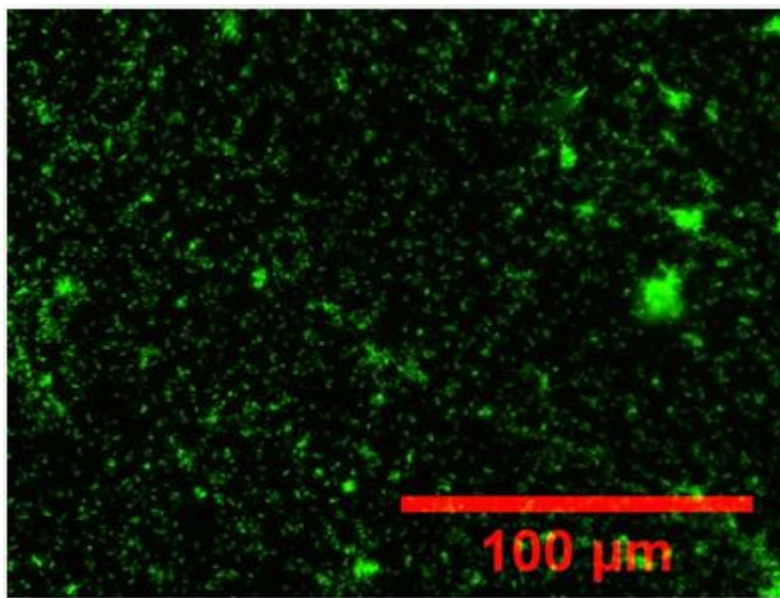
Figure 3.15. Image of a biofilm formed in silver-free control. This represents the maximum amount of colonization/biofilm that was formed in silver-free controls at any time. This particular biofilm was grown from an $OD_{600} = 0.001$ starting culture for 45 h. No silver-free controls in the absence of a media switch, from either starting cell concentration, up to 96 h total growth, showed greater biofilm formation than is observed here. Image is a false color overlay of the images collected with the AF488 (green) and AO (red) filter sets. The diminished biofilm formation compared to AgNP-coated surfaces is apparent.

3.4 Implications of the inoculum effect

The primary observation in this work is that an inoculum effect strongly influences how

surface-adherent silver nanoparticles affect bacterial surface colonization. The inoculum effect is

not considered generally when evaluating antimicrobial surfaces, yet this work shows that it can

be a significant factor in the effectiveness of antimicrobial surfaces that are based on release of

toxic silver ions. For example, the ASTM standard method E2180 – 07 for "determining the

activity of incorporated antimicrobial agents in polymeric or hydrophobic materials"

recommends testing a single inoculum concentration.[205] The method only considers cell killing at a single time point (24 hours is suggested) and does not account for the possibility of long-term recovery of the bacterial population as occurred in the current surface-adherent AgNP system.

Whereas inhibiting surface colonization is the technological goal of anti-fouling materials, in the context of the environmental implications of silver nanoparticles, the preservation of biofilm formation capability after nanoparticle entry into the environment is the desired situation. This work suggests that silver nanoparticle attachment on natural surfaces after release into the environment may not inhibit biofilm formation over the long term. In addition to the diminished bioavailability of silver bound to planktonic bacteria and/or macromolecular byproducts that was noted here, silver ion complexation to many common environmental ligands, such as humic acid, sulfide, and chloride, has been shown to reduce its toxicity.[99,206,207] Therefore, in environmental systems one must consider the possibility that the ionic silver released from adherent nanoparticles may not reach levels capable of causing 100% bacterial viability loss except in the presence of very low bacterial populations, and surface-adhered silver nanoparticles may be less likely to detrimentally affect environmental biofilm formation.

3.5 Experimental Section

3.5.1 Silver Partitioning

The partitioning between dissolved and bacterial biomass-associated Ag^+ was investigated independently. *P. fluorescens* in logarithmic growth was diluted with MDM and predetermined volumes of $AgNO_3$ solution to prepare cultures with $OD_{600} = 0.001, 0.01$ or

0.045. Total Ag^+ concentrations ranged from 0.25 to 50 ppb. Cultures were orbitally mixed for 1 hour at 160 rpm. Afterwards, a 3 mL aliquot was collected and held for silver analysis, while a separate 4 mL aliquot was centrifugally filtered as above. 3 mL of the filtrate was collected. Both the unfiltered sample and the filtrate were treated with 180 µL concentrated HNO_3 and 90 µL H_2O_2 (30%, Fisher Scientific), heated for 15 min at 100°C in a digital heat block (VWR International) and allowed to cool. Silver concentrations were then determined using ICP-MS.

3.5.2 Minimum inhibitory concentration (MIC) and minimum bactericidal concentration (MBC)

The MIC and MBC were determined for AgNPs and for ionic silver introduced as $AgNO_3$. *P. fluorescens* cultures in logarithmic growth were diluted with MDM and a predetermined volume of $AgNO_3$ solution or AgNP dispersion to yield samples with either $OD_{600} = 0.01$ or $OD_{600} = 0.001$, with varying silver concentrations, in black polystyrene clear-bottomed well-plates (Corning Costar). Two-fold serial dilutions ranged from 0.98 to 500 ppb for Ag^+ or 9.8 to 5000 ppb for AgNP for $OD_{600} = 0.01$ cultures and from 0.098 to 50 ppb for Ag^+ or 0.98 to 500 ppb for AgNP for $OD_{600} = 0.001$ cultures. All concentrations are ppb of Ag. One well-plate column was used for bacteria-free silver controls and another for silver-free bacteria controls. The OD_{600} was recorded for each well immediately after filling and again after 24 h, and the MIC was identified as the smallest Ag^+ or AgNP concentration that yielded no increase in OD_{600}. To determine the MBC, 100 µL samples taken from wells from the MIC experiments for all concentrations at and above the MIC were spread on nutrient agar. The MBC was identified as the lowest silver concentration that yielded no colonies after 24 hour growth on agar.

3.5.3 Contact angle measurement

AgNP-coated and uncoated coverslips were incubated in 25 mL sterilized MDM for 20 hours with 160 rpm orbital mixing, rinsed with purified water and gently dried under a purified nitrogen stream. A Ramè-Hart contact angle imaging system was used to measure the advancing and receding contact angles for a drop of purified water deposited on each surface.

3.6 Results and Discussion

3.6.1 MIC and MBC for silver ions and silver nanoparticles

In section 3.3.1 it was observed that the higher initial inoculum concentration of OD_{600} = 0.01 was unaffected by the AgNP-coated coverslip and easily colonized the surface while the lower inoculum concentration of OD_{600} = 0.001 had a significantly delayed growth and required much longer times (>48 h) to recover and colonize the AgNP-coated surface. These differences in performance by the two inoculum concentrations in the presence of the AgNP-coated coverslips with similar surface concentrations of AgNPs, suggest that an inoculum effect is present. To further explore the inoculum effect of silver on *P. fluorescens*, both the MIC and MBC were determined. Both the MIC and MBC were significantly higher for dispersed AgNPs than for Ag^+ (as $AgNO_3$). For OD_{600} = 0.001 cultures, the Ag^+ and AgNP MIC were 4.2 ± 3.7 ppb (n = 15) and 23 ± 14 ppb (n = 12) (P = 3×10^{-5}), respectively, while the Ag^+ and AgNP MBC were 4.9 ± 3.1 ppb (n = 11) and 31 ± 0 ppb (n = 7) (P = 2×10^{-11}), respectively. When the cell concentration was increased to OD_{600} = 0.01, the Ag^+ and AgNP MIC increased to 20 ± 14 ppb (n = 23) and 140 ± 100 ppb (n = 16) (P = 6×10^{-8}), respectively. The Ag^+ and AgNP MBC increased to 32 ± 21 ppb (n = 12) and 156 ± 0 ppb (n = 7) (P = 2×10^{-13}), respectively. Values are

reported as mean $\pm$ standard deviation. A zero reported standard deviation simply indicates that each MBC determination corresponded to the same serial dilution. The observed dependence of the MIC and MBC on the *P. fluorescens* concentration, for both silver forms, indicates an inoculum effect for silver toxicity.

These increased MIC and MBCs suggest that dissolved silver is becoming bound to bacteria or macromolecular products which reduces the amount of bioavailable silver. This is corroborated in Figure 3.9 where the free silver concentrations are at detectable levels when the $OD_{600} = 0.001$ while they are below detection limits when the initial inoculum concentration is $OD_{600} = 0.01$. By effectively decreasing the free silver concentration that is bioavailable to interact with other cells, this decreases its antimicrobial effect. Similar decreases in toxicity have been observed when Ag^+ is bound to humic acid in solution.[99] If suspension phase binding of silver to viable or nonviable cells and/or cell products is sufficient to keep the free silver concentration low, then planktonic bacteria populations are able to recover and overwhelm dissolved silver's antimicrobial effect.

Note that silver complexation to biomass in the $OD_{600} = 0.001$ culture suppressed the free silver concentration to levels that never exceeded 2 ppb in Figure 3.9. This falls just below the ~4 ppb MIC for Ag^+. Thus, planktonic growth in the $OD_{600} = 0.001$ inoculum culture is initially slow, but the culture retains viability, as is evident in the OD_{600} increase in Figure 3.9 at 72 h. Between 45 and 72 h, the planktonic population increased significantly, reaching $OD_{600} = 0.045$. This increase in biomass was accompanied by the free silver decreasing to barely detectable levels (Figure 3.9).

This is corroborated by Figure 3.16, which shows the degree to which silver ion added as $AgNO_3$ binds to planktonic *P. fluorescens*, and/or its products in suspension, at cell

concentrations spanning the range of the surface colonization experiments. The extent of binding is significant and strongly dependent on cell concentration. Figure 3.16 indicates that cells and/or byproducts in an $OD_{600} = 0.045$ bacterial suspension bind 88% of the silver at total silver concentrations as high as 42 ppb. Thus, the $OD_{600} = 0.045$ culture, corresponding to the 72 h population that grew from the $OD_{600} = 0.001$ inoculum (Figure 3.9), could maintain the free silver concentration at only a few ppb for total silver ion concentrations as large as ~ 42 ppb. The black bars in Figure 3.16, corresponding to cell-free control experiments where all silver is free, indicated that the total silver concentration released from the adherent AgNPs over 72 h never exceeded 15 ppb. This is less than the 20 ppb MIC for a planktonic culture with $OD_{600} = 0.01$ (that is, a more dilute culture than the $OD_{600} = 0.045$ culture that existed at 72 h). In experiments with the $OD_{600} = 0.01$ inoculum, no free silver was detected in the media bathing the AgNP half-coated coverslips at any time. This is consistent with the equilibrium Ag^+ binding data in Figure 3.12. For the total silver concentrations of ~ 4 to 6 ppb that Figure 3.5 indicates were released from AgNP-coated coverslips over 1 to 45 h, Figure 3.16 shows that nearly all of the released silver would be in the bound form for $OD_{600} = 0.01$ cultures, even without further planktonic growth.

It is evident that silver binding allows the planktonic population to grow in these experiments. The inoculum effect that is manifested as a strong dependence of MIC and MBC on cell concentration is apparent in the propagation of planktonic cultures in suspension above AgNP-coated coverslips.
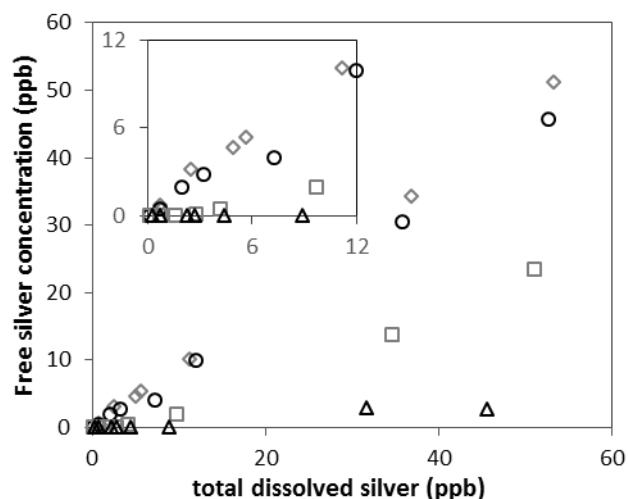
Figure 3.16. Free silver concentrations for AgNO$_3$ added to planktonic P. fluorescens cultures in MDM, as measured by ICP-MS after filtration with a 3 kDa cutoff. Cell-free controls (open diamonds) showed minimal decreases in free silver after filtration while OD$_{600}$ =0.001(open circles), OD$_{600}$ =0.01(open squares) and OD$_{600}$ =0.045 (open triangles) bacterial cultures decreased the free silver concentration to different degrees. The inset highlights low concentration data.

3.6.2 Preferential adsorption to AgNP-coated surface

In section 3.3.3, it was observed that in some situations *P. fluorescens* preferentially adhered to the AgNP-coated surfaces. Collectively, these results indicate that there is an as yet unknown biological reason for the increased adhesion of cells on the AgNP coated surfaces. Additionally, the low numbers of adhering killed cells suggests that the nonviable cells observed on the AgNP-coated surfaces became nonviable after they initially adhered as viable cells. Viability appears to be a necessary condition for the preferential bacterial adhesion to the AgNP-coated surface. It is unclear at this point whether the increased colonization of the AgNP-coated region is caused by some biological recognition of the AgNPs on the surface or whether it may be related to changes in substrate surface properties or roughness that promote the ability of

73

active bacteria to establish an anchorage and colonize the surface. Surface topography has previously been shown to influence bacterial adhesion.[208–210] Although adhered AgNPs did not render the coverslips hydrophobic, they did become slightly less hydrophilic. Clean coverslips incubated in MDM were perfectly wetted by water, while the advancing and receding contact angles of water on AgNP-coated coverslips were 10.7±1° and 6.9±0.9°, respectively, suggesting that surface physico-chemical processes probably are not responsible for preferential attachment to AgNP-coated surface regions. Further investigation into the cause of the preferential adhesion of viable bacteria on AgNP-coated surfaces remains a subject of interest.

3.7 Conclusions

Data obtained on the planktonic population response to silver ion and silver nanoparticle exposure and colonization on silver nanoparticle-laden surfaces confirmed the hypothesis that the inhibition of bacterial surface colonization would exhibit an inoculum effect. Evidence was presented that *P. fluorescens* colonization on surfaces decorated with adsorbed silver nanoparticles is a silver ion stress response, and the inoculum effect was evident in the observation that prevention of surface colonization occurs only when 100% of the planktonic bacterial population is killed. This occurs with a sufficiently low initial inoculum concentration. With higher inoculum concentrations, a small remnant fraction of viable bacteria is sufficient to allow population recovery and surface colonization, proceeding to biofilm formation at long times. The inoculum effect was attributed to silver ion binding to bacteria and/or their macromolecular byproducts and the resulting decrease in free, bioavailable silver ion in solution. Accordingly, the minimal inhibitory concentration and minimal bactericidal concentration, with

respect to silver nanoparticles as well as silver ion administered as $AgNO_3$, both increase with increasing concentration of the planktonic bacterial inoculum.

The "anti-fouling" or colonization inhibitory properties of the AgNP-coated glass surfaces used in this work were controlled by the dissolved silver released from the surface-adhered particles and not by direct bacterial contact with the silver nanoparticles on the surface. A similar absence of contact-mediated bacterial killing was observed by de Prijck and colleagues in their work with silver-ion releasing rubber.[211] When colonization occurred, viable bacteria were observed directly on silver nanoparticle-laden surfaces, without the need for any passivating layer of nonviable bacteria that might have shielded newly arriving bacteria from silver.

The current work of course pertains strictly to *P. fluorescens* and immobilized silver nanoparticles. No claim is made about any particular inoculum concentration that should be considered a threshold, above which a sufficient fraction of a bacterial population may survive a silver ion exposure and colonize a silver-laden surface, either for different species or different silver surface presentation formats. It may be anticipated, for example, that the presentation of larger amounts of silver would require higher inoculum concentrations for a population to survive the initial killing and recover. Other species may differ quantitatively, but the possibility of an inoculum effect should be considered when evaluating a toxin-releasing antimicrobial surface. Future work should address the prominence of the inoculum effect in the context of surface colonization on silver nanoparticle-laden surfaces or other toxin-releasing surfaces. This should include quantitative comparisons of threshold inoculum concentrations, with a broad variety of bacterial species, including pathogenic ones.
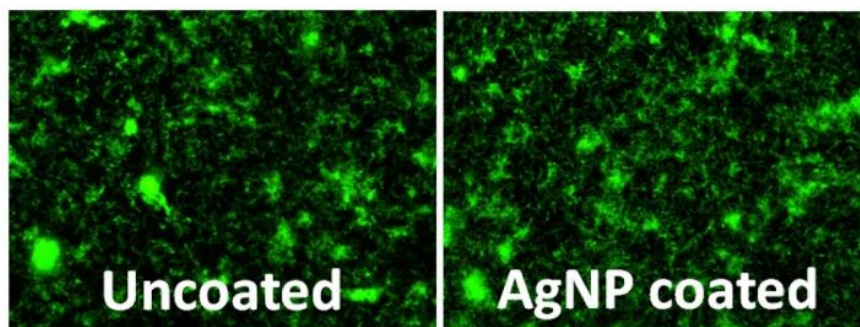
Figure 3.17. *P. fluorescens* colonization on both uncoated and AgNP-coated surfaces. In some cases there was preferable bacterial colonization on the AgNP-coated surface over the uncoated surfaces.

Chapter 4. Silver Sink Effect of Humic Acid on Bacterial Colonization

Reprinted with permission from A. J. Bertuccio and R.D. Tilton. Silver Sink Effect of Humic Acid on Bacterial Surface Colonization in the Presence of Silver Ions and Nanoparticles. *Environmental Science and Technology*, 2017, 51 (3), 1754-1763.[126] All Quartz Crystal Microbalance-Dissipation in this work was performed with the help of Dr. John Riley.

4.1 Introduction

Chapter 3 showed that bacterial colonization on AgNP-decorated surfaces is highly dependent on the initial planktonic concentration. It was hypothesized that at high bacterial concentrations, bacteria serve as a silver sink and reduce the amount of bioavailable silver below toxic levels allowing high concentrations to colonize AgNP-decorated surfaces. Thus, a AgNP-decorated surface may be able to inhibit low concentrations of bacteria from colonization but not high inoculum concentrations. However, in the environment there are a large number of organic materials, such as NOM, that have the potential to bind metals such as silver and one could expect that the efficacy of AgNP-decorated surfaces are much lower when exposed to environmental media.

The objective of the current research is to elucidate the combined effects of initial bacterial inoculum concentration and the presence of NOM on the ability of planktonic bacteria to colonize a surface that displays adherent AgNPs. The governing hypothesis is that NOM, as exemplified by humic acid (HA) in this investigation, will increase bacterial tolerance of AgNP and Ag^+ by functioning as an Ag^+- binding sink that decreases the free silver concentration and thus the amount of bacteria-bound Ag^+, and thereby allows bacteria to proliferate and colonize

AgNP-laden surfaces at lower inoculum concentrations than would be possible in the absence of NOM. We consider a Gram- negative model biofilm-forming species, *P. fluorescens*, suspended in minimal media over glass surfaces decorated with polyvinylpyrrolidone (PVP)-stabilized AgNPs that have been used in previous model system studies. Gram negative bacteria are more vulnerable to AgNP and Ag^+ than Gram positive bacteria which have thicker cell walls that reduce the likelihood of silver uptake.[194–197] Typical aqueous NOM concentrations in the environment range from 2 to 10 mg C/L in rivers and lakes and up to 60 mg C/L in bogs, marshes and swamps.[175] We consider the higher end of the natural HA concentration range to capture the magnitude of NOM effects that may be expected in high organic carbon ecosystems. We will show that HA increases the minimum inhibitory concentration (MIC) and minimum bactericidal concentration (MBC) of silver in both AgNP and Ag^+ form and allows bacteria to colonize the AgNP-laden surface at lower bacterial inoculum concentrations than would otherwise be possible. This study also reveals that the overall effect of HA on surface colonization is complex and involves several competing tendencies. We find that HA exerts two counteracting effects that impact bacterial survival: by competitively binding Ag^+, HA decreases the amount of Ag^+ bound to bacteria for a given total silver concentration, which favors survival, but HA also sensitizes *P. fluorescens* to bound Ag^+ such that growth inhibition and loss of viability both occur at lower extents of Ag^+ binding to bacteria when in the presence of HA than in its absence. The net outcome of these competing effects favors *P. fluorescens* survival, which allows them to withstand silver exposure and proceed to colonize AgNP-laden glass surfaces. That is colonization also occurs despite the observed tendency of HA to otherwise decrease the amount of *P. fluorescens* colonization of glass surfaces, an effect observed here in the absence of silver.

4.2 Experimental

4.2.1 Silver nanoparticle deposition on glass coverslips.

The AgNPs used in this study were described previously.[155] They are stabilized by PVP (MW 55,000) and have a diameter of 9.3 ± 2 nm based on TEM. Their zeta potential (Malvern Zetasizer Nano ZS) in minimal Davis media (MDM) (50 mM ionic strength) was -2.35 ± 4 mV. The hydrodynamic diameter of the AgNPs in minimal Davis media (MDM, see below) was determined by dynamic light scattering (Malvern Zetasizer Nano ZS) to be 10.2 ± 3 nm (Figure 2.1).

4.2.2 AgNP-Decorated Coverslips

To deposit AgNPs onto coverslips, the AgNP stock suspension was diluted with MDM to a final concentration of 10 ppm. 5 mL aliquots were added to 50 mL polypropylene centrifuge tubes (Beckman Coulter). One clean, UV-sterilized slide was placed with flame sterilized forceps into each tube and incubated to allow particles to adhere in the dark for 1 h at $23 \pm 2°C$. Afterwards coverslips were rinsed aseptically with 300 mL of sterilized ultrapure water and immediately added to new sterile 50 mL centrifuge tubes containing 15 mL of MDM to begin a colonization experiment. AgNP-decorated coverslips were analyzed with a Zeiss Axio Observer Z1 microscope and a 20 X LD plan-NEOFLUAR objective (Zeiss) using darkfield microscopy and following the protocol described by Wirth and coworkers.[116] Figure 2.4 shows representative images of a three separate AgNP-decorated coverslips.

4.2.3 Bacterial surface colonization.

A 25 mL volume of bacterial suspension with an initial bacterial inoculum of $OD_{600} = 0.0001$ (~1×10^5 CFU/mL), 0.001 (~1×10^6 CFU/mL), or 0.01 (~1×10^7 CFU/mL) was exposed to a vertically oriented, pristine or AgNP-decorated coverslip in MDM with 0, 20 or 60 mg C/L HA

in 50 mL centrifuge tubes and orbitally shaken at 160 rpm at room temperature for 72 h with loose caps to maintain aerobic conditions.

Bacteria exposed to Ag^+ were exposed to a pristine coverslip. A 25 mL suspension sample with initial inoculum of $OD_{600} = 0.0001$ or $OD_{600} = 0.001$ was exposed to 5 ppb Ag^+ in the form of $AgNO_3$ in MDM with 0, 20 or 60 mg C/L HA in 50 mL centrifuge tubes and orbitally shaken at 160 rpm and 72 h with loose caps to maintain aerobic conditions.

4.2.4 Minimum inhibitory concentration (MIC) and minimum bactericidal concentration (MBC)

P. fluorescens in early log-growth was diluted with MDM containing suspended AgNPs or dissolved $AgNO_3$ in MDM to obtain $OD_{600} = 0.01$, 0.001, or 0.0001 in volumes of 200 µL in black polystyrene clear-bottomed well plates (Corning Costar) with and without HA. OD_{600} was measured initially after filling and again after 24 h. The silver species gave negligible contributions to the optical density. Two-fold serial dilutions ranged from 9.8 to 5000 ppb of AgNP or 0.98 to 500 ppb of Ag^+ for $OD_{600} = 0.01$ and 0.98 to 500 ppb of AgNP or 0.098 to 50 ppb of Ag^+ for $OD_{600} = 0.001$ and $OD_{600} = 0.0001$ inocula. One column of the well plate was left as a silver control with no bacteria and one column as a bacteria control with no silver. The MIC was determined as the lowest concentration yielding no change in OD_{600} over 24 h.

4.2.5 Ag^+ binding to bacteria and HA

Bacteria binding: 25 mL samples in 50 mL centrifuge tubes were prepared to contain $AgNO_3$ at concentrations ranging from 1 to 55 ppb Ag^+ and *P. fluorescens* at $OD_{600} = 0.001$ to 0.045 and equilibrated for 1 h under orbital mixing in the dark at 160 rpm. A 4 mL aliquot was

sampled from each to assay total silver and free silver in each system. To assay total silver, 3 mL of the unfiltered aliquots were analyzed. A 3 kDa molecular weight cutoff cellulose acetate centrifugal filter (Amicon) was used to remove bacteria and bacteria-bound Ag^+. These filters were centrifuged at 4000 rpm (Eppendorf centrifuge 5810 R) for 50 minutes to remove bacteria and bacteria-bound Ag^+. Silver detected in the filtrate is considered free silver. To assay silver concentrations in either the unfiltered sample (total silver) or in the filtrate (free silver), 240 µL HNO_3 (BDH chemicals, Aristar Plus) and 120 µL H_2O_2 (Fisher Scientific) were added to the appropriate samples. The samples were then heated for 15 minutes at 100°C in a digital heat block (VWR International) and allowed to cool. Silver was assayed using inductively coupled plasma-mass spectrometry (ICP-MS, Agilent 7700x). The ICP-MS was calibrated against $AgNO_3$ standards immediately before each experiment.

Humic acid binding: The same procedure was also performed to measure Ag^+ binding to HA at HA concentrations of 1, 5, 10, 20 and 60 mg C/L HA, using the 3 kDa centrifugal filter to remove HA and its bound Ag^+.[99,116] A control experiment without bacteria or HA was conducted to check for Ag^+ losses due to binding to the filter or container surfaces.

Centrifugal filters were washed three times with DI H_2O. The organic carbon contributed after three rinsings was 1.1 mg C/L. Triple washed filters were used to filter 56.6 ± 2.9 mg C/L HA to determine the amount of HA that passes through the filter. Only 1.4 ± 0.1 mg C/L HA was measured in the filtrate. Thus centrifugal filtration removed 97.5% of the HA.

4.2.6 Humic acid adsorption to silica via quartz crystal microbalance-dissipation (QCM-D)

Quartz crystal microbalance with dissipation (QCM-D) measurements were performed on a four-chamber Q-sense E4 instrument (Biolin Scientific). Q-sense SiO_2 coated sensors (QSX

303 or QSX 335) were exposed to MDM, then MDM + humic acid, and then MDM. The frequency shifts are small and positive and dissipation shifts are small and negative when the media changes from MDM to MDM + humic acid but rapidly return to their baseline values when the media switches back to MDM. Adsorption would produce negative frequency shifts and positive dissipation shifts.[212] The results confirm that humic acid does not adsorb to silica under these conditions. The small observed shifts are due to changes in viscosity and density of the bulk liquid.

4.3. Results and Discussion

4.3.1 AgNP-decorated surfaces

AgNP adhesion was measured on six coverslips; two sets of three coverslips were prepared from independent AgNP dispersions, with representative images in Figure 2.4. The average deposition density was $(3.5 \pm 0.8) \times 10^5$ particles/mm^2. Clean coverslips were also analyzed and averaged 500 ± 150 "spots"/mm^2 indicating that any extraneous scattering contributions from dust or surface defects were insignificant. Wirth and coworkers showed that AgNP detachment is not significant during subsequent colonization experiments.[116]

4.3.2 Effect of initial inoculum and presence of humic acid on bacterial colonization

Bacterial colonization on glass coverslips with or without adherent AgNPs, in MDM or MDM augmented with 60 mg C/L HA, after 72 hours of orbital shaking, is shown in Figure 4.1. In the absence of HA (Figure 4.1 D) colonization was significant for each initial inoculum concentration on pristine AgNP-free coverslips and exceeded monolayer coverage, where the

82

maximum countable amount of bacteria would be ~26,800 cells/mm^2 for this microscope. When

adherent AgNPs were present, colonization was greatly reduced to sub-monolayer coverages, by

a factor of at least 360, except for the most concentrated initial inoculum, ~10^7 CFU/mL, which

showed similarly extensive colonization as on the pristine coverslips.
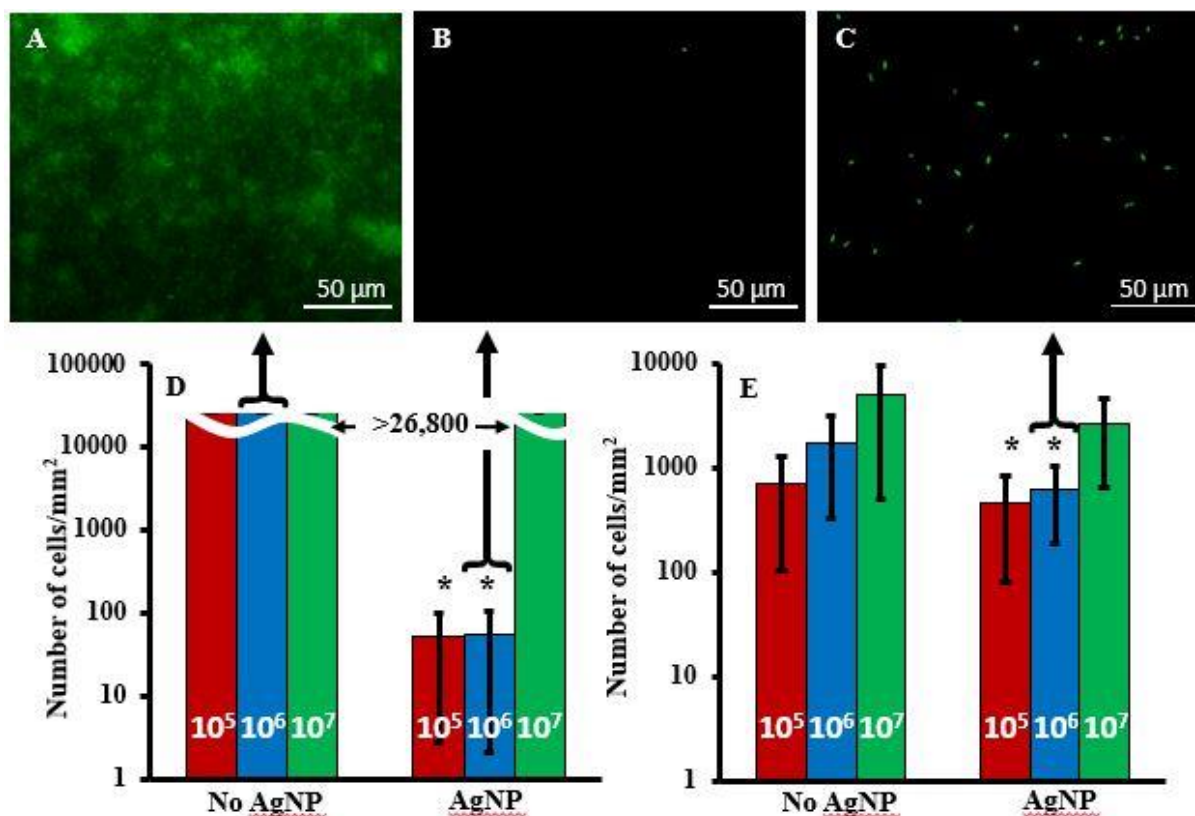
Figure 4.1. Representative images with a false color overlay for *P. fluorescens* colonization on AgNP-decorated coverslips at > 26,800 (A), 60 (B) and 700 cells/mm^2 (C). Bacterial colonization over 72 h on coverslips without and with adherent AgNPs in HA-free MDM (D) or in MDM with 60 mg C/L HA (E). Red, blue and green bars correspond to initial inoculum concentrations of 10^5, 10^6, and 10^7 CFU/mL respectively. Initial inoculum concentrations below a certain amount resulted in statistically significant reductions in colonization on AgNP-decorated coverslips compared to pristine ones (comparing 10^5 and 10^6 CFU/mL with AgNP in D against similar inocula with no AgNP in D, $p < 0.001$). *P. fluorescens* showed a statistically significant increase in colonization in MDM with HA on AgNP-decorated surfaces compared to HA-free MDM (comparing 10^5 and 10^6 CFU/mL with AgNP in E against the same inocula with AgNP in D, $p < 0.001$). Data points represent at least three replicate coverslips and 10 random locations measured per coverslip.

During these colonization experiments OD_{600} was monitored to identify changes in planktonic bacterial concentration. In the absence of HA, the optical density did not change over 72 h in the presence of adherent AgNPs, *i.e.* there was no growth, for 10^5 or 10^6 CFU/mL initial inocula, but OD_{600} increased 14-fold, from 0.010 ± 0.001 to 0.14 ± 0.1, for 10^7 CFU/mL. This strong inoculum concentration dependence in both planktonic growth and colonization of the AgNP-decorated surface corroborates the prior observation of an inoculum effect whereby silver toxicity is highly dependent on initial planktonic bacterial concentrations.[116] High initial planktonic bacterial concentrations provide an excess of silver binding sites that decrease the amount of free silver in solution. By distributing the silver among a large number of binding sites among the bacterial population, most bacteria take up a sublethal amount of silver which allows the majority of the population to survive, proliferate and colonize the AgNP-decorated surface.

Adherent cell viability on the AgNP-decorated coverslips in MDM and MDM augmented with HA was also measured. In MDM, the average percentages of viable cells on coverslips were $84 \pm 16\%$ ($n_{total} = 55$ cells distributed over 30 fields of view) and $61 \pm 22\%$ ($n_{total} = 57$ over 30 fields of view) for initial inocula of 10^5 and 10^6 CFU/mL respectively. A thick biofilm was observed with an initial inoculum of 10^7 CFU/mL and no dead cells were observed by LIVE/DEAD staining with epifluorescence microscopy. When MDM was augmented with 60 mg C/L HA, viability was $99 \pm 2\%$ ($n_{total} = 501$ over 30 fields of view), $94 \pm 2\%$ ($n_{total} = 1414$ over 30 fields of view), and $91 \pm 6\%$ ($n_{total} = 2774$ over 30 fields of view) for 10^5, 10^6, 10^7 CFU/mL respectively. Viability from the low initial inoculum concentrations of 10^5 and 10^6 CFU/mL was greater in the presence of HA.

Comparing data for colonization of the AgNP-decorated surface in the presence of 60 mg C/L HA (Figure 4.1 E) with the similar data in its absence (Figure 4.1 D) indicates that HA

allowed significantly greater surface colonization on AgNP-decorated surfaces for the 10^5 and 10^6 CFU/mL inocula. Colonization increased by factors of 7.7 ($p < 0.001$) and 9.4 ($p < 0.001$) relative to the HA-free experiments for 10^5 and 10^6 CFU/mL inocula, respectively (based on the statistical sign test[213]). This supports the hypothesis that HA provides a protective effect that enables low concentrations of *P. fluorescens* to colonize AgNP-decorated surfaces to a significantly greater extent. This protective effect on the bacterial surface colonization phase is consistent with prior evidence that HA can increase bacterial tolerance to silver ions and nanoparticles for bacteria in either the planktonic or the biofilm state.[96,99,117,118]

Colonization on the AgNP-decorated surface by the 10^7 CFU/mL inoculum was decreased in the presence of HA compared to its absence. This is not due to a failure of HA to provide a protective silver sink. Comparing colonization on AgNP-free surfaces with (Figure 4.1 E) and without (Figure 4.1 D) HA indicates that HA has an overall effect of significantly decreasing colonization, by 37-, 15- and 4-fold for initial inocula of 10^5, 10^6, and 10^7 CFU/mL respectively. Even though bacteria have a decreased overall tendency to colonize coverslips in media containing HA, the lower inoculum concentration data show that there is a greater extent of colonization on AgNP-decorated coverslips in media with HA than in media without HA.

The greater colonization of AgNP-decorated surfaces in the presence of HA, despite the otherwise unfavorable effect of HA on colonization, is attributable to the preservation of planktonic growth in the presence of HA. The optical density of the planktonic suspension bathing the AgNP-decorated coverslips in the presence of 60 mg C/L HA increased by 286% from 0.294 ± 0.001 to 1.135 ± 0.009, by 272% from 0.295 ± 0.003 to 1.1 ± 0.04, and by 253% from 0.271 ± 0.002 to 0.96 ± 0.090 over 72 h for 10^5, 10^6 and 10^7 CFU/mL inocula respectively.

For each inoculum planktonic growth was far more extensive in the presence of HA than in its absence; in fact, HA allowed growth and colonization on AgNP-decorated surfaces in the two most dilute inocula that exhibited no growth and minimal colonization in its absence.

The decreased bacterial colonization on AgNP-free surfaces in the presence of HA is considerable. We considered the hypothesis that HA inhibits *P. fluorescens* colonization of silica glass surfaces by adsorbing to the surface and creating an electrosteric barrier to bacterial adhesion, but prior literature indicates that HA does not adsorb to silica.[214] We verified that Pahokee peat HA does not adsorb to silica via a quartz crystal microbalance with dissipation (QSense E4) experiment (Figure 4.2).
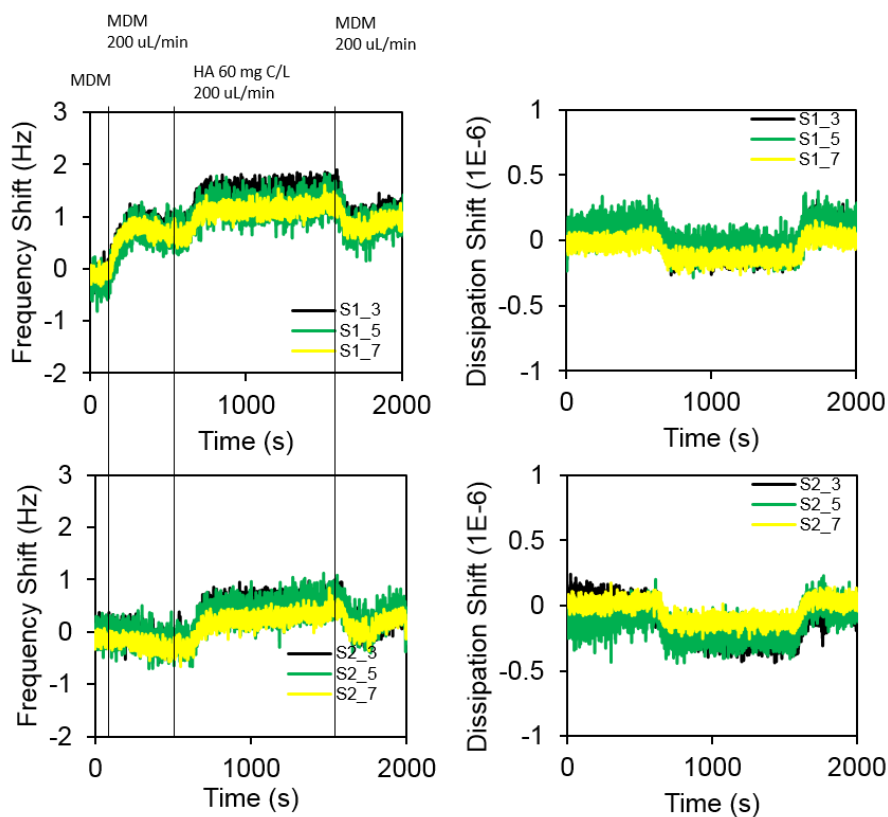
Figure 4.2. QCM-D graphs for two separate experiments where the left represents frequency shifts while the ones on the right represent dissipation shifts for the third, fifth and seventh overtones. The compositions of the liquid in the sample cell during different time intervals marked by vertical lines are indicated.

The decreased colonization may be a result of HA making the bulk solution environment more favorable for *P. fluorescens*. Figure 4.3 shows that *P. fluorescens* growing in MDM has a greater growth rate in the presence of HA than in its absence. The growth rate constants were 0.101 ± 0.001 h^{-1} in the absence of HA and 0.21 ± 0.06 h^{-1} in the presence of 60 mg C/L HA. The faster growth in media with HA may suggest that *P. fluorescens* are able to metabolize HA as a carbon source, but independent growth experiments conducted with *P. fluorescens* in MDM containing no carbon source other than HA exhibited no growth. *P. fluorescens* cannot metabolize HA alone. It was also determined that HA did not significantly affect media pH, ruling out a buffering effect on growth. The origins of the growth rate increase have yet to be established, but it is clear that HA makes the planktonic phase more suitable for *P. fluorescens* growth, which could decrease a biological driving force for bacteria to select the surface environment. There also may be a colloidal basis for the lessened colonization in the presence of HA. The electrophoretic mobility of *P. fluorescens* in 10-fold diluted MDM was -1.1 ± 0.25 µmcm/Vs in the absence of HA, but increased in magnitude significantly ($p = 0.016$, using the rank-sum test[213]) to -1.48 ± 0.08 µmcm/Vs with the addition of 60 mg C/L HA. The increased negative electrophoretic mobility is consistent with HA adsorption to bacteria, which would increase their negative surface charge and could inhibit deposition on negatively charged silica surfaces.
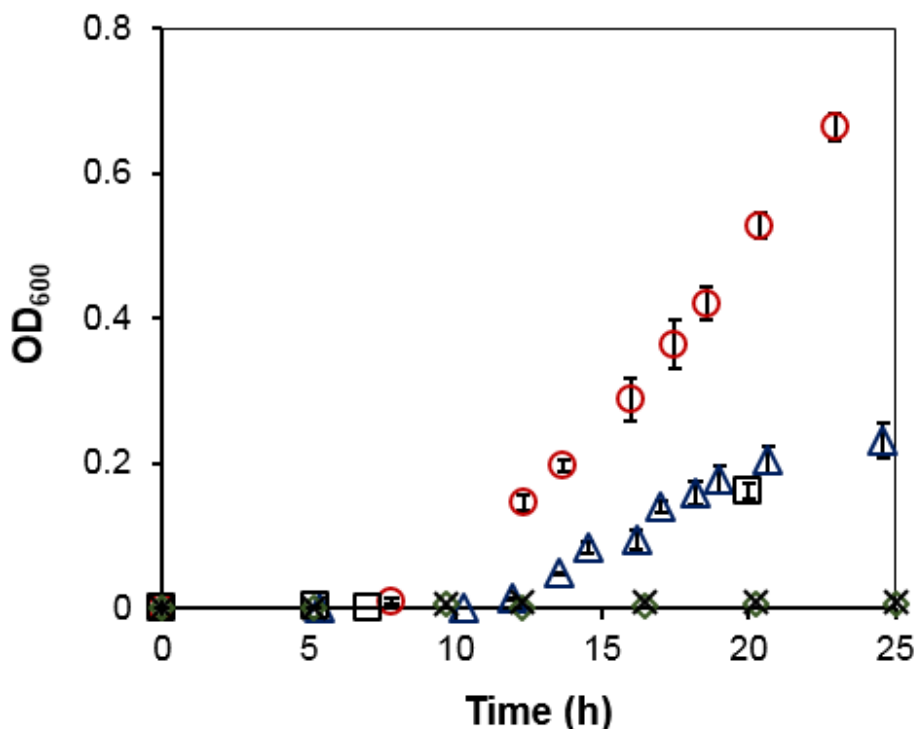
Figure 4.3. Representative growth curves for *P. fluorescens* when subcultured to an OD_{600} = 0.001 in HA-free MDM (open blue triangles), MDM with 60 mg C/L HA (open red circles), MDM without any carbon sources (green diamonds), and MDM augmented with 60 mg C/L HA (black crosses). These experiments have no silver. Error bars represent standard deviations based on triplicate samples. Bacterial growth is represented as optical density.

4.3.3 Bacteria and humic acid Ag⁺ binding isotherms

Isotherms were measured for Ag⁺ binding to *P. fluorescens* and to HA. Figure 4.4 shows the normalized amounts of silver bound per unit amount of *P. fluorescens* (N_{bac} = number of Ag ions bound per CFU) or per unit amount of HA (N_{HA} = number of Ag ions per mg C HA). The normalized isotherms collapse reasonably well onto single curves for 45-fold and 60-fold variations in bacteria or HA concentration respectively. Normalized isotherms were fitted to empirical equations (4.1) and (4.2) to analyze the silver material balance in cell growth experiments. Coefficients were determined by regression. These equations have the form of a

two-site binding model for *P. fluorescens* and a one-site Langmuir model for HA, but we do not ascribe any physical significance to the coefficients beyond curve fitting. The fitted isotherms give the normalized number of silver ions bound as a function of the free silver concentration, C_{free} for binding to *P. fluorescens* as

$$N_{bac} = \left(\frac{1.31 \, C_{free}}{0.1 + C_{free}} + \frac{81.88 \, C_{free}}{100.9 + C_{free}} \right) 10^6 \qquad (4.1)$$

and for binding to Pahokee peat HA as

$$N_{HA} = \left(\frac{4.14 \, C_{free}}{19.54 + C_{free}} \right) 10^{16} \qquad (4.2)$$
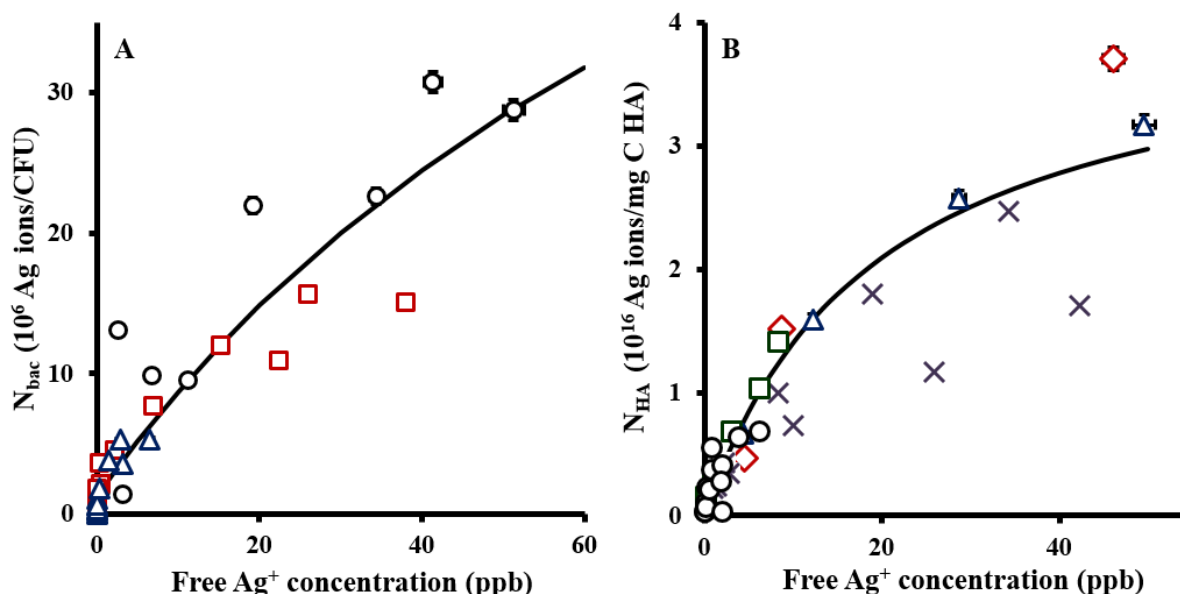
Figure 4.4. Ag$^+$ binding isotherms to *P. fluorescens* (A) and to Pahokee peat humic acid (B). Different symbols represent different bacterial inocula of OD$_{600}$ = 0.001 (black circles), 0.01 (red squares) and 0.045 (blue triangles) (A) or HA concentrations of 1 (red diamonds), 5 (blue triangles), 10 (purple crosses), 20 (green squares) or 60 mg C/L HA (black circles) (B). Curves are fitting equations [4.1] and [4.2]. Error bars are included to represent instrumental uncertainty and are typically smaller than the markers. To aid comparison of bacteria or HA binding, assuming a dry mass of 0.33 pg per bacterium,[242] with carbon content 47%[243], 10 million Ag ions/CFU would correspond to 6.4×10^{16} Ag ions/mg C bacteria.

4.3.4 *P. fluorescens* MIC and MBC for Ag$^+$ and AgNP.

P. fluorescens MIC and MBC were determined for Ag$^+$ and AgNPs for 10^5, 10^6, and 10^7 CFU/mL in MDM and MDM with 20 or 60 mg C/L HA. All results are reported in Tables 4.1 and 4.2. Figure 4.5 uses some of the MIC and MBC data to highlight important trends observed. Figure 4.5 A show Ag$^+$ (as AgNO$_3$) MIC (threshold concentration for complete growth inhibition) and MBC (threshold concentration for 100% viability loss) values at different initial bacterial concentrations. Increasing initial inoculum concentration increases both the MIC and MBC, consistent with the greater capacity for sublethal Ag$^+$ binding. In Figure 4.5 B, when

the bacterial inoculum is held constant at $OD_{600} = 0.0001$, corresponding to 10^5 CFU/mL, as the

HA concentration increases the MIC and MBC both increase. The MBC values were consistently

50% greater than the respective MIC values. These same trends were established for 10^6 and 10^7

CFU/mL inocula and when AgNPs were the silver source (Figure 4.5 C and 4.5 D). These results

confirm that HA functions as a silver binding sink and that it significantly protects against silver

toxicity.
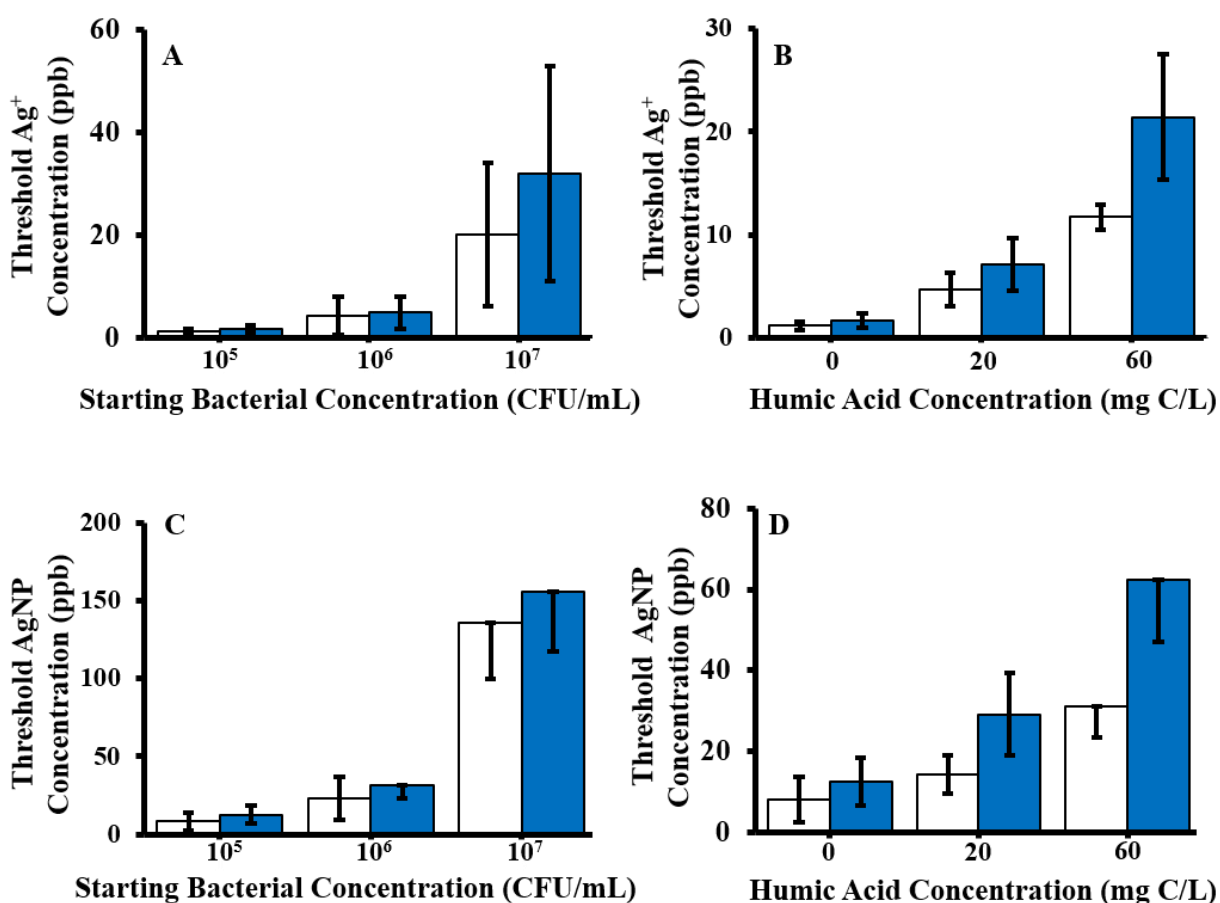
Figure 4.5. MIC and MBC values for Ag^+ (added as $AgNO_3$) and AgNPs for varying initial bacterial concentrations without HA (A) and (C) and for varying concentrations of Pahokee peat HA with an initial bacterial inoculum of 10^5 CFU/mL (B) and (D). White bars represent MICs and blue bars represent MBCs.

The reported values in Tables 4.1 and 4.2 are in the form of mean ± standard deviation. In the case of only a minus sign it is a conservative low estimate of uncertainty since there was no growth at the reported MBC concentration but the true MBC value may be inbetween the reported concentration and the next lower one (e.g. 156 to 78 ppb).

Table 4.1. Ag^+ MIC and MBC (ppb Ag) for *P. fluorescens* at inoculum concentrations of 10^5, 10^6 or 10^7 CFU/mL in MDM with 0, 20 or 60 mg C/L Pahokee peat humic acid

Ag^+	MDM	20 mg C/L HA	60 mg C/L HA
10^5 CFU/mL	MIC 1.2 ± 0.4 (n = 8) MBC 1.7 ± 0.7 (n = 8)	MIC 4.7 ± 1.6 (n = 7) MBC 7.1 ± 2.5 (n=8)	MIC 11.7 ± 1.2 (n = 12) MBC 21.4 ±6.1 (n=8)
10^6 CFU/mL	MIC 4.2 ± 3.7 (n = 15) MBC 4.9 ± 3.1 (n = 11)	MIC 6.3 − 1.6 (n = 8) MBC 11.6 ± 2.4 (n = 8)	MIC 11.5 ± 2.4 (n = 12) MBC 26.1 ± 8.8 (n = 12)
10^7 CFU/mL	MIC 20 ± 14 (n = 16) MBC 31.9 ± 20.9 (n = 12)	MIC 15.6 − 3.9 (n = 8) MBC 29.3 ± 5.5 (n = 8)	MIC 29.3 ± 5.5 (n = 8) MBC 164.1 ± 74.2 (n = 8)

Table 4.2. AgNP MIC and MBC (ppb Ag) for *P. fluorescens* at inoculum concentrations of 10^5, 10^6 or 10^7 CFU/mL in MDM with 0, 20 or 60 mg C/L Pahokee peat humic acid

AgNP	MDM	20 mg C/L HA	60 mg C/L HA
10^5 CFU/mL	MIC 8.3 ± 5.6 (n = 4) MBC 12.7 ± 5.9 (n = 4)	MIC 14.3 ± 4.7 (n = 7) MBC 29.2 ± 10.2 (n=8)	MIC 31.25 − 7.8 (n = 8) MBC 62.5 − 15.6 (n=8)
10^6 CFU/mL	MIC 23 ± 14 (n = 12) MBC 31.3 − 7.8 (n = 7)	MIC 37.5 ± 28.2 (n = 15) MBC 60.1 ± 39.2 (n = 15)	MIC 116.7 ± 22 (n = 15) MBC 221.2 ± 104 (n = 15)
10^7 CFU/mL	MIC 136 − 36 (n = 7) MBC 156 − 39 (n = 7)	MIC 175.8 ± 55.2 (n = 8) MBC 507.8 ± 161.7 (n = 8)	MIC 312.5 − 78.1 (n = 7) MBC 833.3 ± 322.7 (n = 7)

4.3.5 Silver material balance and silver binding toxicity thresholds

The sink effect of HA decreases the free Ag^+ concentration from any silver source in the system. The total silver material balance below incorporates the binding isotherms, equations (4.1-4.2) and allows a threshold amount of silver binding per bacterium to be determined for growth inhibition (N_{bac} at the MIC) or for 100% viability loss (N_{bac} at the MBC):

$$N_{tot} = V(C_{free} + N_{bac}C_{bac} + N_{HA}C_{HA}) \tag{4.3}$$

where N_{tot} is the total amount of dissolved silver ions in the system, V is the media volume, C_{bac} is the bacterial concentration, and C_{HA} is the HA concentration.

Threshold degrees of silver binding to bacteria at the MIC and MBC were calculated via equations (4.1- 4.3) from the MIC and MBC results obtained for Ag^+ (added as $AgNO_3$) and presented for various inoculum and HA concentrations in Figure 4.6. When HA is absent, the lethal threshold amount of Ag ions bound per bacterium, N_{bac} (MBC) is on the same order of magnitude for each inoculum, 2.5 ± 0.6, 4.5 ± 2.1 and 10.6 ± 6.2 million Ag ions bound per CFU for 10^5, 10^6 and 10^7 CFU/mL inocula respectively. The trend of observing similar threshold amounts of Ag ions bound per CFU for the different inocula is also observed with respect to the values of N_{bac} at the MIC (Table 4.3). The order of magnitude similarity for threshold Ag^+ binding across three orders of magnitude in inoculum concentration suggests a critical degree of silver binding needed for 100% lethality.

Table 4.3. Effect of humic acid on threshold levels of Ag^+ bacterial binding. Values are the ratio of the number of Ag ions bound per bacterium in MDM to the number of Ag ions bound per bacterium in MDM augmented with HA at the MIC and at the MBC. Results are shown for the fitted parameters that best represent the measured binding data for *P. fluorescens* and HA, as well as the adjusted parameters to represent the binding extrema.

OD_{600}	HA Conc. (mg C/L HA)	Calculated Ag atoms bound per bacterium (millions)	Fitted Data $N_{bac, MDM}/ N_{bac,MDM+HA}$ ($B_{II} = 81.88$) ($B = 4.14$)	Extreme Case $N_{bac, MDM}/ N_{bac,MDM+HA}$ ($B_{II} = 134.1$) ($B = 1.8$)
0.0001	0	at MIC = 2.111 at MBC = 2.530	at MIC: 1 at MBC: 1	at MIC: 1 at MBC: 1
	20	at MIC = 0.009 at MBC = 0.012	at MIC: 247 at MBC: 196	at MIC: 132 at MBC: 110
	60	at MIC = 0.007 at MBC = 0.013	at MIC: 297 at MBC: 195	at MIC: 159 at MBC: 109
0.001	0	at MIC = 4.003 at MBC = 4.47	at MIC: 1 at MBC: 1	at MIC: 1 at MBC: 1
	20	at MIC = 0.011 at MBC = 0.021	at MIC: 350 at MBC: 214	at MIC: 201 at MBC: 125
	60	at MIC = 0.007 at MBC = 0.016	at MIC: 302 at MBC: 284	at MIC: 328 at MBC: 166
0.01	0	at MIC = 9.666 at MBC = 10.591	at MIC: 1 at MBC: 1	at MIC: 1 at MBC: 1
	20	at MIC = 0.028 at MBC = 0.052	at MIC: 249 at MBC: 205	at MIC: 125 at MBC: 107
	60	at MIC = 0.018 at MBC = 0.114	at MIC: 395 at MBC: 93	at MIC: 196 at MBC: 51

Despite the overall protective effect of HA manifested as higher MIC and MBC values, the critical threshold for lethal binding is substantially lower in the presence of HA compared to when HA is absent. N_{bac} (MBC) decreased by two orders of magnitude relative to HA-free conditions ($p < 0.001$, based on the rank-sum test[213]). In the presence of 20 mg C/L HA the amount of Ag ions bound per bacterium at the MBC is 0.012 ± 0.001, 0.021 ± 0.002 and 0.052 ± 0.004 million Ag ions bound per CFU for bacterial concentrations of 10^5, 10^6, and 10^7 CFU/mL, respectively. In the presence of 60 mg C/L HA the amount of Ag ions bound per bacterium at the MBC is 0.013 ± 0.001, 0.016 ± 0.003 and 0.114 ± 0.003 million Ag ions bound per CFU for bacterial concentrations of 10^5, 10^6, and 10^7 CFU/mL, respectively. Comparing Figure 4.6 A and 4.6 B also shows that N_{bac} (MIC) also decreased with the addition of HA. The significant decrease in the amount of silver ions bound per bacterium at the MIC and MBC when HA is present compared to when it is absent suggests that *P. fluorescens* is more sensitive to silver in systems with HA.
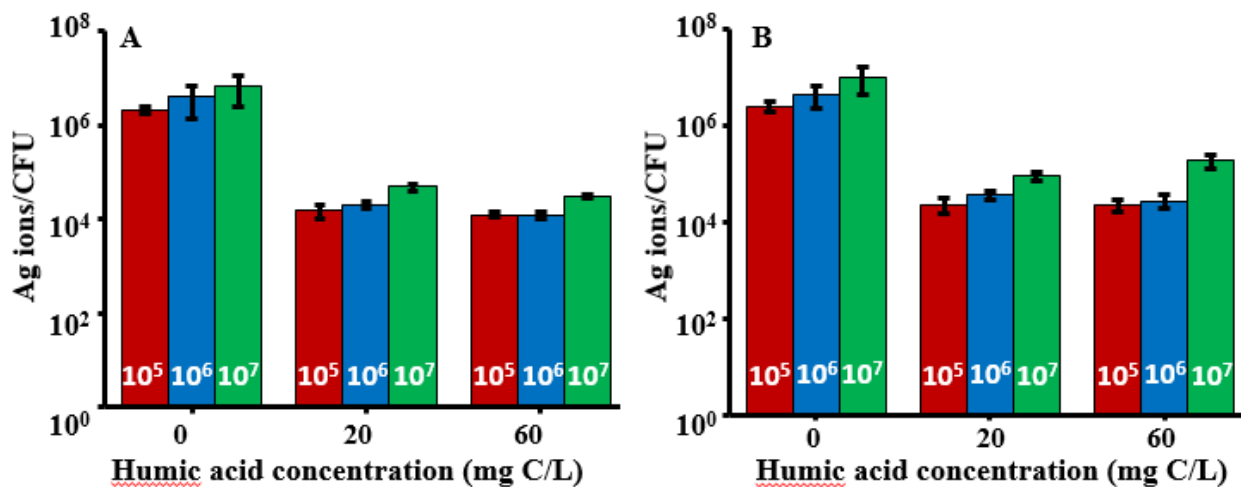
Figure 4.6. Ag$^+$ bound per bacterium at the MIC (A) or MBC (B) in 0, 20 and 60 mg C/L humic acid with minimal Davis media for bacterial inoculum concentrations of 10^5, 10^6, and 10^7 CFU/mL which are represented by the red, blue and green bars, respectively.

Since there is scatter in the Ag^+ binding data, in order to validate the conclusions regarding the MIC and MBC threshold levels of bacterial Ag^+ binding in the presence of HA, silver material balance calculations were repeated using binding isotherm equations that represent the extrema of the binding data. For example, upper bound estimates of the amount of Ag ions bound per bacterium at the MIC or MBC were determined by using a binding isotherm that would overestimate the amount of bacterial Ag^+ binding (see Figure 4.7 A) and a binding isotherm that would underestimate the HA binding data set (see Figure 4.7 B).
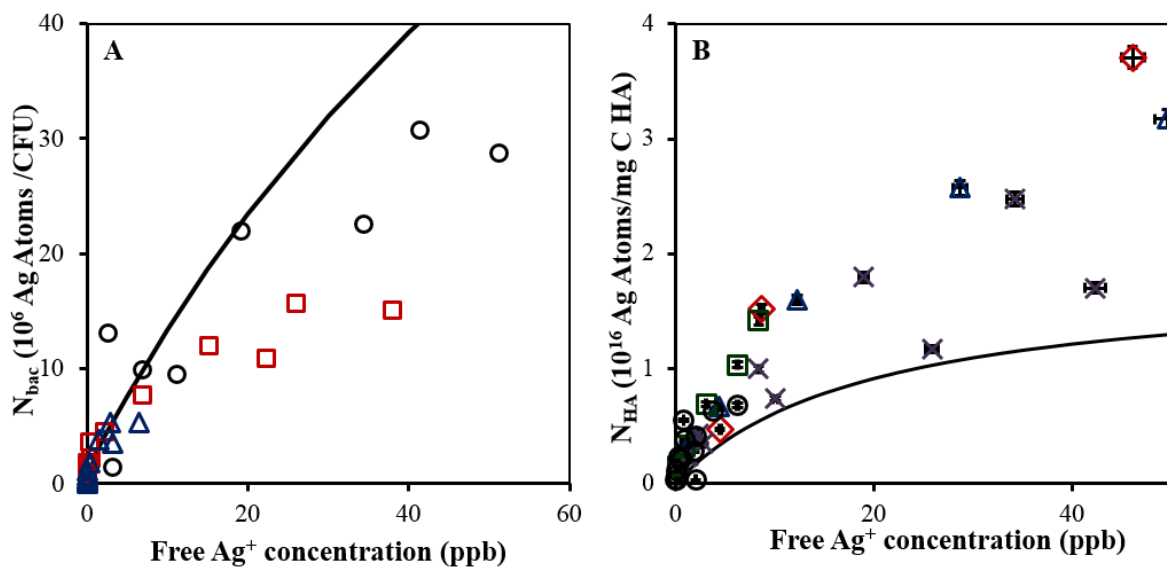
Figure 4.7. Ag^+ model binding isotherms to *P. fluorescens* (A) representing an overestimation of binding to *P. fluorescens* and to Pahokee peat humic acid (B) representing an underestimation of binding to humic acid.

The general form for the Ag$^+$ binding isotherm to *P. fluorescens* is represented as

$$N_{bac} = \left(\frac{B_I \, C_{free}}{K_I + C_{free}} + \frac{B_{II} C_{free}}{K_{II} + C_{free}} \right) 10^6 \qquad (4.4)$$

and for binding to Pahokee peat HA as

$$N_{HA} = \left(\frac{B \, C_{free}}{K + C_{free}} \right) 10^{16} \qquad (4.5)$$

where N_{bac} is the number of Ag ions bound per CFU, N_{HA} is the number of Ag ions per mg C

HA, and C_{free} is the free silver concentration. B_I, K_I, B_{II} and K_{II} are fitting parameters for Ag$^+$

binding to *P. fluorescens* while B and K are fitting parameters for Ag$^+$ binding to Pahokee peat

humic acid. The parameters B_{II} and B (original fitted values listed in Table 4.3) were altered to

represent the most extreme case that would result in *P. fluorescens* having the highest amount of

Ag ions bound per CFU using the upper extreme of Ag$^+$ binding to *P. fluorescens* (see Figure 4.7

A) and the lower extreme of Ag$^+$ binding to Pahokee peat humic acid (see Figure 4.7 B). The

equation for *P. fluorescens* with an adjustable parameter that can be used to over-estimate

bacterial binding is shown below as

$$N_{bac} = \left(\frac{1.31 \, C_{free}}{0.1 + C_{free}} + \frac{B_{II} C_{free}}{100.9 + C_{free}} \right) 10^6 \qquad (4.6)$$

and for binding to Pahokee peat HA with an adjustable parameter to under-estimate HA binding

as

$$N_{HA} = \left(\frac{B \, C_{free}}{19.54 + C_{free}} \right) 10^{16} \qquad (4.7)$$

In each case the adjusted models that represent the binding extrema do not affect the

conclusion determined using the fitted binding isotherms, that the threshold amounts of Ag$^+$

bound per CFU at the MIC and at the MBC are much greater in the absence of humic acid. (HA

makes *P. fluorescens* more sensitive to Ag$^+$.) Even using binding extreme representations that de-emphasize HA binding, the threshold amounts of bacterial silver binding without HA remain well over one order of magnitude greater than with HA (Table 4.3). Uncertainty in the binding isotherms does not affect the conclusion that *P. fluorescens* is more sensitive to the toxic effects of bacterial bound Ag$^+$ in the presence of HA.

The overall protective effect of HA is due primarily to the decrease in the free silver concentration, since *P. fluorescens* is apparently more intrinsically vulnerable to silver toxicity (lower lethality threshold of silver bound per bacterium) in the presence of HA than its absence. That is, HA has two opposing effects: it decreases free silver concentrations but makes *P. fluorescens* more sensitive to each silver ion bound. Here the net effect is overall protective. The mechanism for the apparent increase in vulnerability is as yet unknown. One possible explanation for the increased sensitivity is that HA adsorbs and shuttles bound Ag$^+$ to the cell wall. This would be consistent with electrophoretic mobility results in Section 4.3.2.

4.3.6 Bacterial colonization in the presence of Ag$^+$ and humic acid

The main toxic agent associated with AgNPs is believed to be Ag$^+$ released from the nanoparticles.[47,88,206,215] ICP-MS analysis of the bacteria suspensions bathing the AgNP-decorated coverslips showed that the total silver ion concentration (in either free, bacteria-bound or HA-bound states) released from the AgNPs after 3 h of exposure was 3.2 $\pm$ 1.5 ppb in MDM, 5.8 $\pm$ 0.8 ppb in MDM augmented with 20 mg C/L HA, and 5.4 $\pm$ 0.4 ppb in MDM augmented with 60 mg C/L HA. For comparison, the MIC values for 10^5 CFU/mL are 1.2 $\pm$ 0.4 ppb in MDM, 4.7 $\pm$ 1.6 ppb in MDM with 20 mg C/L HA and 11.7 $\pm$ 1.2 ppb in MDM with 60 mg C/L HA. The MIC values for 10^6 CFU/mL are 4.2 $\pm$ 3.7 ppb in MDM, 6.3 – 1.6 ppb in MDM with

20 mg C/L HA and 11.5 $\pm$ 2.4 ppb in MDM with 60 mg C/L HA. (Where the uncertainty is indicated only by a minus sign, it means every serial dilution experiment yielded the same MIC, so the uncertainty is estimated as half the difference between the observed MIC and the next lower concentration in the serial dilution.)

For both 10^5 and 10^6 CFU/mL initial inocula in the absence of HA, the silver released after 3 h exceeded the MIC. Accordingly, there was no detected growth and minimal colonization of the AgNP-decorated coverslips. However, in the presence of 60 mg C/L HA, the silver released after 3 h was less than the MIC for these initial inocula, and there was significant planktonic growth and surface colonization of the AgNP-decorated coverslips for both initial inocula.

After 72 h the total concentrations of released Ag^+ had increased to 6.1 $\pm$ 2.4 ppb in MDM, 16.9 $\pm$ 1.0 ppb in MDM with 20 mg C/L HA and 20.4 $\pm$ 4.2 ppb with 60 mg C/L HA. These concentrations somewhat exceeded the MIC values for 10^5 and 10^6 CFU/mL initial inocula. Yet, the results in Figure 4.1 showed that the AgNP-decorated coverslips were colonized in the presence of 60 mg C/L HA for both these initial inocula. This is attributed to the growth that occurs during the early stages of exposure to AgNP-decorated surfaces, when the released Ag^+ concentrations remain below the MIC. That growth produces higher planktonic concentrations, and since the MIC increases with increasing bacterial concentration, the planktonic growth and colonization evidently outpace the release of Ag^+. The relative kinetics of silver release and bacterial growth are important.

When *P. fluorescens* are exposed to concentrations of Ag^+ below the MIC they can grow to higher inoculum concentrations that require considerably higher concentrations of silver to inhibit growth. To illustrate, Table 4.4 shows the amount of growth in 24 hours for 10^5 and 10^6

CFU/mL initial inocula of *P. fluorescens* when exposed to a concentration of Ag^+ that is half of

the corresponding MIC. In every case, growth after 24 h was substantial – increasing OD_{600} by

orders of magnitude. This relates to the observed bacterial proliferation and growth when the

short-term release of Ag^+ from AgNPs was less than the MIC, but the long-term release

exceeded the MIC that would correspond to the *initial* inoculum concentration. If the initial

release of Ag^+ exceeds the MIC of the bacterial population that exists at the beginning of the

exposure, there is no growth. However, if the early growth outpaces the silver ion release, the

amount of Ag^+ released as a function of time as the exposure continues to longer times may

never reach the threshold concentration needed to inhibit growth of the existing bacterial

population at any particular point in time.

Table 4.4. Change in OD_{600} of *P. fluorescens* after 24 h exposure to half the MIC for Ag^+.

Initial OD_{600}	HA Conc. (mg C/L HA)	0.5 Ag^+ MIC (ppb)	Change in OD_{600}
0.0001	0	0.6 ± 0.2	0.03 ± 0.01
	20	2.3 ± 0.8	0.28 ± 0.21
	60	5.8 ± 0.6	0.16 ± 0.14
0.001	0	2.5 ± 2.2	0.15 ± 0.05
	20	3.1 ± 0	0.66 ± 0.29
	60	5.5 ± 1.5	0.78 ± 0.04

These concentrations are reasonable ones to work with because over 24 hours *P.*

fluorescens can grow up to an optical density greater than the respective silver dosage needed to

inhibit growth and under the right conditions *P. fluorescens* will grow to bacterial concentrations that far exceed the amount of silver released from these AgNP-laden coverslips.

Since released Ag^+ may influence bacteria in the nearby vicinity of AgNP deposition sites in the environment, it is also important to investigate the potential for HA to aid bacterial colonization on bare surfaces in the presence of dissolved Ag^+. 10^5 and 10^6 CFU/mL *P. fluorescens* inocula were exposed to 5 ppb Ag^+ in MDM and MDM augmented with 20 and 60 mg C/L HA. This concentration was selected because it approximated the 3 h release of Ag^+ from surface-adherent AgNPs. Both inocula concentrations have MIC values near or below 5 ppb Ag^+ for 0 or 20 mg C/L HA and well above 5 ppb Ag^+ with 60 mg C/L HA. Thus, we expected bacterial growth would be inhibited in all media except MDM containing 60 mg C/L HA for both bacterial concentrations. Since hindered growth correlated with significantly diminished colonization (with adherent AgNPs, Figure 4.1), we also anticipated diminished colonization on bare glass with 0 or 20 mg C/L, but not with 60 mg C/L HA.

Compared to silver-free systems (Figure 4.1), the only appreciable amount of colonization in the presence of 5 ppb $AgNO_3$ (Figure 4.8) occurred in MDM with 60 mg C/L HA. Accordingly, there was no detectable change in OD_{600} in the presence of MDM or MDM with 20 mg C/L HA, while in the presence of 60 mg C/L HA, OD_{600} increased by 0.80 ± 0.05 and 0.84 ± 0.02 for 10^5 and 10^6 CFU/mL, respectively. HA had a concentration-dependent effect of preserving colonization on bare glass surfaces when all silver was added in the form of dissolved silver, and the effect was quantitatively consistent with the effect of HA addition on the MIC.
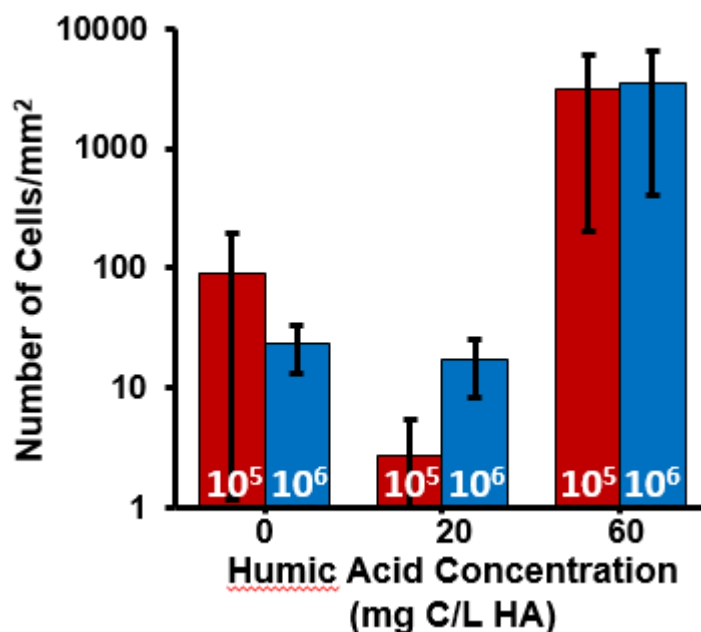
Figure 4.8. Bacterial colonization on AgNP-free coverslips when exposed to 5 ppb Ag^+ as $AgNO_3$ in 0, 20 or 60 mg C/L HA in MDM. Initial inoculum concentrations are represented by the red and blue bars for 10^5 and 10^6 CFU/mL, respectively.

4.3.7. Relationship between Ag released from AgNP-decorated coverslip and binding isotherm

Figure 4.9 shows that the amount of silver bound per bacterium after 72 h is above the critical threshold when 10^5 CFU/mL are exposed to a AgNP-decorated coverslip in MDM. However, even though the critical threshold is reduced by two orders of magnitude when HA is present and the amount of Ag in the system increases, the amount of Ag ions bound per bacterium is still below the new critical threshold to explain why *P. fluoresces* is able to grow in the planktonic state and ultimately colonize the AgNP-coated coverslip.
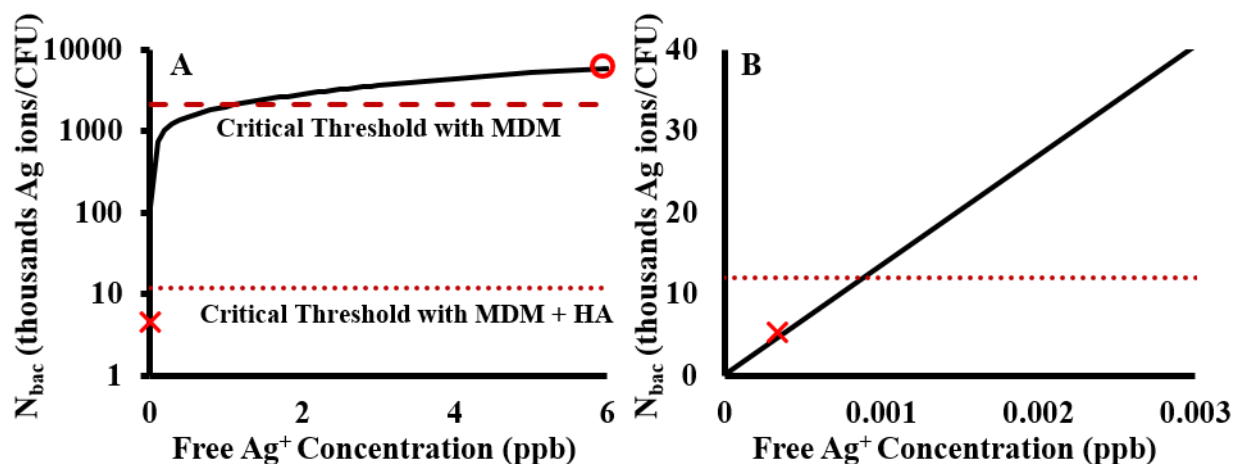
Figure 4.9. Ag^+ model binding isotherm to *P. fluorescens* (represented by the black line) with the critical threshold of Ag ion bound per bacterium when MDM and when MDM is augmented with HA represented by the red dashed and red dotted lines respectively (A) and subsection (B). The red circle represents the amount of Ag ions bound per bacterium if the total silver in the system was 6.1 ppb, the amount released from a AgNP-decorated coverslip in MDM and the initial inoculum was 10^5 CFU/mL. The red cross represents the amount of silver bound per bacterium when amount of silver released is 20.4 ppb, the amount Ag^+ released from coverslips in MDM augmented with 60 mg C/L HA and the initial inoculum was 10^5 CFU/mL.

4.3.8. Environmental Implications

Provided that inoculum concentrations exceed a threshold level, bacteria can directly colonize surfaces displaying an abundance of silver nanoparticles. The key is whether the population is large enough that a fraction of the original population survives and proliferates. Surviving bacteria colonize the nanoparticle-decorated surface. Silver ion binding to humic acid extends the range of this inoculum effect, allowing bacterial populations to proliferate and colonize silver nanoparticle-decorated surfaces at inoculum concentrations much smaller than would otherwise be required in the absence of humic acid. Silver sinks such as humic acid are abundant in many environments and can be expected to offer significant bacterial protective effects against silver and potentially other toxic metals. The increased tolerance provided by

these silver sinks may allow bacteria to proceed through normal lifecycle phases under conditions where AgNP disruption of surface colonization and biofilm formation may be expected otherwise. A more subtle but still significant consequence of the presence of humic acid is an apparent sensitization of *P. fluorescens* to bound silver ions; the amount of Ag ions bound per bacterium at the MIC and MBC are significantly lower when humic acid is present compared to when it is absent. This effect opposes the protective effect of humic acid binding to Ag^+ to decrease the free silver ion concentration. In the current system, the balance of these competing effects favored *P. fluorescens* proliferation and colonization, but it cannot be certain that the balance would be favorable for other species if this sensitization also exists for other bacteria.
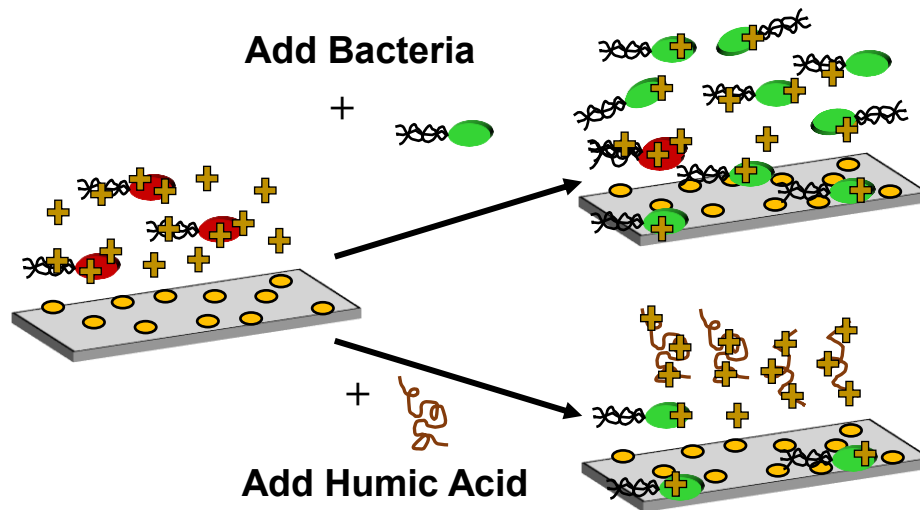
Figure 4.10. Addition of bacteria or natural organic matter can reduce the amount of silver ions distributed per bacterium enabling bacteria to survive in the presence of the antibacterials Ag^+ and AgNPs and colonize AgNP-decorated surfaces.

Chapter 5. Natural organic matter effect on copper toxicity

5.1 Introduction

In Chapters 3 and 4 the effects of the initial inoculum concentration and the presence of humic acid on silver toxicity were explored. However, for the past two decades, in addition to AgNP containing products, CuONPs have also been increasingly used in consumer products such as textiles, electronics and biomedical devices for their antimicrobial properties.[3,33–36] Extensive usage of these products leads to increased nanoparticles in wastewater runoff. Wastewater treatment sludge is typically used as fertilizer, providing another potentially significant route for copper entry into ecosystems in agricultural regions.[37,38] Additionally, copper-containing nanoparticles such as Kocide are directly applied in agriculture as a pesticide.[132] Since copper has known antimicrobial properties and may affect bacterial populations in the environment, it is important to assess copper toxicity to bacteria in environmentally relevant systems.

The objective of this research is to determine the combined effects of bacterial concentration and the presence of NOM on mitigating copper toxicity. The governing hypothesis is that NOM will increase bacterial tolerance to copper by serving as a copper sink to reduce free copper concentrations to sublethal levels so bacteria can proliferate. We consider *Escherichia coli* as a model Gram-negative bacterium that has a well characterized genome for these studies. Minimal inhibitory and bactericidal concentrations will be determined for *E. coli* with and without NOM, exemplified as HA, at different initial inoculum concentrations to determine the effects of bacterial concentration and the presence of NOM. For this study, similar to Chapter 4, we consider the higher end of natural HA concentration ranges to capture the magnitude of NOM effects that may be expected in high organic carbon environments. Copper binding isotherms to

E. coli and HA are also obtained to determine copper removal by each organic material. To further probe the mitigating potential for HA, copper responsive genes *copA*, *cueO*, *cusC* and a protein membrane repair gene, *cpxP*, and ROS production were measured with and without HA. It was observed that the presence of humic acid decreased all gene responses to copper. ROS produced inside bacteria that was induced by copper was indirectly observed to decrease in the presence of humic acid as well. Analysis of gene responses were performed with the help of Ph.D. candidate Joe D. Moore in Civil and Environmental Engineering at Carnegie Mellon University.

5.2 Materials and Methods

5.2.1 Bacterial Strain and Conditions

Escherichia coli (ATCC® 11775™) was grown in modified minimal Davis media (MDM) that contains 1.58 g/L K_2HPO_4 ($\geq$ 99%, Acros Organics), 2.5 g/L KH_2PO_4 ($\geq$ 99%, J.T. Baker), 1.0 g/L $(NH_4)_2SO_4$ ($\geq$ 99%, Sigma-Aldrich), 0.1g/L $MgSO_4 \cdot 7H_2O$ (Acros Organics), modified Wolfe's vitamin and mineral solutions (see Tables 2.2 and 2.3), and 4 g/L glucose ($\geq$ 99.5%, Amresco) as the primary carbon source. The MDM pH was adjusted to 6.5 ± 0.02 by addition of 0.1 M H_2SO_4 (Acros Organics). All water was purified by a Barnstead Nanopure, > 18 MΩ cm resistivity.

A frozen stock of *E. coli* stored at $- 80°C$ was inoculated aerobically in an orbital shaker (Corning LSE digital microplate shaker) at 160 rpm at room temperature. *E. coli* suspensions were orbitally shaken until the early log-growth phase (occurring at $OD_{600} = 0.07 - 0.10$) and then subcultured to the desired inoculum concentration for experiments.

Pahokee Peat Humic Acid (International Humic Substances Society) solutions were prepared and sterile filtered as described previously.[126] HA stock solution concentrations were determined as total organic carbon using a Sievers Innovox TOC analyzer (General Electric Analytical Instruments) and reported as milligrams of organic carbon per liter (mg C/L).

5.2.2 Minimal Inhibitory Concentration and Minimum Bactericidal Concentration

E. coli in the early log-growth phase was diluted to $OD_{600} = 0.01$, 0.001 or 0.0001, corresponding to ~10^7, ~10^6, and ~10^5 CFU/mL, respectively, verified by agar plating, and placed in black polystyrene clear-bottomed 96-well plates (Corning Costar). A 10,000 ppm Cu^{2+} stock solution prepared with $CuSO_4 \cdot 5 H_2O$ (Fisher Scientific) in de-ionized water was sterile-filtered with a 0.22 µm syringe filter. Cu^{2+} solution aliquots were added to bacteria suspensions in MDM in the well plates. Cu^{2+} exposure concentrations ranged from 40 to 220 ppb for the inoculum with initial $OD_{600} = 0.0001$ (10^5 CFU/mL), 40 to 400 ppb for $OD_{600} = 0.001$ (10^6 CFU/mL) and 80 to 1200 ppb $OD_{600} = 0.01$ (10^7 CFU/mL). In MDM augmented with 60 mg C/L HA, $OD_{600} = 0.0001$, 0.001 and 0.01 inocula were all exposed to two-fold serial dilutions that ranged from 100 ppb to 50,000 ppb of Cu^{2+}. The total sample volume in each well was 200 µL.

96-well Plates were orbitally shaken at room temperature at 160 rpm for 48 hours to allow *E. coli*, exposed to sub-lethal Cu^{2+} concentrations, an opportunity to recover and grow if there was a significant lag time for growth. *E. coli* was grown for 48 hours to allow low initial inoculum concentrations (10^5 CFU/mL) sufficient time to grow, especially when copper is present since no observable growth is measured until 20 hours after setting up the experiment.

Figure 5.1 shows that when bacteria are subcultured to an initial $OD_{600} = 0.0001$ it takes about 20 h before a change in optical density is observed.
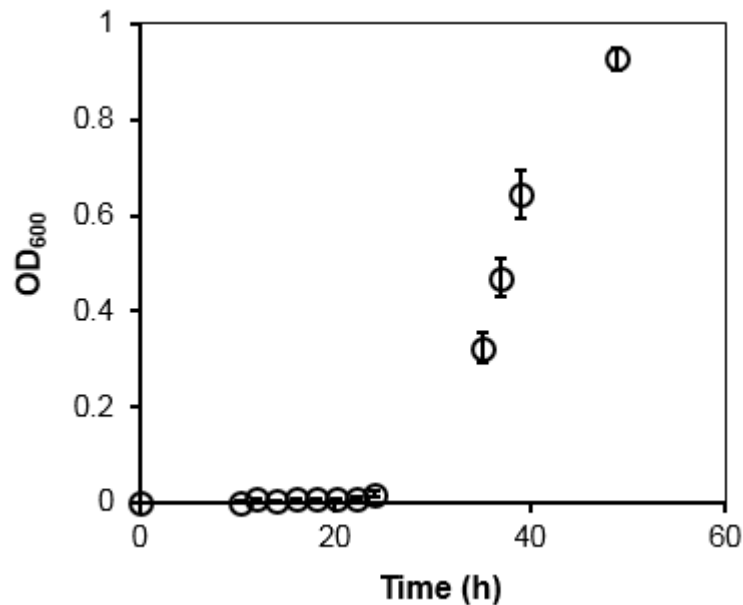
Figure 5.1 Representative growth curve for *E. coli* subcultured to an $OD_{600} = 0.0001$ from bacteria in early log-phase growth ($0.07 - 0.10$).

The OD_{600} was measured for each well using a plate reader (Spectramax M2, Molecular Devices) as a function of time during the 48 h experiment. The lowest Cu^{2+} concentration for which there was no significant change in OD_{600} was determined to be the MIC. MBC determinations were performed after each 48 hour MIC experiment. 100 µL samples were collected from wells corresponding to the highest concentration that was still below the MIC and all higher concentrations. These were spread on agar plates, which were maintained at 37 °C for 24 hours. The MBC was determined to be the lowest concentration for which no colonies were observed to form. Agar plates were prepared by pouring an autoclaved mixture of 4 g of Difco

nutrient broth (BD Diagnostics) and 7.5 g Bacto Agar (BD Diagnostics) in 500 mL of ultrapure water.

5.2.3 Determining Growth Rate Constant

The growth rate constant was determined by taking values from the growth curves of bacteria at different copper concentrations and plotting $Ln(OD_{600})$ vs. time. Since the bacterial optical densities did not reach levels that deviated from Beer's law ($OD_{600} > 0.40$), the optical densities could be used instead of converting to bacterial concentrations since the slope of each curve should be equivalent. The data points plotted were chosen based on linearity. All points that followed the same linear trend were plotted. The slope of the line is the growth rate constant since a reformatted version of the bacterial growth curve is:

$$Ln(C) = Ln(C_o) + kt \qquad (5.1)$$

Where: C_o is the initial bacterial concentration, C is the current concentration of bacteria, k is the growth rate constant (h^{-1}), and t is time (h). A representative plot for obtaining the growth rate constant is shown in Figure 5.1
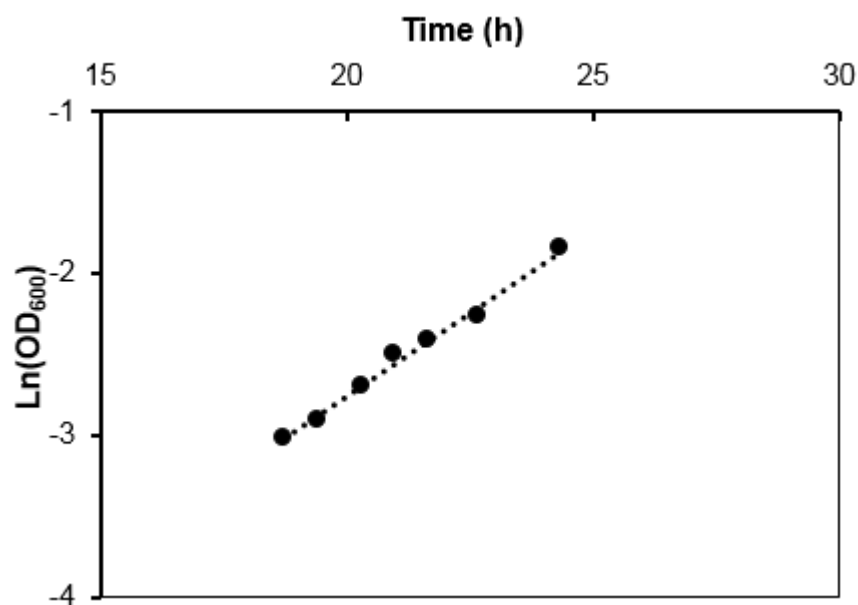
Figure 5.2. A representative of how growth rate constants are determined. This one is for initial inoculum concentration of $OD_{600} = 0.001$ at 80 ppb Cu^{2+}. The slope of this curve is 0.207 h^{-1} which is the growth rate constant.

5.2.4 Cu^{2+} Binding to Bacteria and HA

To measure Cu^{2+} binding to *E. coli* 5 to 50 ppb of Cu^{2+} were mixed with 10^6, 10^7 or 5×10^7 CFU/mL *E. coli* suspensions prepared by diluting suspensions that were in the early log-growth phase. To measure Cu^{2+} binding to HA in solution, 10 to 500 ppb of Cu^{2+} were mixed with humic acid at concentrations ranging from 3 to 60 mg C/L.   In each case the total volume was 10 mL and the mixtures were orbitally shaken for one hour. 4 mL samples were removed and centrifugally filtered with a 3 kDA molecular weight cutoff centrifugal filter (Amicon) at 4000 *g* (Eppendorf Centrifuge 5415 D) for 50 min. To prepare the samples for copper analysis by inductively coupled plasma- mass spectrometry (ICP-MS), the filtrates and original samples were then oxidized by adding concentrated nitric acid and 30% H_2O_2. For a 3 mL sample, 180 µL of concentrated HNO_3 (Aristar plus) and 90 µL 30% v/v of H_2O_2 (Fisher Scientific) were

added. Samples were then heated for 15 minutes at 100 °C with a digestion chamber (VWR). Copper concentrations were then determined via ICP-MS (Agilent 7700x).[171]

5.2.5 Transcriptional Response Experiments

For quantitative polymerase chain reaction (qPCR) gene expression assays, *E. coli* suspensions were sub-cultured from $OD_{600} = 0.2 - 0.3$ suspensions to produce $\sim 2 \times 10^8$ or 2×10^7 CFU/mL suspensions with a total volume of 5 mL. Samples were prepared with the following media conditions: MDM, MDM + 300 ppb Cu^{2+}, MDM + 60 mg C/L HA, and MDM + 60 mg C/L HA + 300 ppb Cu^{2+}. Samples were orbitally mixed for 30 min at 160 rpm at room temperature. Afterwards, for 10^8 CFU/mL, 1 mL of the bacterial suspension was removed and mixed with 2 mL of RNAprotect (Qiagen). For 10^7 CFU/mL, 10 mL of RNAprotect was added to the 5 mL bacterial sample. All samples were centrifuged at 4000 g for 20 min and the supernatant was decanted. Samples were stored frozen at -20 °C until until analysis.

RNA was isolated using the RNeasy Mini Kit (Qiagen) following the manufacturer's procedure with slight alterations, including an on-column DNase treatment (Qiagen). RNA was quantitated fluorometrically using a high-sensitivity RNA kit and a Qubit 2.0 fluorometer (Life Technologies, Carlsbad, CA). Quality information was derived from a 1.3% agarose gel and using a NanoDrop UV-Vis spectophotometer (Thermo Fisher Scientific). cDNA was synthesized from 185 ng RNA using iScript Reverse Transcription Supermix (Bio-Rad) and was quantitated using a ssDNA kit and the Qubit fluorometer. cDNA quality was also assessed on the NanoDrop. Aliquots of cDNA were diluted to 1 ng/µL in RNase/DNase-free water.

Relative quantification was performed on a 7500 Real-Time PCR System (Applied Biosystems) using PowerUP SYBR Green master mix (Life Technologies) according to the manufacturer's protocol and primers designed with PrimerQuest (IDT). Each 20 µL reaction

consisted of 1 ng cDNA, 10 µL master mix, 8 µL molecular biology grade water, and 1 µL of a 10 µM solution containing both forward and reverse primers (for a final primer concentration of 500 nM). Triplicate technical replicates were performed on each sample. (Primer sequences can be found in Table 5.1.) The 16S rRNA gene, *rrsA*, was used as a housekeeping gene against which target genes were normalized. *rrsA* has been validated for this function before.[216] Fold control, ϕ, was calculated using the $\Delta\Delta$Ct method[217] (Equation 5.2) dividing the normalized gene expression of a target gene (x) under a given treatment (y) by the normalized gene expression of the same gene for the undosed control (*undosed*):

$$Fold\ Control = \ \phi_{xy} = 2^{-(\Delta C_y - \Delta C\ control)} \tag{5.2}$$

Table 5.1. RT-qPCR gene primer sequences

Gene	Primer sequences
rrsA	F: CCTCATAAAGTGCGTCGTAGTC
	R: CGTATTCACCGTGGCATTCT
copA	F: GAACAGGCGGATGTGTCTATC
	R: TTAGCCTTTGGGTGGCTTAC
cueO	F: GGGCTGGAAAGATACCGTTAAG
	R: GATGGCAGTGCGCCATATAA
cusC	F: CAGCAGTCGGTGGTGAATTA
	R: TTGCAGCGATGCCAGATAA
cpxP	F: CTGACGCTGATGTTCGGTTA
	R: GAAGTCGGTTCAGGCGATAA

5.3 Results and Discussion

5.3.1 Impacts of Cu Concentrations on Bacterial Growth Rates.

Growth curves over 48 h for initial inoculum concentrations of 10^5, 10^6, and 10^7 CFU/mL at various copper concentrations in MDM are shown in Figure 5.3 (A – C). Time zero corresponds to the time at which *E. coli* suspensions were sub-cultured at the indicated conditions. As copper concentrations increase, the lag time for bacterial growth increases and the bacterial growth rate constant decreases smoothly (Figure 5.3 D, see Figure 5.2 for representative growth curve fits to first order kinetic model). When comparing growth rate constants, larger bacterial inoculum concentrations require larger copper concentrations to reduce the growth rate constant to a similar extent. The dependence, for copper inhibition of growth, on the initial *E. coli* inoculum concentration indicates that an inoculum effect is present. This is consistent with the observations of Franklin and co-workers for *Pseudokirchneriella subcapitata*.[130]
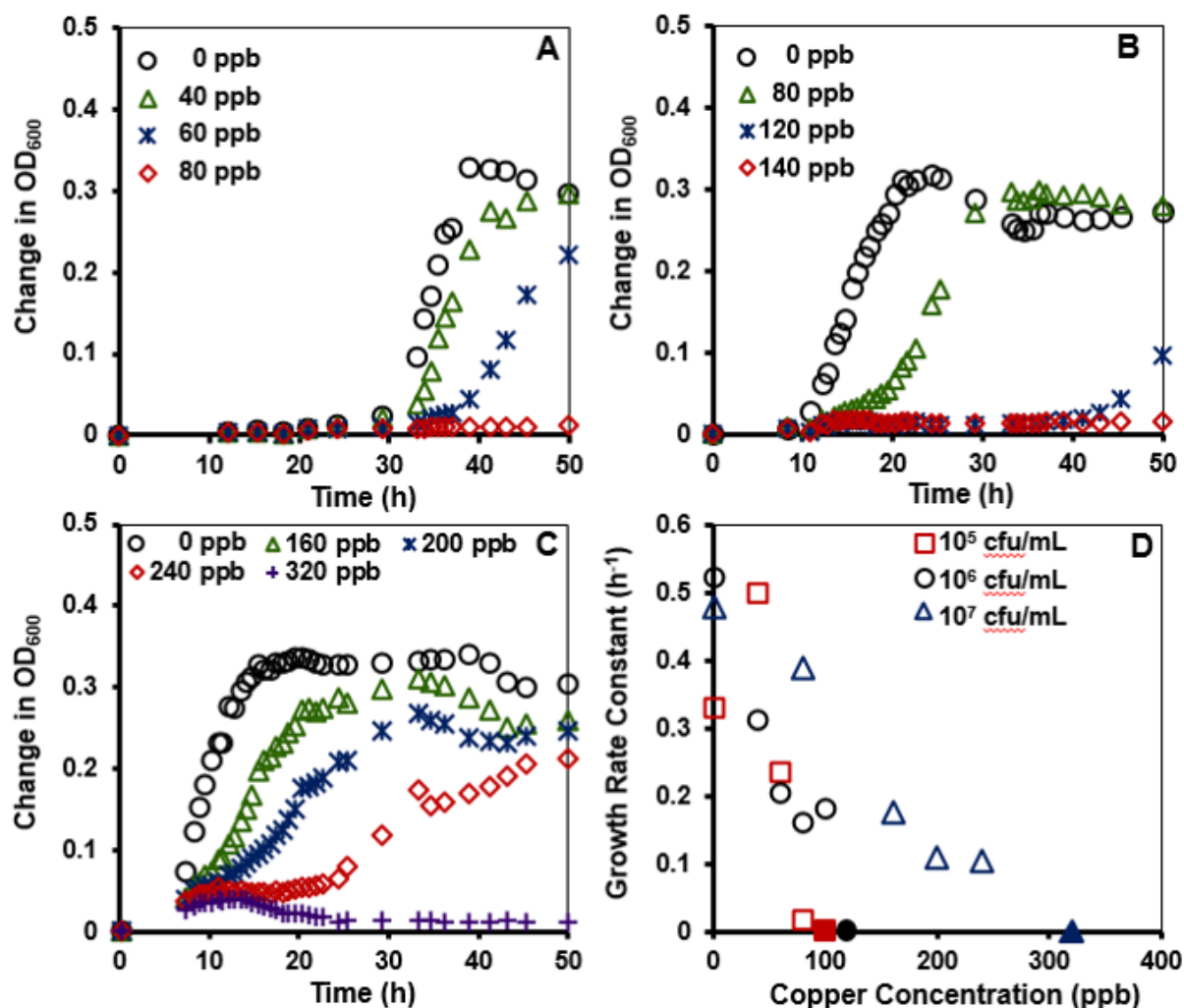
Figure 5.3. Growth curves for initial inoculum concentrations of 10^5 CFU/mL (A), 10^6 CFU/mL (B) and 10^7 CFU/mL (C) at various Cu^{2+} concentrations in MDM containing no HA. Error bars are smaller than the symbols Corresponding growth rate constants are displayed in D. Filled symbols in D indicate the MIC determined as the concentration yielding no growth.

When HA is added to MDM there is still a smooth trend of decreasing growth rate constants as copper concentrations increase for initial bacterial inoculum concentrations of 10^5, 10^6 and 10^7 CFU/mL (Figure 5.4 A – C). The addition of 60 mg C/L HA requires an order of magnitude greater copper concentrations to inhibit bacterial growth. For example, when MDM is augmented with 60 mg C/L HA, bacterial growth in the most dilute inoculum, 10^5 CFU/mL, is

not affected by 813 ppb Cu^{2+} while in HA-free MDM, growth of 10^5 CFU/mL inoculum is fully suppressed 80 ppb Cu^{2+}. Humic acid shows a strong potential for mitigating copper toxicity to *E. coli*, similar to previous reports of silver ion bacterial toxicity mitigation. [99,126]
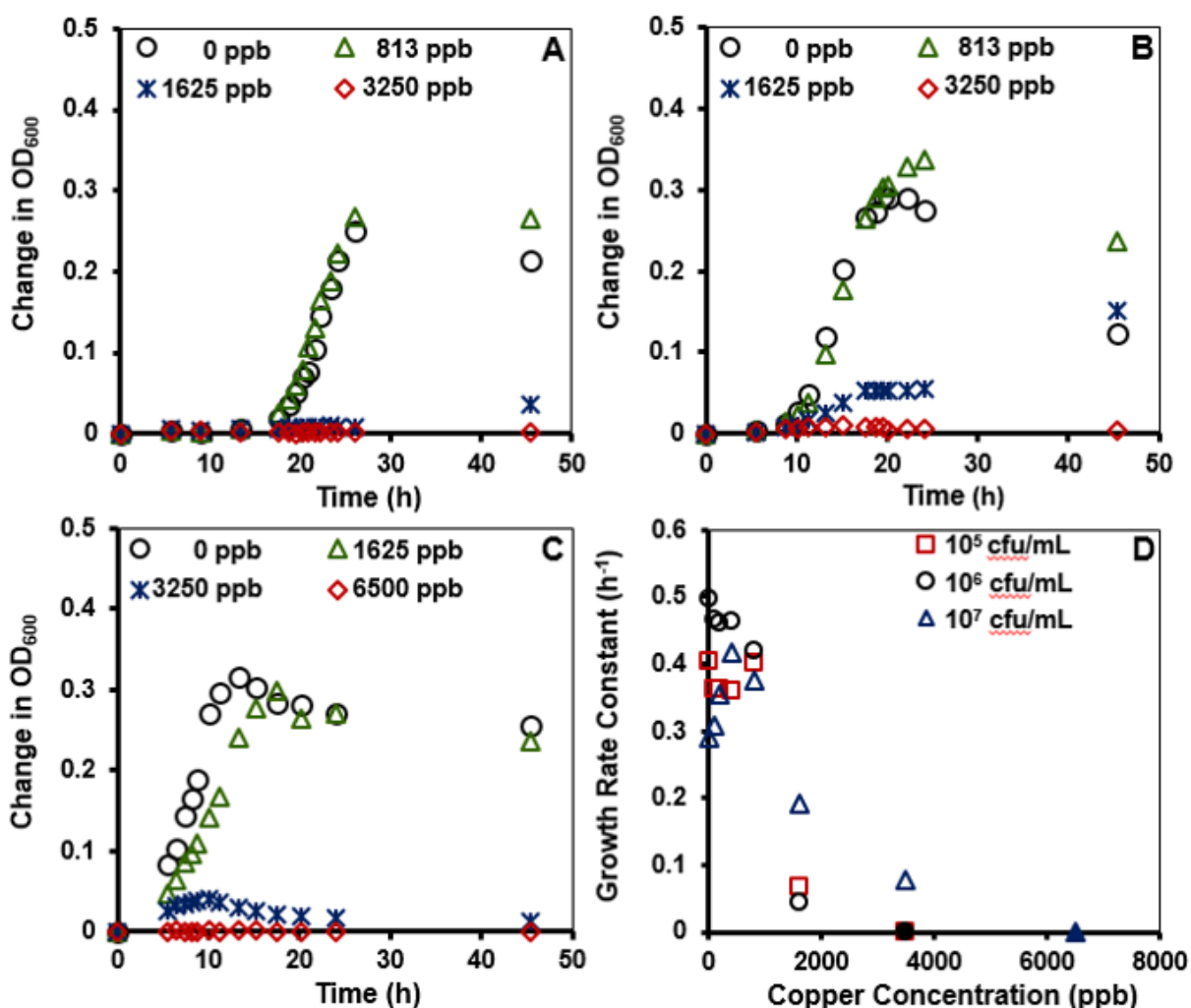
Figure 5.4. Growth curves for initial inoculum concentrations of 10^5 CFU/mL (A), 10^6 CFU/mL (B) and 10^7 CFU/mL (C) at various Cu^{2+} concentrations in MDM augmented with 60 mg C/L HA. Error bars are smaller than the symbols. Corresponding growth rate constants are displayed in D. Filled symbols in D indicate the MIC determined as the concentration yielding no growth (10^6 and 10^5 CFU/mL MIC overlap.)

5.3.2 *E. coli* MIC and MBCs for Cu^{2+}

The inoculum effect for Cu^{2+} toxicity to *E. coli* is evident in Figure 5.5, where Cu^{2+} MIC

and MBC values corresponding to the above experiments are summarized. (All MIC and MBC

values are tabulated in Table 5.2.) Increasing the initial bacterial inoculum concentration

increases the MIC and MBC in MDM. When 60 mg C/L HA is added to MDM (Figure 5.4 B)

the MIC and MBC are much greater than in the absence of HA. MIC values increase

approximately 10-fold relative to HA-free MDM. Increases in MBC are more pronounced. The

MBC for the 10^7 CFU/mL inoculum increased approximately 40-fold, from ~1.2 to 40 ppm with

addition of HA. The inoculum effect persists in the presence of HA, although it is stronger for

the MBC than for the MIC. The MIC and MBCs for Cu^{2+} in MDM augmented with HA was

almost the same for 10^5 and 10^6 CFU/mL. This lack of an inoculum effect may be attributed to

the nature of the MIC experiment where 2-fold dilutions were performed. It is possible that better

concentration gradations would provide a statistical difference between the MIC and MBCs for

the two inoculum concentrations.

Table 5.2. MIC and MBC values (ppb Cu^{2+}) for *E. coli* in MDM and MDM augmented with 60 mg C/L Pahokee peat humic acid at initial inoculum concentrations of 10^5, 10^6 and 10^7 CFU/mL.

Inoculum	MDM		MDM + 60 mg C/L HA	
10^5 CFU/mL	MIC:	78 ± 7 (n = 8)	MIC:	3000 ± 660 (n = 6)
	MBC:	118 ± 20 (n = 8)	MBC:	3800 ± 1300 (n = 6)
10^6 CFU/mL	MIC:	$140 - 10$ (n = 8)	MIC:	$3300 - 810$ (n = 7)
	MBC:	270 ± 41 (n = 8)	MBC:	7600 ± 2700 (n = 7)
10^7 CFU/mL	MIC:	$320 - 40$ (n = 8)	MIC:	$6500 - 1600$ (n = 7)
	MBC:	$1200 - 90$ (n = 8)	MBC:	$41000 - 14000$ (n = 7)
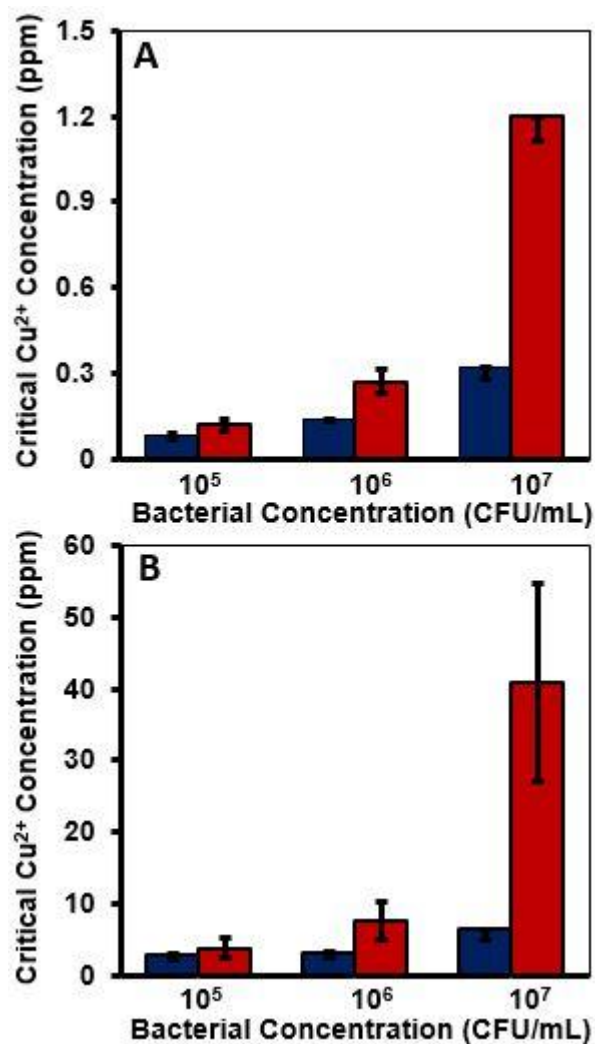
Figure 5.5. Minimal inhibitory concentrations and minimal bactericidal concentrations represented by the blue and red bars respectively for initial bacterial concentrations of 10^5, 10^6 and 10^7 CFU/mL in MDM (A) and MDM augmented with 60 mg C/L HA (B)

Evidently, both the initial inoculum concentration and the presence of HA play a role in mitigating copper toxicity. We hypothesize that both *E. coli* and HA serve as copper sinks and reduce the concentration of copper that is freely available in solution to below toxic levels, similar to the silver ion sink effect reported by Bertuccio and Tilton[126] for silver toxicity to *P. fluorescens*. There it was shown that sub-lethal binding to bacteria and binding to HA decreased free solution Ag^+ concentrations and increased the MIC and MBC. It is interesting to note that

the humic acid increased the Cu^{2+} MIC and MBCs for *E. coli* 20 and 30-fold while humic acid

only increased the Ag^+ MIC and MBCs for *P. fluorescens* 5 and 3-fold. The authors acknowledge

that these are two different species of bacteria being compared for two different metal ions and

cannot conclude that HA is more effective at mitigating copper over silver from this comparison.

Similar to Bertuccio and Tilton,[126] binding isotherms were measured for Cu^{2+} binding to

HA in solution and to *E. coli* in order to evaluate the Cu^{2+} material balance as it partitions

between free solution, HA-bound and *E. coli*-bound states. Copper binding isotherms for *E. coli*

and Pahokee peat humic acid (Figure 5.6) to determine the bioavailable copper.

5.3.3 Copper binding isotherms for *E. coli* and HA

Different concentrations of *E. coli* (in the absence of HA) or HA (in the absence of *E.*

coli) were incubated, in separate experiments, with a range of copper concentrations, and the free

solution Cu^{2+} was subsequently assayed in filtrates. Depletion of Cu^{2+} from the filtrate relative to

the concentration in the original sample directly reports the amount bound to bacteria or to HA.

Control experiments verified that neither bacteria nor HA pass through the 3 kDa molecular

weight cutoff centrifugal filters. The concentration of copper bound was normalized by the

bacterial concentration or the HA concentration, and the free concentration reported on the

ordinate is the Cu^{2+} concentration in the filtrate. Visual MINTEQ 3.0 was used to identify copper

species and the potential formation of copper precipitates in VDMD. It was observed that in the

absence of organic matter 570 ppb Cu^{2+} is the solubility limit of Cu^{2+} before copper phosphate

precipitates form. When humic acid is added, modeled as DOC (Nica-Donnan), the solubility

limit increased up to about 3200 ppb Cu^{2+}. All binding experiments were conducted below the

model-predicted solubility limits of copper phosphate. Solubility limits and mineral

concentrations in this system can be found in the Appendix in Tables A1 – A4.

In the case of bacteria, the term "binding" is used in a general sense to convey any mechanism for Cu^{2+} sequestration from solution, whether by adsorption or ionic binding to cell constituents or any mode of internalization. The *E. coli* Cu^{2+} binding isotherm (Figure 5.6 A) is scattered and indicates a low degree of binding. The data presented shows a 10% or less removal of Cu^{2+} from solution when the total copper concentration is 10 ppb or greater.

The copper binding isotherm for HA is shown in Figure 5.6 B. Normalized data for Cu^{2+} binding collapse onto a single isotherm for HA concentrations ranging from 3 to 60 mg C/L. For subsequent material balance analyses, the normalized isotherm data, expressed as N_{HA} = number of Cu ions bound per mg C HA, were fitted to an empirical equation:

$$N_{HA} = \left(\frac{3.34\ C_{free}}{40.49 + \ C_{free}} \right) 10^{17} \tag{5.3}$$

where C_{free} is the free copper concentration in ppb. The empirical equation for Cu^{2+} binding to HA fits well to a Langmuir isotherm fit, though we do not ascribe any physical meaning to this. It is meant solely as a means to estimate copper binding. Bertuccio and Tilton also obtained a binding isotherm with a Langmuir fit for HA binding to silver.[126] One can compare the slopes of the two equations in the linear region to compare the affinity of both metal ions to HA. When comparing these two slopes, the slope for the Cu^{2+} binding isotherm was 4.7 times higher than the slope for the Ag^+ binding isotherm. This significantly higher slope for Cu^{2+} suggests that this ion has a much higher thermodynamic binding affinity for HA than Ag^+ and would support the idea that HA is better at mitigating copper than silver toxicity as observed earlier.
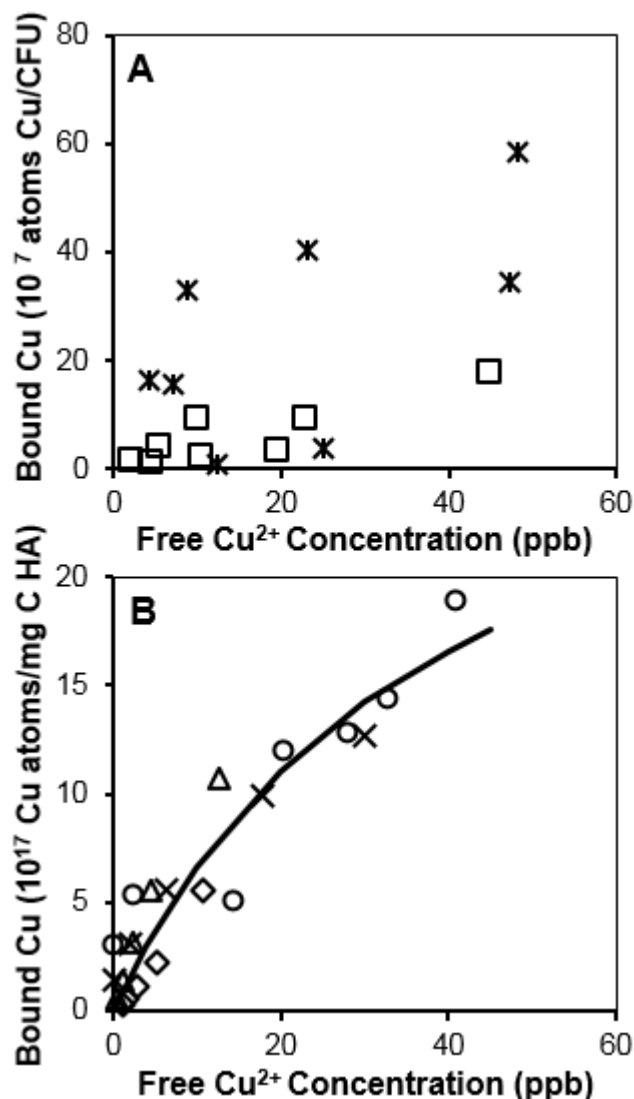
Figure 5.6. Binding data for Cu to *E. coli* (A) and to Pahokee peat humic acid (B). Different symbols represent different inoculum concentrations of $OD_{600} = 0.01(\sim 10^7 \, CFU/mL$, black stars) and 0.05 ($\sim 5 \times 10^7$, black squares) (A) or HA concentrations of 3 (black circles), 6 (crosses), 12 (triangles) and 60 mg C/L HA (diamonds). To aid comparison of bacteria or HA binding, assuming a dry mass of 0.33 pg per bacterium,[242] with carbon content 47%[243], 10 million Cu atoms/CFU would correspond to 6.4×10^{16} Cu ions/mg C bacteria.

A material balance was performed around the entire system for unbound free copper concentrations when *E. coli* and humic acid are both present. For 10^5, 10^6 and 10^7 CFU/mL

without HA, the respective MICs are 78 ± 7 ppb Cu^{2+}, $140 - 10$ ppb Cu^{2+} and $320 - 40$ ppb Cu^{2+} (In cases where the symbol is only a negative sign, no growth was seen at the reported concentration and the conservative estimate was made for potential lower MIC values). Since minimal binding to *E. coli* was observed and no copper-phosphate precipitates form at these listed concentrations we assume that the MIC is the free Cu^{2+} necessary to inhibit growth. When 60 mg C/L HA is present, after using the humic acid binding isotherm, the free available copper concentrations decrease to 2.84 ± 0.2 ppb Cu^{2+}, $4.31 - 2.82$ ppb Cu^{2+}, and $9.10 - 8.54$ ppb Cu^{2+} for 10^5, 10^6, and 10^7 CFU/mL respectively. These free copper concentrations are significantly lower than the MICs, indicating that the decrease in free Cu^{2+} concentration caused by HA binding is the likely cause of the reduced copper toxicity to *E. coli*.

5.3.4 Effect of HA on Oxidative Stress and Gene Expression

For ROS experiments, *E. coli* were exposed to 300 ppb Cu^{2+} with initial inoculum concentrations of 10^7 and 10^8 CFU/mL. 300 ppb Cu^{2+} is near the MIC for the initial inoculum concentration of 10^7 CFU/mL. The fluorescent probe H_2DCFDA was used to indirectly assess ROS levels inside *E. coli* with and without copper. H_2DCFDA is a non-fluorescent molecule that freely enters *E. coli* and then is hydrolyzed by esterases to remove the diacetate group and further reacts with ROS to form the fluorescent molecule dichlorofluorescein (DCF).[190,191] Greater ROS concentrations yield greater fluorescence emission. For 10^7 CFU/mL initial inocuum concentration, 300 ppb Cu produced a negligible amount of ROS produced after 3 h of exposure that was indistinguishable from the copper-free control (Figure 2.8). However, after longer periods of exposure to 300 ppb Cu^{2+} (18 to 24 h), significant increases in ROS were observed. Thus, 20 h was selected as the exposure time for all subsequent ROS analysis

experiments.　Minimal ROS production after short copper exposure periods has been reported previously.[42,190].

ROS determinations for 20 h exposure to 300 ppb Cu^{2+} are summarized in Figure 5.7. The 10^8 CFU/mL initial inoculum samples yielded 26.7-fold lower ROS production as indicated by fluorescence emission intensity than 10^7 CFU/mL. These ROS signals correspond to 1.8-fold or 23-fold increases relative to copper-free controls. The inoculum effect observed in the context of growth inhibition is also manifested in terms of an inoculum concentration-dependent level of ROS production.

Before considering the effect of HA on Cu^{2+}-induced ROS production, control experiments were conducted to determine whether HA may have an intrinsic effect on ROS production in *E. coli* suspensions. ROS signals for control *E. coli* suspensions that were not exposed to copper were twice as high in MDM with 60 mg C/L HA as in HA-free MDM, but subsequent experiments determined that this was not the result of an HA effect on ROS production. Rather, fluorescence measurements with HA but no cells or ROS probes showed that this increase was simply due to fluorescence emission from HA. This has been reported previously.[218,219] . *E. coli* 20 h copper exposure experiments conducted with 60 mg C/L HA with

an initial inoculum concentration of 10^7 CFU/mL yielded the same results with 300 ppb Cu^{2+} and with no added Cu^{2+}. ROS production was completely suppressed by 60 mg C/mL HA.
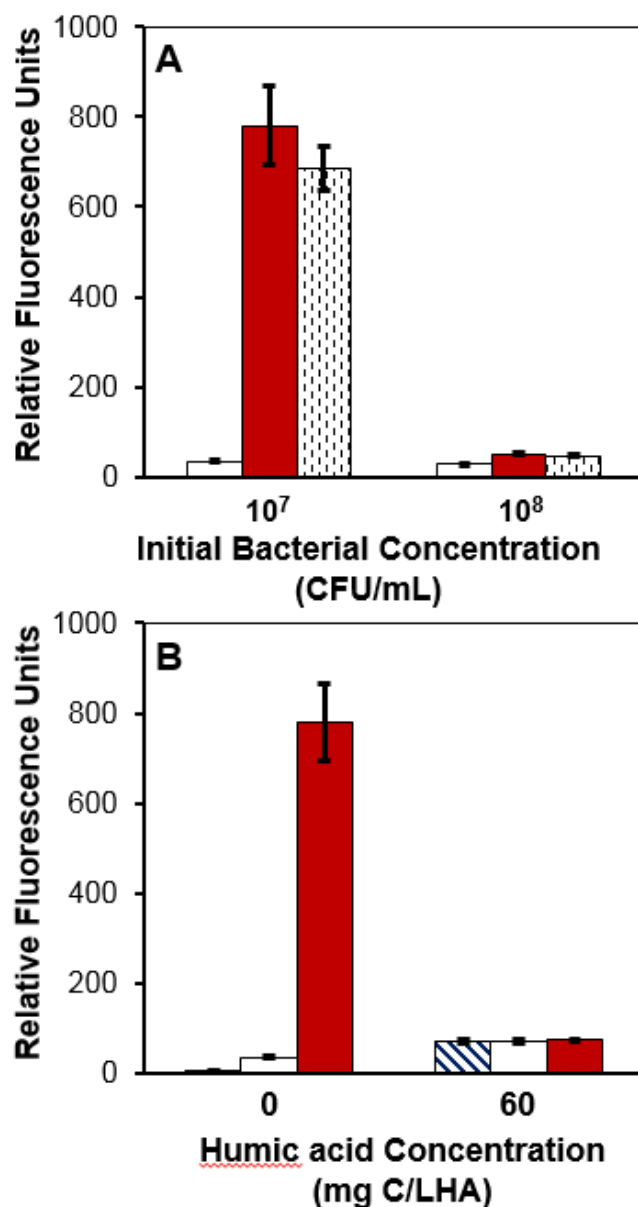
Figure 5.7. Fluorescence measurements from probe molecule H_2DCFDA after 20 h of exposure. ROS signals when comparing two different inoculum concentrations (A) and when humic acid is added to media for an initial inoculum concentration of 10^7 CFU/mL (B). White bars represent the control, when bacteria are only exposed to signaling molecule, red bars represent *E. coli* exposed to 300 ppb Cu^{2+}, black dashed bars represent the signal after exposure to 2 mM H_2O_2 (positive control), and blue striped bars represent media without any bacteria or probe molecules.

Measurement of fluorescence from the H_2DCFDA probe did not suggest enhanced oxidative stress after short times of exposure. It is important to also monitor other signs of copper toxicity for bacteria. Moore and coworkers observed that ROS is not produced in short periods of *E. coli* copper exposure and also determined by gene expression analysis for five genes that are related to oxidative stress (*ahpC*, *btuE*, *katG*, *sodA*, and *yqhD*) that oxidative stress responses were not present after 30 minutes of copper exposure.[143] They showed that copper- and protein damage-responsive genes, e.g., *cpxP*, are significantly upregulated in *E. coli* within 30 min of Cu^{2+} exposure. Thus, in addition to monitoring ROS, four genes, *copA*, *cueO*, *cusC*, and *cpxP*, were measured to quantify amounts of gene upregulation when *E. coli* are exposed to 300 ppb Cu^{2+} for 30 minutes in MDM and MDM with 60 mg C/L HA. Fold changes in gene expression for *E. coli* when dosed or undosed with 300 ppb Cu^{2+} are presented in Figure 5.8 for *copA*, *cueO* and *cpxP*. Expression of *cusC* was also detected in the presence of Cu^{2+}; however, a fold-change comparison between dosed and undosed expression could not be made because after 40 cycles there were undetectable levels of *cusC* in all samples without copper. When 300 ppb Cu^{2+} was present, it was only in the absence of HA that this gene was expressed. Critical qPCR threshold values (C_t) for all genes and treatments can be found in Tables 5.3 and 5.4.
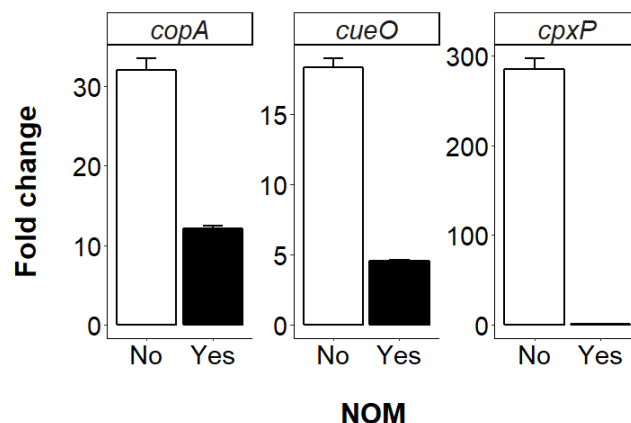
Figure 5.8. Relative gene expression for *copA*, *cueO*, and *cpxP* for *E. coli* at an initial inoculum concentration of 10^8 CFU/mL. Each fold change represents the increase in gene expression aftr 30 min exposure when comparing bacteria exposed to 300 ppb Cu^{2+} to when there is no Cu^{2+} added. Fold changes are compared in HA-free MDM (No) and MDM augmented 60 mg C/L HA (Yes). Measurements are from triplicate samples. Error bars represent standard deviations.

Table 5.3. *E. coli*, at an initial inoculum of 10^8 CFU/mL, was exposed to different concentrations of Cu^{2+} and humic acid. Changes in gene response were monitored via qT-PCR. This table shows the critical qPCR threshold values (C_t) for housekeeping gene *rrsA* as well as *copA, cueO, cusC and cpxP*. The higher the signal the fewer cycles are run to reach the detection signal.

Treatment	*rrsA*	*copA*	*cueO*	*cusC*	*cpxP*
No Cu^{2+} No HA	15.65 ± 0.33	28.26 ± 0.62	31.79 ± 0.49	NA	33.03 ± 0.49
300 ppb Cu^{2+} No HA	15.34 ± 0.18	23.05 ± 0.55	27.37 ± 0.35	38.06 ± 0.42	24.67 ± 0.62
300 ppb Cu^{2+} No HA	15.64 ± 0.18	29.69 ± 0.48	32.21 ± 0.24	NA	29.26 ± 0.43
300 ppb Cu^{2+} 60 mg C/L HA	15.53 ± 0.15	25.97 ± 0.21	29.9 ± 0.17	NA	29.6 ± 0.23

126

Table 5.4. *E. coli*, at an initial inoculum of 10^7 CFU/mL, was exposed to different concentrations of Cu^{2+} and humic acid. Changes in gene response were monitored via qT-PCR. This table shows the critical qPCR threshold values (C_t) for housekeeping gene *rrsA* as well as *copA, cueO, cusC and cpxP*. The higher the signal the fewer cycles are run to reach the detection signal.

Treatment	*rrsA*	*copA*	*cueO*	*cusC*	*cpxP*
No Cu^{2+} No HA	15.25 ± 0.07	26.71 ± 0.21	30.43 ± 0.12	NA	31.11 ± 0.24
300 ppb Cu^{2+} No HA	15.63 ± 0.13	23.34 ± 0.17	27.81 ± 0.18	38.78 ± 0.21	24.29 ± 0.2
300 ppb Cu^{2+} No HA	18.28 ± 0.06	31.72 ± 0.19	33.62 ± 0.28	NA	30.5 ± 0.16
300 ppb Cu^{2+} 60 mg C/L HA	18.45 ± 0.16	30.53 ± 0.2	31.46 ± 0.17	NA	30.56 ± 0.07

The significant decrease in gene expression in the presence of HA provides further support that the HA reduces bioavailable copper. Even though HA does bind a large amount of copper there is still some copper that is bioavailable. When using the isotherm for copper binding to HA (Figure 5.6 B), if 60 mg C/L HA is present for a total copper concentration of 300 ppb Cu^{2+} there is about 10 ppb Cu^{2+} that remains free. The results in Figure 5.3 would suggest that no *E. coli* growth inhibition would be expected for the 10^8 CFU/mL inoculum with such a low Cu^{2+} concentration, since even higher copper concentrations were required to inhibit growth of less concentrated inocula. Yet, *copA* and *cueO* genes were still upregulated 12-fold and 4.5-fold, respectively, for 300 ppb Cu^{2+} exposure at 10^8 CFU/mL. It has been reported that free copper concentrations as low as 10^{-21} M will induce an upregulation of copper regulatory genes.[220,221] The *cpxP* gene had similar levels of expression when HA is introduced in combination with Cu^{2+}

as when *E. coli* are in MDM without any copper (or HA). HA completely suppressed Cu^{2+}-induced *cpxP* upregulation. This constant level of gene expression indicates that HA binding decreased the free Cu^{2+} concentration to levels at which periplasmic protein degradation was not significant.

5.4 Conclusions

Copper toxicity is a gradual process where a range of copper concentrations can affect bacterial growth. Toxicity depends on a variety of conditions such as the initial inoculum concentration and the presence of NOM. In the environment there is a high presence of HA, especially in soils, which can effectively serve as a copper sink to protect microorganisms from copper toxicity. We see that HA is especially effective at reducing copper stress induced on bacteria within 30 min, as indicated by decreases in *copA*, *cueO* and *cpxP* gene expression, and over extended periods of exposure as indicated by decreased ROS production. The Cu^{2+} binding capability of HA would need to be taken into account when designing application regimens for intentionally applied antimicrobial Cu treatments, and it may mitigate microbial impacts of inadvertent Cu release into the environment. After comparing our binding isotherm results for Cu^{2+} results with Ag^+ binding isotherm obtained by Bertuccio and Tilton, the Cu^{2+} has a higher affinity for HA. Binding isotherms for different types of HA could be useful in estimating free copper concentrations for both toxicity and application analyses and could also be used for other metals of concern.

Chapter 6. Tween 80 influences on bacterial quorum sensing

6.1 Introduction

Chapters 3 – 5 showed the impact that metal salts and nanoparticles can have on bacteria. Silver and copper ion toxicity as well as silver nanoparticle toxicity towards bacteria are greatly dependent on a variety of factors including the metal used, the concentration of humic acid and the initial inoculum concentration.

Another potential threat to bacteria is the usage of surfactants for oil spill remediation. Surfactants used for oil spills have hydrophilic heads and hydrophobic tails that disperse oil into small droplets in the ocean. Certain bacteria are able to colonize petroleum/water interfaces, form biofilms, and metabolize the oil. This natural attenuation process plays a significant role in regulating the environmental response to both natural oil seepage and to spills. Dispersing oil into smaller droplets increases surface area available for oil consuming bacteria to metabolize.[222–226] This could be beneficial. However, other possible effects may disrupt the bacterial response. When the concentration of surfactant exceeds the critical micelle concentration (CMC) they will form micelles. A micelle is a self-assembled colloid that forms because of the amphiphilic character of surfactants. They are closed structures. Depending on concentration and surfactant type, they may be spheres, ellipsoids, or elongated worm-like structures. In water, the hydrophobic surfactant tails face the inside of the micelle and the polar head groups are on the surface facing the water to reduce polar-nonpolar interactions. Because of their low-polarity interior, micelles readily solubilize nonpolar compounds. Other amphiphilic compounds, such as long chain alcohols, often partition into micelles and serve as co-surfactants, mixing with the surfactants to promote micellization. This tendency for amphiphilic molecules to

partition into surfactant micelles could disrupt the quorum sensing process that plays a critical role in bacterial community behaviors, including biofilm formation. This possibility is addressed in this chapter.

Quorum sensing is the process where bacteria release molecules known as autoinducers in order for them to be able to monitor the bacterial population density, and when bacterial concentrations are high enough a population of bacteria will exhibit an upregulation in one or several gene(s). Quorum sensing allows bacteria to function similar to a multicellular organism with these responses, and some examples of quorum sensing include: bioluminescence, virulence and biofilm formation. Like surfactants, autoinducers are amphiphilic, with spatially separated hydrophilic and hydrophobic portions, much like the polar headgroup and nonpolar alkyl tail of a surfactant.[82,84,189,227]

Since autoinducers and surfactants both have amphiphilic structures, it is possible that autoinducers could interact with surfactants to reduce bioavailability. It is possible that autoinducers could be integrated into the micelle of a surfactant, potentially cluster with surfactant molecules or surfactants could interfere with autoinducers binding to bacterial receptors. These are all scenarios that could reduce available autoinducer concentrations and alter the ability of bacteria to sense local population density. If surfactants decrease the bioavailable autoinducer concentration, then a higher bacterial population density would be needed to produce the quorum sensing response. Since quorum sensing is important for bacterial populations to act together potential interference by surfactants could affect community behavior and ultimately affect aquatic ecosystems, especially since some studies have shown that surfactants found in Corexit can persist for up to four years in the environment.

The objective of this work is to identify potential effects that Tween 80, one surfactant found in the commercial oil dispersant Corexit, can have on bacterial growth and quorum sensing. *V. harveyi* will be used a model quorum sensing bacterium. One of the gene expressions upregulated through *V. harveyi* quorum sensing is bioluminescence. We will show that bacterial growth rates are affected minimally at concentrations below 40 mM Tween 80. The amount of luminescence detected in the presence of various Tween 80 concentrations decreased and when luminescence was normalized by optical density, a reporter of bacterial concentration, there was a decrease in luminescence at the same optical density when Tween 80 was present.

Bacterial growth curves were obtained with the help of undergraduate students Michelle Karabin and Tamara Amin. All LC-MS work and chromatograms were obtained with the help of Ph.D. candidate Eric McGivney in Civil and Environmental Engineering at Carnegie Mellon University.

6.2 Materials and Methods

6.2.1. Growth and Luminescence curves of *V. harveyi* with Tween 80

100 mL of AIM was inoculated with *V. harveyi* (ATCC-BAA 1116) in a 250 mL Erlenmeyer flask overnight at 30 °C. *V. harveyi* was orbitally rotated at 200 rpm. A black polystyrene clear-bottomed (Corning Costar) and an opaque white polystyrene 96 well-plate (Corning Costar) were used to monitor the optical density and the bioluminescence respectively. Both plates were treated with a UV light (Spectroline EN-180, 365 nm, 0.2A) for 20 minutes prior to use. Wells were filled with 100 µL of AIM, and two-fold serial dilutions were carried out between 0.08 mM and 40 mM of Tween 80. A stock of 80 mM Tween 80 was prepared by dissolving Tween 80 in AIM and then filter sterilizing the solution with a 0.22 m cellulose

acetate filter. When the suspension of *V. harveyi* reached an OD_{600} of 0.4 to 0.5 the suspension

was subcultured to and OD_{600} = 0.002. 100 µL of OD_{600} was added to all but one column which

was a cell-free control. Another column served as a surfactant-free control. These two plates

were then measured for initial optical density (Spectramax M2 Plate Reader, Molecular Devices)

and luminescence (Synergy H1 Hybrid Multi-Mode Microplate Reader, Biotek) and then

allowed to orbitally shake. Optical density and luminescence measurements were taken once

every 45 to 60 mins for 10 h.

6.2.2 Doping *V. harveyi* with autoinducers

N-butyryl homoserine lactone (AI-2, Cayman chemical) is an autoinducer produced by *V.*

harveyi for quorum sensing to induce luminescence. Studies have shown *V. harveyi* is sensitive

to the amount of AI-2 added and at high AI-2 concentrations, luminescence is reduced instead of

increased.[228] For this experiment a white, opaque 96-well plate was used and the plate was set up

the same as in 6.2.1. However, before adding the *V. harveyi* four adjacent rows were doped with

AI-2. In separate plates the final AI-2 concentration *V. harveyi* was exposed to was 0.4 µM

which were diluted down from a stock solution of 8 mM AI-2. Stock solutions were prepared

shortly before *V. harveyi* were added to the plates and were made in AIM.

6.2.3. Liquid Chromatography – Mass Spectrometry

Qualitative LC-MS analysis of Tween 80 – AI-2 interactions were performed on an

Agilent 1100 Series HPLC stack with an Agilent Eclipse XDB-C18 column and an Agilent 6430

Triple Quad MS operated in "MS2 Scan" mode. Run conditions are shown in Table 6.1. The

procedure is described in further detail here.[229]

The concentration of AI-2 was 250 µM and was dissolved in a buffered solution containing 0.22 g/L $(NH_4)HCO_3$ (≥99.0%,Sigma Aldrich). The pH was adjusted to 7.5 ± 0.02 by adding 0.2 N HCl. A stock solution of 80 mM Tween 80 was also prepared in this buffered solution. Samples were prepared fresh and run on the LC-MS within several hours after preparation. Four samples were prepared in the buffered solution: 250 µM AI-2, 20 mM Tween 80, 250 µM AI-2 + 20 mM Tween 80, and 250 µM AI-2 + 0.4 µM Tween 80 and run on LC-MS.

Table 6.1 LC-MS run conditions	
Injection volume	5.00 µL
Mobile phase A	H_20, 0.1% formic acid
Mobile phase B	Acetonitrile, 0.1% formic acid
Solvent run type	Isocratic, 1:1 mixture of mobile phase A:B
Flow rate	0.450 mL/min
LC column	Agilent Eclipse XBD-C18, 5 µM, 4.6 x 150 mm
Column temperature	30.0 °C
Ion source	ESI
Scan type	MRM
AI-2	
Precursor ion	172.2 u
Product ions (Frag., CE. energies)	102.1 u (130 V, 3 V)
Cell accelerator voltage	4 V
Polarity	Positive
Gas temperature	300 °C

Gas flow	11.0 L/min
Nebulizer	15.0 psi
Chromatogram type	Total ion count

6.3 Results and Discussion

6.3.1 Effects of Tween 80 on *V. harveyi* Growth

Tween 80 is a nonionic surfactant found in Corexit[56] and the CMC of Tween 80 is 0.01 mM. Tween 80 has been documented to solubilize proteins, isolate nuclei from cells and emulsifying and dispersing substances in medical and food products. [230,231] Since Tween 80 has solubilizing properties with other biological materials it is possible that it could also solubilize autoinducers.

In this study, *V. harveyi* were exposed to a range of Tween 80 concentrations between 0.08 mM and 40 mM. Optical densities and luminescence were measured over time for the different Tween 80 concentrations (Figures 6.1 and 6.3 respectively). The change in optical density was monitored to indicate the increase in bacterial concentration. The contribution of Tween 80 to optical density was small. The optical densities at 0 h were 0.034 ± 0.001 and 0.051 ± 0.005 for 0 mM and 40 mM Tween 80, respectively, with an initial bacterial concentration equal to an $OD_{600} = 0.001$. The growth rate constants (shown in Figure 6.2) are 0.63 ± 0.06 h^{-1} for all Tween 80 concentrations except 40 mM where the growth was minimal. The similar growth rate constants for the majority of Tween 80 concentrations suggests that Tween 80 is minimally inhibitory towards *V. harveyi* growth except at high concentrations of Tween 80 of 40 mM and above. Although toxicity, as indicated by impaired growth rates, is minimal until the

high concentrations, it is observed that higher concentrations of Tween 80 yield increased lag

phases for growth. It is possible that *V. harveyi* are using Tween 80 as an additional carbon

source. Other groups have suggested this for other surfactants found in Corexit.[150,153,232]   It is not

clear whether the growth rate constant was significantly decreased with 40 mM Tween 80 or the

lag phase extended beyond the end of the experiment.
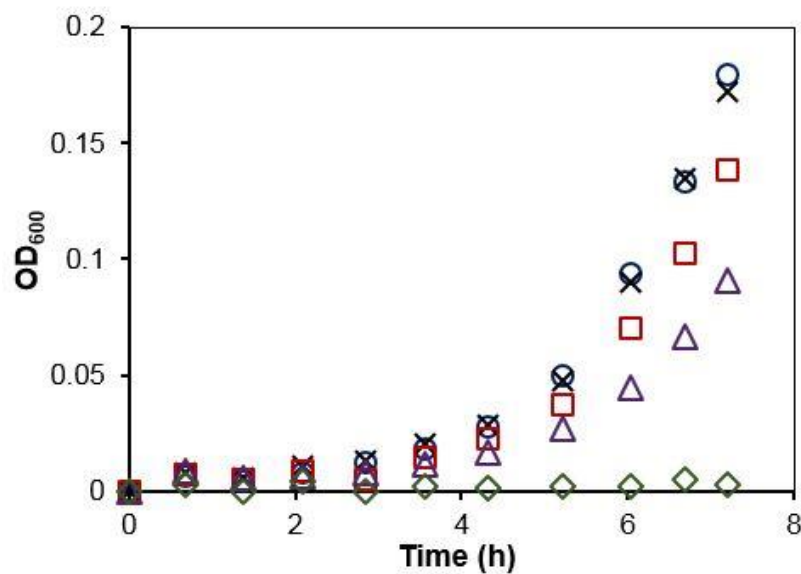
Figure 6.1. Representative growth curves for *V. harveyi* at an initial inoculum of OD_{600} = 0.001 when exposed to 0 mM (blue circles), 0.08 mM (black crosses), 2.5 mM (red squares), 10 mM (purple triangles) and 40 mM (green diamonds) of Tween 80 (n = 8). Error bars are smaller than markers
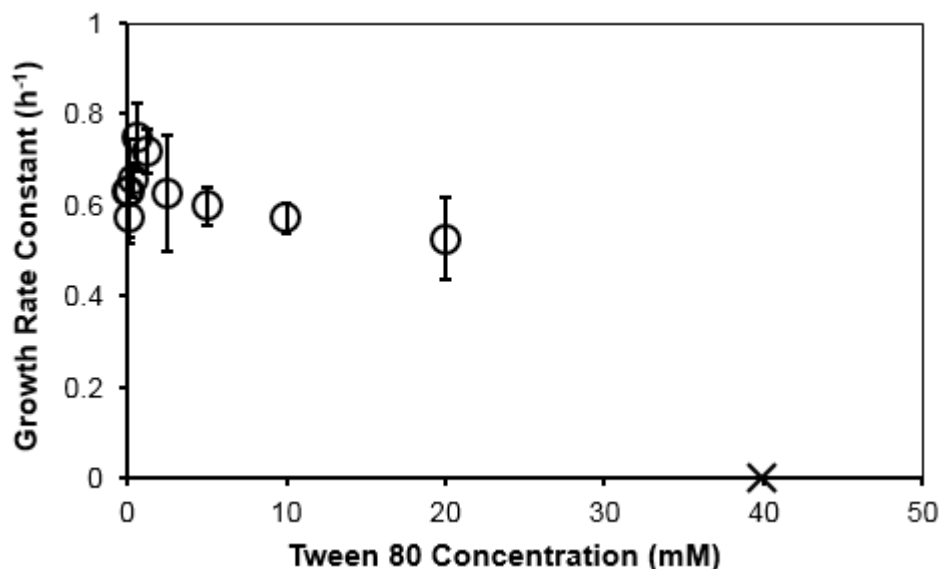
Figure 6.2. Growth rate constants for *V. harveyi* when exposed to concentrations between 0.08 and 40 mM of Tween 80 (n = 8). Error bars represent 95% confidence intervals. 40 mM is marked with an x to indicate uncertain origin of effect.

6.3.2 Effects of Tween 80 on Quorum Sensing

Bioluminescence is one product from the quorum sensing of *V. harveyi*. This is an ideal system to use for monitoring quorum sensing since luminescence can be read with a plate reader. The luminescence intensity is reported in "relative luminescence units" as is customary for luminescence instruments. It is "relative" only in the sense that the intensity has not been calibrated against a reference standard. It is useful for relative comparisons for different experimental conditions. The word "relative" does not imply that the data is normalized in any way. Figure 6.3 shows the luminescence of *V. harveyi* over time for different Tween 80 concentrations. In these cases there are significant differences in the luminescence signal between *V. harveyi* with and without Tween 80. Even concentrations as low as 0.08 mM Tween

80 greatly reduced the amount of luminescence emitted by the *V. harveyi*. Note that 0.08 mM is still well above the CMC for Tween 80, so micelles were present.
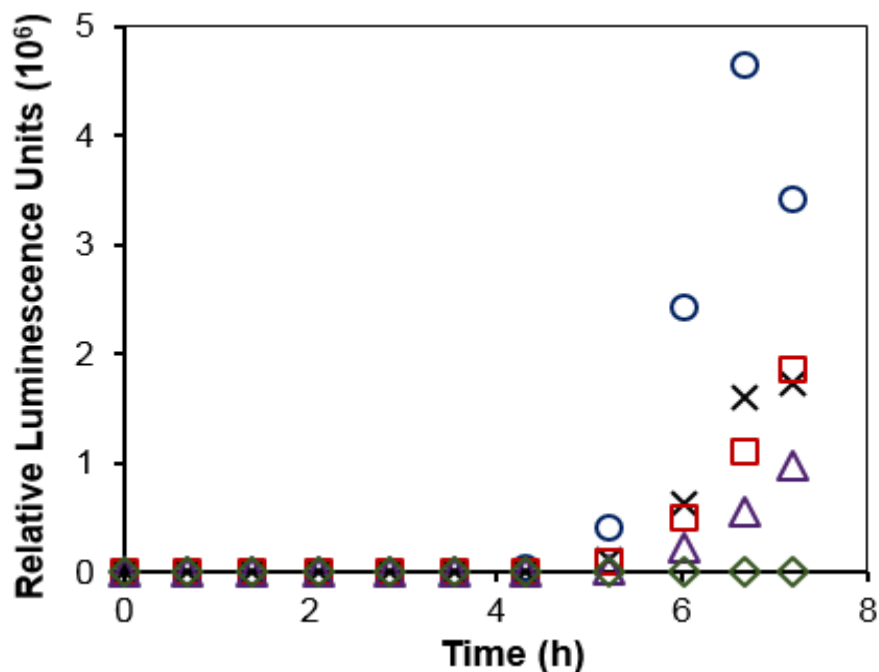
Figure 6.3. Luminescence curves for *V. harveyi* at an initial inoculum of $OD_{600} = 0.001$ when exposed to 0 mM (blue circles), 0.08 mM (black crosses), 2.5 mM (red squares), 10 mM (purple triangles) and 40 mM (green diamonds) of Tween 80 (n = 8). Error bars are smaller than markers

As seen in Figure 6.1 there was an increase in lag times for bacterial growth. It is possible that these delays in growth could affect the amounts of luminescence at the different times, simply because there were fewer bacteria producing autoinducers and fewer bacteria to luminesce. At high Tween concentrations, if there are low concentrations of *V. harveyi* due to the increased lag phase, the low levels of luminescence could be attributed to the differences in bacterial concentrations and not due to an inhibition of quorum sensing. Thus, we show in Figure 6.4 the amounts of luminescence at the respective optical densities for several Tween 80 concentrations.

Here luminescence is used as a proxy for monitoring quorum sensing. The decreases in luminescence for *V. harveyi* at optical densities that are approximately the same when Tween is added indicates that Tween is indeed affecting the process of *V. harveyi* quorum sensing, in a manner that would be consistent with decreased bioavailability of autoinducers. However, the mechanism is uncertain.
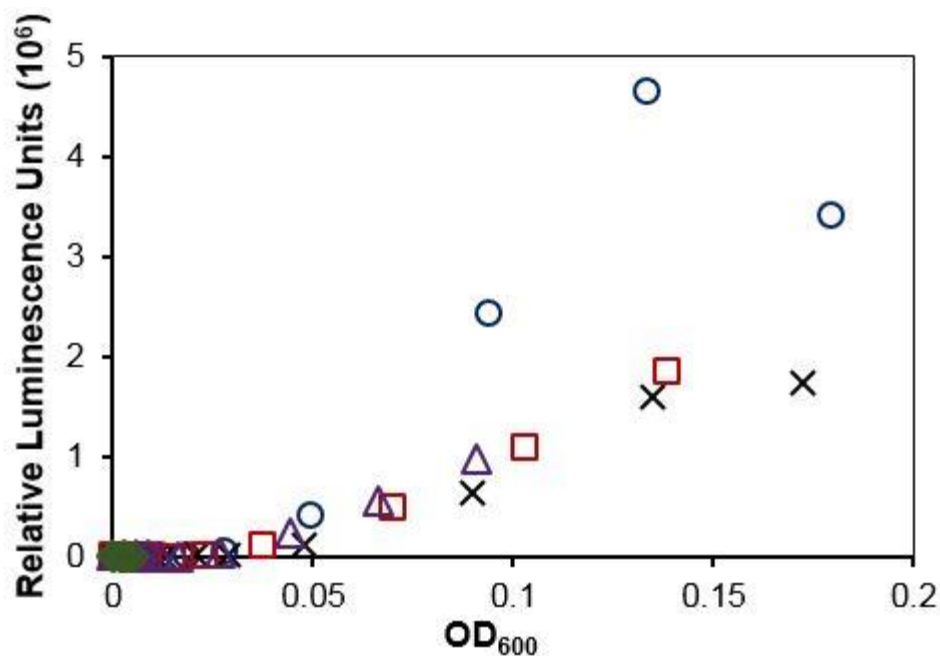
Figure 6.4. *V. harveyi* luminescence profiles at the respective optical densities when measurements were taken. The initial inoculum of $OD_{600} = 0.001$ when exposed to 0 mM (blue circles), 0.08 mM (black crosses), 2.5 mM (red squares), 10 mM (purple triangles) and 40 mM (green diamonds) of Tween 80 (n = 8). Error bars are smaller than markers

6.3.3 Tween 80 interactions with AI-2

AI-2 is an autoinducer produced by *V. harveyi* for quorum sensing. This autoinducer is involved in turning on the luminescence gene for *V. harveyi*.[82,83] AI-2 was used as a means to probe the mechanism behind Tween 80 interfering with the quorum sensing process. AI-2 was

added to suspensions of *V. harveyi* to determine if Tween 80 prevents receptors on the bacteria from receiving the autoinducer.

Vilchez and coworkers have shown that bacteria are sensitive to the ambient concentration of autoinducer and if the concentration of autoinducer is too high quorum sensing is inhibited rather than enhanced.[228] The same group identified appropriate AI-2 concentrations to enhance the gene response, luminescence, for *V. harveyi*. Based on the findings of this group, *V. harveyi* were exposed to a final concentration of 0.4 µM AI-2. Figure 6.5 shows the luminescence of *V. harveyi* with and without AI-2 when exposed to several Tween 80 concentrations. When the AIM was augmented with 0.4 µM AI2, *V. harveyi* responded positively and luminesced more than in the absence of AI-2. This elevated response by *V. harveyi* suggests that Tween 80, at least, does not completely inhibit receptors from receiving AI-2 molecules.
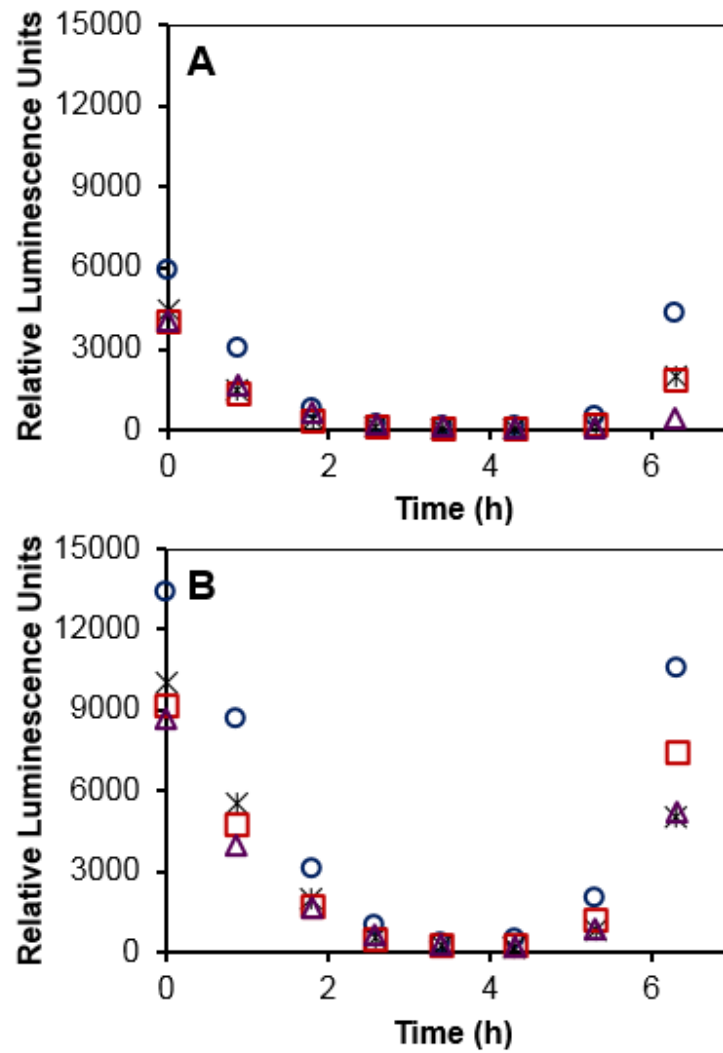
Figure 6.5. *V. harveyi* luminescence profiles over time with 0 µM AI2 (A) and 0.4 µM AI2 added. Symbols represent Tween 80 concentrations of 0 mM (blue circles), 0.63 mM (black stars), 2.5 mM (red squares) and 10 mM (purple triangles). *V. harveyi* were subcultured to an initial $OD_{600} = 0.001$.

The initial decrease in luminescence is because the bacterial culture was diluted form a high concentration of bacteria that were luminescing, down to $OD_{600} = 0.001$. Thus the early stages represent the response of the bacteria to dilution. The main point is the subsequent

increase in luminescence at later times, as the bacteria population increases and crosses the luminescence quorum sensing threshold again. AI-doped samples developed luminescence to a greater extent than undoped samples.

Since *V. harveyi* are able to receive autoinducers in the presence of autoinducers there must be another mechanism to explain the decrease in quorum sensing with Tween 80. Since the molecular structures of autoinducers are generally "surfactant-like" possessing hydrophilic heads and hydrophobic tails, it is possible that the hydrophilic and hydrophobic moieties of Tween 80 could interact with the ones of AI-2 to change its bioavailability. At concentrations above the critical micelle concentration (CMC) it could be possible that the Tween 80 solubilizes the autoinducers and incorporates them into their micelles. The CMC of Tween 80 is 0.01 mM and the Tween 80 concentrations *V. harveyi* were exposed to in this study were 0.08 mM to 40 mM, all higher than the CMC of Tween 80. If Tween 80 interacts with the autoinducer it may reduce the free autoinducer concentration to reduce quorum sensing.

LC-MS was used to detect mass peaks for AI-2, 20 mM Tween 80 and mixtures of AI-2 and Tween 80 to identify any changes in AI-2 availability (shown in Figure 6.6). Samples were injected directly to the MS, bypassing the chromatography system. A peak signal was monitored for AI-2 with an m/z of 172.2, the molecular weight of AI-2 with addition of a proton. The m/z of 172.2 was also monitored for 20 mM Tween 80 to identify any contributions Tween 80 may have at this signal, but no counts were measured. The counts detected at an m/z of 172.2 were measured for 0.4 µM of AI-2 and served as the control. Any reduction in counts was assumed to be attributed to an interaction between AI-2 and Tween 80. When 20 mM Tween 80 was added to AI-2 the signal at an m/z of 172.2 was eliminated. However, when 0.4 µM of Tween 80, several orders of magnitude less than the CMC of Tween 80, was added to AI-2, there was only a

slight decrease in counts. These differences in counts at an m/z of 172.2 suggest that the Tween 80 micelles are interacting with AI-2 in a manner that prevented its detection by MS. More work needs to be done to determine how the interaction prevented AI-2 detection, but is taken as evidence for a strong interaction. This interaction may be the same interaction that reduces the quorum sensing response, and may serve to decrease the amount bioavailable and offset the natural process of quorum sensing performed by *V. harveyi*. This is consistent with AI partitioning into micelles, but this is not yet fully proven. We do not claim that this is the only mechanism explaining the dampening of quorum sensing.
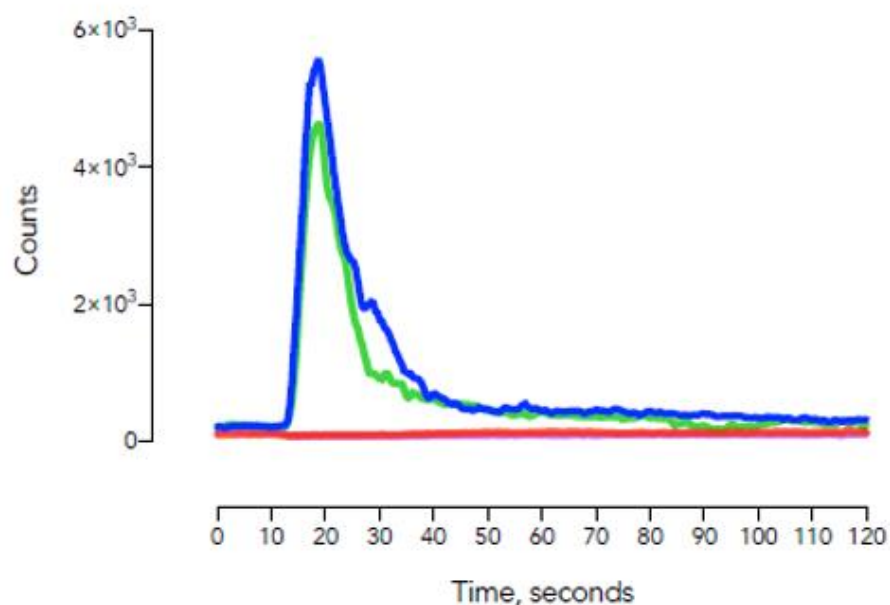
Figure 6.6. Chromatograms for 250 µM AI-2 in buffered solution (blue line), in buffered solution with 0.4 µM Tween 80 (green line), in buffered solution with 20 mM Tween 80 (red line), and 20 mM Tween 80 (purple line) in buffered solution without AI-2.

6.4 Conclusions

Since the BP oil spill of 2010 there have been many questions surrounding the current means to remediate oil spills. As of now, a surfactant solution such as Corexit is added to oil slicks to break up oil into small droplets that can be processed by oil consuming organisms such as bacteria.[57,61,150] Although some groups have seen no toxicity of surfactants to bacteria,[66,70,153] the findings in this study suggest that toxicity may not be the only metric necessary to evaluate the effects of dispersants on the environment. It is possible that this can extend to a much larger number of bacterial species in the environment that use quorum sensing.

Quorum sensing is commonly used by bacteria to perform a community function. The usage of dispersants could greatly affect this process and furthermore affect the interactions within a microbial community and cause microbial population shifts as seen by several other groups.[66–70]. Further studies should be performed to determine the impact that these dispersants have on quorum sensing for other bacteria and to develop a better understanding between autoinducers and surfactants.

Chapter 7. Conclusions and Future Directions

The overall objective of this work was to determine the impact of metal species on bacterial populations and the effects surfactants have on bacterial communities. This work addresses a wide range of issues concerning bacteria but most importantly two in particular, that is, (1) that toxicity for silver nanoparticles, as well as silver and copper ions, is highly dependent on the system for bacterial exposure, and (2) that surfactants may affect the ability for bacteria to communicate via quorum sensing.

This work suggests that toxicity from silver and copper ions and nanoparticles towards bacteria in the environment could be minimal if there are sufficient sinks to bind these metals and reduce the amount that is bioavailable. The presence of natural organic matter, extracellular polymeric substances and other organic material found in the environment provide a plethora of sinks that can mitigate silver and copper toxicity to bacteria in the environment.

Additionally this work indicates that synthetic surfactants such as Tween 80 can interrupt the quorum sensing amongst a bacterial community. This unintended effect could be significant if dispersants for oil spill remediation continue to be used and these surfactants persist for extended periods of time in the environment. The mechanism behind Tween 80 interference for *V. harveyi* quorum sensing should be further explored along with the impact that other surfactants can have in the quorum sensing process.

7.1 Summary of Observations

Determine silver toxicity in "environmentally" relevant systems and how this impacts bacterial colonization on surfaces coated with silver nanoparticles

Silver toxicity is dependent on a variety of factors. The initial inoculum concentration is one way to affect silver toxicity. The higher the initial inoculum concentration, the higher the silver dosage required to have the same effect on the bacteria. This inoculum effect is true for silver in the ionic and nanoparticle forms. The presence of humic acid can also increase *P. fluorescens* tolerance to silver ions and nanoparticles.

Humic acid and *P. fluorescens* both serve as effective silver sinks. Silver binding isotherms for humic acid and *P. fluorescens* were obtained from binding data and each batch of data collapsed onto a unique isotherm. MIC and MBCs were also collected for *P. fluorescens* for Ag^+ and AgNPs in MDM and MDM augmented with 60 mg C/L HA. These MICs and MBCs were used with the binding isotherms to estimate the critical amount of silver atoms per bacterium necessary to inhibit bacterial growth and kill bacteria. For the different inoculum concentrations tested in the same media the silver bound per bacterium was on the same order of magnitude. However, it was observed that when humic acid was added to the minimal media that *P. fluorescens* had a heightened sensitivity towards silver and the estimated critical thresholds for growth inhibition and death were reduced by several orders of magnitude. We hypothesize that the surface properties of *P. fluorescens* may change when humic acid is present.

During the colonization process for *P. fluorescens*, the key factor that affected the ability of *P. fluorescens* colonization on AgNP-decorated surfaces was the amount of silver sinks present to bind and reduce the amount of bioavailable silver. If the amount of silver bound per bacterium is below the critical threshold to kill bacteria (determined in Chapter 4) then the bacterial population could recover from the silver and eventually colonize the AgNP-decorated surface. However, if the bacterial population was exposed to enough silver to be above this critical threshold the planktonic bacteria would be unable to colonize the surface and would die.

Humic acid played a significant role and greatly affected the ability of *P. fluorescens* to colonize AgNP-decorated surfaces. Humic acid was able to mitigate toxicity so AgNP-decorated surfaces would be colonized by low inoculum concentrations of *P. fluorescens* that normally would be unable to colonize those same surfaces in the absence of humic acid. However, it was observed that humic acid reduces the driving force for bacteria to colonize glass substrates with and without AgNPs. It was hypothesized that the minimal media augmented with humic acid provides a more favorable media (as seen with the increased growth in media augmented with humic acid) so planktonic bacteria have a reduced driving force to colonize the surface.

Determine how initial inoculum concentrations and the presence of humic acid affect copper toxicity and identify potential mechanisms for copper toxicity mitigation

Copper toxicity is slightly dependent on the initial inoculum concentration, but to a much lesser extent than observed with *P. fluorescens*. However, this could be attributed to differences with species of bacteria, changes in the type of minimal media used, or the metal ion used. When humic acid is added to media it increased the MIC and MBCs for three different inoculum concentrations that spanned two orders of magnitude, by a factor of ten compared to the MIC and MBCs without humic acid.

Similar to the silver studies, copper binding isotherms for humic acid and *E. coli* were performed. There was minimal observed copper binding to *E. coli*, but there was significant copper binding to humic acid. The binding data for copper and humic acid collapsed onto a single isotherm.

Bacterial gene expressions and oxidative stress levels were measured to further understand how humic acid mitigates toxicity. It was observed that when humic acid is present the gene expressions for the copper responsive genes (*copA, cueO,* and *cusC*) as well as *cpxP*, a

146

gene that codes for membrane repair,[148] were significantly reduced. This decrease in gene expression suggests that less copper was present to upregulate genes. Additionally, when *E. coli* was exposed to cupric ions for longer times ROS levels were greatly reduced when humic acid was present as well as when the inoculum concentration was increased ten-fold. These observations further support the hypothesis by adding humic acid less copper is available to induce a toxic effect on *E. coli*.

Determine the impact that surfactants in commercial dispersants used for bioremediation can have on bacterial growth and quorum sensing

Tween 80 was used to probe the impact that commercial dispersants have on quourum sensing. *V. harveyi* were used as a model bacterium to identify potential effects. These bacteria were ideal since bioluminescence is one product of quorum sensing for *V. harveyi*. It was observed that Tween 80 concentrations up to 20 mM (on the same order of magnitude as the solubility limit of Tween 80) do not affect *V. harveyi* growth rates, though there was an observed increase in the lag time for growth. This increased lag time was 2 – 3 hours. Other groups have hypothesized this change could be in part due to *V. harveyi* attempting to metabolize surfactants in Corexit.[61,70]

Although most concentrations of Tween 80 did not have an effect on *V. harveyi* growth rates, it was observed that Tween 80 considerably affected quorum sensing. It was observed that luminescence was reduced up to 60% in media with Tween 80. Luminescence was a proxy used to monitor quorum sensing. The reduction in luminescence was an indication that quorum sensing was quenched in solutions with Tween 80. Using LC-MS, a mixture of Tween 80 and AI-2 were run through a size exclusion column. The peak for AI-2 was reduced when Tween 80

was above the CMC suggesting the autoinducer was incorporated into the Tween 80 micelle. Since autoinducer molecules possess hydrophilic and hydrophobic moieties this is a possibility. The solubilization of the autoinducers would then reduce the concentration of autoinducers available for communication amongst the bacterial population.

7.2 Original Contributions of this Work

The following is a list of the notable contributions of this work:

- Demonstrated that silver toxicity is highly dependent on the initial inoculum concentration. It was seen when using *P. fluorescens*- silver binding isotherms that the amount of Ag atoms/ bacterium was on the same order of magnitude for each inoculum concentration.

- Found that when free silver concentrations are below a critical threshold, bacteria are capable of colonizing a AgNP-decorated surface, but in the presence of humic acid there is a decreased driving force for colonization.

- Demonstrated that the presence of humic acid greatly reduces copper and silver toxicity to bacteria. The presence of humic acid reduces the bioavailable amount of copper and silver.

- Developed copper and silver binding isotherms to Pahokee peat humic acid. In both cases, data collapsed onto individual isotherms for copper and silver.

- Showed that quorum sensing for the bacterium *V. harveyi* is affected by Tween 80, one of the components for Corexit.

7.3 Future Directions

7.3.1 Surfactant effects on bacterial quorum sensing

Tween 80 was observed quenching quorum sensing for *V. harveyi*. To the authors knowledge this is the first time a group has observed this phenomenon. Since other groups have seen that surfactants can persist for up to years in the environment[58–60] it would be beneficial to investigate the extent that surfactants, used for oil spill remediation, affect quorum sensing. This combination of Tween 80 and AI2 is only one out of hundreds or thousands of potential surfactant-autoinducer interactions. Many species of bacteria produce their own autoinducer so it would be informative to determine if surfactant-autoinducer interactions can be classified based on certain chemical groups within both surfactant and autoinducer families. A comparison between synthetic and naturally produced surfactants should be compared to identify which ones are less intrusive on quorum sensing.

Another part that could be further explored is surfactant interactions with the bacteria surface. Since bacteria have receptors to receive the autoinducers it is possible that the surfactants could interact with the receptors in some way to decrease the rate at which autoinducer molecules are received.

One other part that is important to study is the change in response when bacteria are supposed to perform a particular function based on quorum sensing. A variety of bacteria with different quorum sensing-induced genes should be studied to observe how the quorum responsive genes are affected when different surfactants are present. For example, biofilm formation is often initiated from quorum sensing. Since over 99% of bacteria exist in the biofilm state[76,233] this is an especially important process that should be researched to identify effects.

Hopefully this type of work could be used to make better suggestions for dispersants to be used for oil spill remediation if dispersants will continue to be used.

7.3.2 Investigation of metal nanoparticle toxicity to bacteria in the presence of human proteins

AgNPs and CuONPs are effective antibacterial agents. From this research binding isotherms for both silver and copper ions were developed for Pahokee peat humic acid. It is possible that binding isotherms could be expanded and applied for other organic material in more biomedically relevant systems. A large amount of work in the biomedical field has investigated the inhibition of bacterial colonization on AgNP and CuONP coated surfaces.[36,234–239] However, a continuous issue is that a large amount of this research has been conducted in ideal systems with minimally organic material commonly found inside humans being present in the study.

For these studies it would be prudent to investigate metal ion and nanoparticle toxicity to *P. aeruginosa* and *S. aureus* which are two opportunistic pathogens that often infect hospital patients with compromised immune systems. *P. aeruginosa* and *S. aureus* have different cell wall structures where *P. aeruginosa* is Gram-negative and has a thinner wall and *S. aureus* which is Gram-positive has a thicker cell wall. MIC and MBCs in systems with and without human proteins (or human-like) proteins on those bacteria could be used to compare the mitigating effects of different proteins as well as differences in toxicity between the two species of bacteria. Along with this metal binding isotherms could be developed for each bacteria to assess how many metal ions needs to be delivered per bacterium to kill the cell. These types of studies could be useful to aid in future designs for metal nanoparticle coatings on prosthetics.

References

(1)   Wiesner, M. R.; Lowry, G. V; Alvarez, P.; Dionysiou, D.; Biswas, P. Assessing the Risks of Manufactured. *Environ. Sci. Technol.* **2006**, 4336–4345.

(2)   Eustis, S.; El-sayed, M. A. Why gold nanoparticles are more precious than pretty gold : Noble metal surface plasmon resonance and its enhancement of the radiative and nonradiative properties of nanocrystals of different shapes. *Chem. Soc. Rev.* **2006**, *35*, 209–217.

(3)   Project on Emerging Nanotechnologies http://www.nanotechproject.org/inventories/consumer/.

(4)   Navarro, E.; Baun, A.; Behra, R.; Hartmann, N. B.; Filser, J.; Antonietta, A. M.; Quigg, A.; Santschi, P. H.; Sigg, L. Environmental behavior and ecotoxicity of engineered nanoparticles to algae, plants, and fungi. *Ecotoxicology* **2008**, *17*, 372–386.

(5)   Radniecki, T. S.; Stankus, D. P.; Neigh, A.; Nason, J. A.; Semprini, L. Influence of liberated silver from silver nanoparticles on nitrification inhibition of Nitrosomonas europaea. *Chemosphere* **2011**, *85*, 43–49.

(6)   Kallman, E. N.; Oyanedel-Craver, V. A.; Smith, J. A. Ceramic Filters Impregnated with Silver Nanoparticles for Point-of-Use Water Treatment in Rural Guatemala. *J. Environ. Eng.* **2011**, *137*, 407–415.

(7)   Lin, S.; Huang, R.; Cheng, Y.; Liu, J.; Lau, B. L. T.; Wiesner, M. R. Silver nanoparticle-alginate composite beads for point-of-use drinking water disinfection. *Water Res.* **2013**, *47*, 3959–3965.

(8)   Quadros, M. E.; Pierson IV, R.; Tulve, N. S.; Willis, R.; Rogers, K.; Thomas, T. A.; Marr, L. C. Release of Silver from Nanotechnology-Based Consumer Products for Children. *Environ. Sci. Technol.* **2013**, *47*, 8894–8901.

(9)   von Goetz, N.; Lorenz, C.; Windler, L.; Nowack, B.; Heuberger, M.; Hungerbuhler, K. Migration of Ag- and TiO 2‑ (Nano)particles from Textiles into Artificial Sweat under Physical Stress: Experiments and Exposure Modeling. *Environ. Sci. Technol.* **2013**, *47*, 9979–9987.

(10)   Ren, D.; Smith, J. A. Proteinate-Capped Silver Nanoparticle Transport in Water-Saturated

151

Sand. *J. Environ. Eng.* **2013**, *139*, 781–787.

(11)   Peyrot, C.; Wilkinson, K. J.; Desrosiers, M.; Sauvé, S. Effects of silver nanoparticles on soil enzyme activities with and without added organic matter. *Environ. Toxicol. Chem.* **2014**, *33*, 115–125.

(12)   Piccinno, F.; Gottschalk, F.; Seeger, S.; Nowack, B. Industrial production quantities and uses of ten engineered nanomaterials in Europe and the world. *J. Nanoparticle Res.* **2012**, *14*, 1–11.

(13)   European_Commission. *Nanotechnology : the invisible giant tackling Europe's future challenges*; 2013.

(14)   Keller, A. A.; McFerran, S.; Lazareva, A.; Suh, S. Global life cycle releases of engineered nanomaterials. *J. Nanoparticle Res.* **2013**, *15*, 1–17.

(15)   Gottschalk, F.; Nowack, B. The release of engineered nanomaterials to the environment. *J. Environ. Monit.* **2011**, *13*, 1145–1155.

(16)   Peralta-Videa, J. R.; Zhao, L.; Lopez-Moreno, M. L.; de la Rosa, G.; Hong, J.; Gardea-Torresdey, J. L. Nanomaterials and the environment : A review for the biennium 2008 – 2010. *J. Hazard. Mater.* **2011**, *186*, 1–15.

(17)   Gomes, T.; Pinheiro, J. P.; Cancio, I.; Pereira, C. G.; Cardoso, C.; Bebianno, M. J. Effects of Copper Nanoparticles Exposure in the Mussel Mytilus galloprovincialis. *Environ. Sci. Technol.* **2011**, *45*, 9356–9362.

(18)   Shaw, B. J.; Handy, R. D. Physiological effects of nanoparticles on fish : A comparison of nanometals versus metal ions. *Environ. Int.* **2011**, *37*, 1083–1097.

(19)   Baker, T. J.; Tyler, C. R.; Galloway, T. S. Impacts of metal and metal oxide nanoparticles on marine organisms. *Environ. Pollut.* **2014**, *186*, 257–271.

(20)   Nowack, B.; Bucheli, T. D. Occurrence, behavior and effects of nanoparticles in the environment. *Environ. Pollut.* **2007**, *150*, 5–22.

(21)   Klaine, S. J.; Koelmans, A. A.; Horne, N.; Carley, S.; Handy, R. D.; Kapustka, L.; Nowack, B.; von de Kammer, F. Paradigms to assess the environmental impact of

manufactured nanomaterials. **2012**, *31*, 3–14.

(22) Maynard, A. D. A decade of uncertainty. *Nat. Nanotechnol.* **2014**, *9*, 159–160.

(23) Marambio-Jones, C.; Hoek, E. M. V. A review of the antibacterial effects of silver nanomaterials and potential implications for human health and the environment. *J. Nanoparticle Res.* **2010**, *12*, 1531–1551.

(24) Benn, T. M.; Westerhoff, P. Nanoparticle silver released into water from commercially available sock fabrics. *Environ. Sci. Technol.* **2008**, *42*, 4133–4139.

(25) Qin, H.; Cao, H.; Zhao, Y.; Zhu, C.; Cheng, T.; Wang, Q.; Peng, X.; Cheng, M.; Wang, J.; Jin, G.; et al. In vitro and in vivo anti-biofilm effects of silver nanoparticles immobilized on titanium. *Biomaterials* **2014**, *35*, 9114–9125.

(26) Roe, D.; Karandikar, B.; Bonn-Savage, N.; Gibbins, B.; Roullet, J.-B. Antimicrobial surface functionalization of plastic catheters by silver nanoparticles. *J. Antimicrob. Chemother.* **2008**, *61*, 869–876.

(27) Jonas, R. B. Acute copper and cupric ion toxicity in an estuarine microbial community. *Appl. Environ. Microbiol.* **1989**, *55*, 43–49.

(28) Thornton, J. A.; Rast, W. *Handbook of Copper Compounds and Applications*; 1997.

(29) Borkow, G.; Gabbay, J. Copper as a biocidal tool. *Curr. Med. Chem.* **2005**, *12*, 2163–2175.

(30) Taylor, E. L.; Holley, A. G.; Kirk, M. Pesticide Development. *South. Reg. Ext. For.* **2007**, *10*, 1–7.

(31) Liu, R.; Lal, R. Potentials of engineered nanoparticles as fertilizers for increasing agronomic productions. *Sci. Total Environ.* **2015**, *514*, 131–139.

(32) Grass, G.; Rensing, C.; Solioz, M. Metallic copper as an antimicrobial surface. *Appl. Environ. Microbiol.* **2011**, *77*, 1541–1547.

(33) Gabbay, J.; Borkow, G.; Mishal, J.; Zatcoff, R.; Shemer-Avni, Y. Copper Oxide Impregnated Textiles with Potent Biocidal Activities. *J. Ind. Text.* **2006**, *35*, 323–335.

(34)   Ren, G.; Hu, D.; Cheng, E. W. C.; Vargas-Reus, M. A.; Reip, P.; Allaker, R. P. Characterisation of copper oxide nanoparticles for antimicrobial applications. *Int. J. Antimicrob. Agents* **2009**, *33*, 587–590.

(35)   Gunawan, C.; Teoh, W. Y.; Marquis, C. P.; Amal, R. Cytotoxic Origin of Copper (II) Oxide Nanoparticles : Comparative Studies and Metal Salts. *ACS Nano* **2011**, 7214–7225.

(36)   Agnihotri, S.; Dhiman, N. K. Development of Nano-antimicrobial Biomaterials for Biomedical Applications. In *Advances in Biomaterials for Biomedical Applications*; Springer Singapore, 2016; pp. 479–545.

(37)   Suppan, S. Nanomaterials In Soil: Our Future Food Chain? *Inst. Agric. Trade Policy* **2013**, 1–17.

(38)   Islam, F.; Yasmeen, T.; Ali, Q.; Mubin, M.; Ali, S.; Arif, M. S.; Hussain, S.; Riaz, M.; Abbas, F. Copper-resistant bacteria reduces oxidative stress and uptake of copper in lentil plants: potential for bacterial bioremediation. *Environ. Sci. Pollut. Res.* **2016**, *23*, 220–233.

(39)   Klaine, S. J.; Alvarez, P. J. J.; Batley, G. E.; Fernandes, T. F.; Handy, R. D.; Lyon, D. Y.; Mahendra, S.; McLaughlin, M. J.; Lead, J. R. Nanomaterials in the environment: behavior, fate, bioavailability, and effects. *Environ. Toxicol. Chem.* **2008**, *27*, 1825–1851.

(40)   Colman, B. P.; Espinasse, B.; Richardson, C. J.; Matson, C. W.; Lowry, G. V; Hunt, D. E.; Wiesner, M. R.; Bernhardt, E. S. Emerging contaminant or an old toxin in disguise? Silver nanoparticle impacts on ecosystems. *Environ. Sci. Technol.* **2014**, *48*, 5229–5236.

(41)   Zevenhuizen, L. P.; Dolfing, J.; Eshuis, E. J.; Scholten-Koerselman, I. J. Inhibitory effects of copper on bacteria related to the free ion concentration. *Microb. Ecol.* **1979**, *5*, 139–146.

(42)   Bondarenko, O.; Ivask, A.; Käkinen, A.; Kahru, A. Sub-toxic effects of CuO nanoparticles on bacteria: Kinetics, role of Cu ions and possible mechanisms of action. *Environ. Pollut.* **2012**, *169*, 81–89.

(43)   Aruoja, V.; Dubourguier, H.; Kasemets, K.; Kahru, A. Toxicity of nanoparticles of CuO , ZnO and TiO 2 to microalgae Pseudokirchneriella subcapitata. *Sci. Total Environ.* **2008**, *407*, 1461–1468.

(44)   Blinova, I.; Ivask, A.; Heinlaan, M.; Mortimer, M.; Kahru, A. Ecotoxicity of nanoparticles of CuO and ZnO in natural water. *Environ. Pollut.* **2010**, *158*, 41–47.

(45)   Heinlaan, M.; Ivask, A.; Blinova, I.; Dubourguier, H.-C.; Kahru, A. Toxicity of nanosized and bulk ZnO, CuO and TiO2 to bacteria Vibrio fischeri and crustaceans Daphnia magna and Thamnocephalus platyurus. *Chemosphere* **2008**, *71*, 1308–1316.

(46)   Chernousova, S.; Epple, M. Silver as antibacterial agent: ion, nanoparticle, and metal. *Angew. Chem. Int. Ed. Engl.* **2013**, *52*, 1636–1653.

(47)   Xiu, Z.; Zhang, Q.; Puppala, H. L.; Colvin, V. L.; Alvarez, P. J. J. Negligible Particle-Specific Antibacterial Activity of Silver Nanoparticles. *Nano Lett.* **2012**, *12*, 4271–4275.

(48)   Cornelis, G.; Pang, L.; Doolette, C.; Kirby, J. K.; McLaughlin, M. J. Transport of silver nanoparticles in saturated columns of natural soils. *Sci. Total Environ.* **2013**, *463–464*, 120–130.

(49)   Suresh, A. K.; Pelletier, D. A.; Doktycz, M. J. Relating nanomaterial properties and microbial toxicity. *Nanoscale* **2013**, *5*, 463–474.

(50)   Dale, A. L.; Casman, E. A.; Lowry, G. V; Lead, J. R.; Viparelli, E.; Baalousha, M. Modeling Nanomaterial Environmental Fate in Aquatic Systems. *Environ. Sci. Technol.* **2015**, *49*, 2587–2593.

(51)   Fabrega, J.; Luoma, S. N.; Tyler, C. R.; Galloway, T. S.; Lead, J. R. Silver nanoparticles: behaviour and effects in the aquatic environment. *Environ. Int.* **2011**, *37*, 517–531.

(52)   Sun, T. Y.; Bornhoft, N. A.; Hungerbuhler, K.; Nowack, B. Dynamic Probabilistic Modeling of Environmental Emissions of Engineered Nanomaterials. *Environ. Sci. Technol.* **2016**, *50*, 4701–4711.

(53)   Garner, K. L.; Suh, S.; Keller, A. A. Assessing the Risk of Engineered Nanomaterials in the Environment: Development and Application of the nanoFate Model. *Environ. Sci. Technol.* **2017**, *51*, 5541–5551.

(54)   Alongi, D. M. The role of bacteria in nutrient recycling in tropical mangrove and other coastal benthic ecosystems. *Dev. Hydrobiol.* **1994**, *98*, 19–32.

(55)   *An Ecosystem Services Approach to Assessing the Impacts of the Deepwater Horizon Oil Spill in the Gulf of Mexico*; 2013.

(56)   Place, B.; Anderson, B.; Mekebri, A.; Furlong, E. T.; Gray, J. L.; Tjeerdema, R.; Field, J. A Role for Analytical Chemistry in Advancing our Understanding of the Occurrence, Fate, and Effects of Corexit Oil Dispersants. *Environ. Sci. Technol. Viewp.* **2010**, *44*, 6016–6018.

(57)   NRC. *Understanding oil spill dispersants: Efficacy and effects*; 2005.

(58)   Kujawinski, E. B.; Soule, M. C. K.; Valentine, D. L.; Boysen, A. K.; Longnecker, K.; Redmond, M. C. Fate of Dispersants Associated with the Deepwater Horizon Oil Spill. *Environ. Sci. Technol.* **2011**, *45*, 1298–1306.

(59)   White, H. K.; Lyons, S. L.; Harrison, S. J.; Findley, D. M.; Liu, Y.; Kujawinski, E. B. Long-Term Persistence of Dispersants following the Deepwater Horizon Oil Spill. *Environ. Sci. Technol. Lett.* **2014**, *1*, 295–299.

(60)   Gray, J. L.; Kanagy, L. K.; Furlong, E. T.; Kanagy, C. J.; Mccoy, J. W.; Mason, A.; Lauenstein, G. Presence of the Corexit component dioctyl sodium sulfosuccinate in Gulf of Mexico waters after the 2010 Deepwater Horizon oil spill. *Chemosphere* **2014**, *95*, 124–130.

(61)   Kleindienst, S.; Paul, J. H.; Joye, S. B. Using dispersants after oil spills: impacts on the composition and activity of microbial communities. *Nat. Rev. Microbiol.* **2015**, *13*, 388–396.

(62)   Goodbody-gringley, G.; Wetzel, D. L.; Gillon, D.; Pulster, E.; Miller, A.; Ritchie, K. B. Toxicity of Deepwater Horizon Source Oil and the Chemical Dispersant , Corexit H 9500 , to Coral Larvae. *PLoS One* **2013**, *8*, 1–10.

(63)   Almeda, R.; Hyatt, C.; Buskey, E. J. Ecotoxicology and Environmental Safety Toxicity of dispersant Corexit 9500A and crude oil to marine microzooplankton. *Ecotoxicol. Environ. Saf.* **2014**, *106*, 76–85.

(64)   Davis, B. M.; Richens, J. L.; Shea, P. O. Label-Free Critical Micelle Concentration Determination of Bacterial Quorum Sensing Molecules. *Biophys. J.* **2011**, *101*, 245–254.

(65)   You, J.; Xue, X.; Cao, L.; Lu, X.; Wang, J.; Zhang, L.; Zhou, S. Inhibition of Vibrio

biofilm formation by a marine actinomycete strain A66. *Appl. Microbiol. Biotechnol.* **2007**, *76*, 1137–1144.

(66) Overholt, W. A.; Marks, K. P.; Romero, I. C.; Hollander, D. J.; Snell, T. W.; Kostka, J. E. Hydrocarbon-Degrading Bacteria Exhibit a Species-Specific Response to Dispersed Oil while Moderating Ecotoxicity. *Appl. Environ. Microbiol.* **2016**, *82*, 518–528.

(67) Venosa, A. D.; Holder, E. L. Biodegradability of dispersed crude oil at two different temperatures. *Mar. Pollut. Bull.* **2007**, *54*, 545–553.

(68) Swannell, R. P. J.; Daniel, F. Effect of dispersants on oil biodegradation under simulated marine conditions. In *International Oil Spill Conference Proceedings*; 1997; pp. 169–176.

(69) Bælum, J.; Borglin, S.; Chakraborty, R.; Fortney, J. L.; Lamendella, R.; Mason, O. U.; Auer, M.; Zemla, M.; Bill, M.; Conrad, M. E.; et al. Deep-sea bacteria enriched by oil and dispersant from the Deepwater Horizon spill. *Environ. Microbiol.* **2012**, *14*, 2405–2416.

(70) Radniecki, T. S.; Schneider, M. C.; Semprini, L. The influence of Corexit 9500A and weathering on Alaska North Slope crude oil toxicity to the ammonia oxidizing bacterium , Nitrosomonas europaea. *Mar. Pollut. Bull.* **2013**, *68*, 64–70.

(71) Kalin, M. Passive mine water treatment: the correct approach? *Ecol. Eng.* **2004**, *22*, 299–304.

(72) McAnulla, C.; McDonald, I. R.; Murrell, J. C. Methyl chloride utilising bacteria are ubiquitous in the natural environment. *FEMS Microbiol. Lett.* **2001**, *201*, 151–155.

(73) Paul, D.; Pandey, G.; Pandey, J.; Jain, R. K. Accessing microbial diversity for bioremediation and environmental restoration. *Trends Biotechnol.* **2005**, *23*, 135–142.

(74) Moore, J. D.; Stegemeier, J. P.; Bibby, K.; Marinakos, S. M.; Lowry, G. V; Gregory, K. B. Impacts of Pristine and Transformed Ag and Cu Engineered Nanomaterials on Sur fi cial Sediment Microbial Communities Appear Short-Lived. *Environemntal Sci. Technol.* **2016**, *50*, 2641–2651.

(75) Toole, G. A. O.; Kolter, R. Flagellar and twitching motility are necessary for Pseudomonas aeruginosa biofilm development. *Mol. Microbiol.* **1998**, *30*, 295–304.

(76)   Stoodley, P.; Sauer, K.; Davies, D. G.; Costerton, J. W. Biofilms as complex differentiated communities. *Annu. Rev. Microbiol.* **2002**, *56*, 187–209.

(77)   Wingender, J.; Neu, T. R.; Flemming, H.-C. *Microbial Extracellular Polymeric Substances: Characterization, Sturcture and Function*; 1999.

(78)   Wingender, H.-C. F. and J. Relevance of microbial extracellular polymeric substances (EPSs) - Part 1: Structural and ecological aspects. *Water Sci. Technol.* **2001**, *43*, 1–8.

(79)   Watnick, P.; Kolter, R. Biofilm , City of Microbes. *J. Bacteriol.* **2000**, *182*, 2675–2679.

(80)   Costerton, J. W.; Lewandowski, Z.; Caldwell, D. E.; Korber, D. R.; Lappin-scott, H. M. Microbial biofilms. *Ann. Rev. Microbiol.* **1995**, *49*, 711–745.

(81)   Dunne Jr., W. M. Bacterial Adhesion : Seen Any Good Biofilms Lately ? *Clin. Microbiol. Rev.* **2002**, *15*, 155–166.

(82)   Miller, M. B.; Bassler, B. L. Quorum Sensing in Bacteria. *Annu. Rev. Microbiol.* **2001**, *55*, 165–199.

(83)   Waters, C. M.; Bassler, B. L. Quorum sensing: cell-to-cell communication in bacteria. *Annu. Rev. Cell Dev. Biol.* **2005**, *21*, 319–346.

(84)   Bassler, B. L.; Losick, R. Bacterially Speaking. *Cell* **2006**, *125*, 237–246.

(85)   Sondi, I.; Salopek-Sondi, B. Silver nanoparticles as antimicrobial agent: a case study on E. coli as a model for Gram-negative bacteria. *J. Colloid Interface Sci.* **2004**, *275*, 177–182.

(86)   Hwang, E. T.; Lee, J. H.; Chae, Y. J.; Kim, Y. S.; Kim, B. C.; Sang, B.-I.; Gu, M. B. Analysis of the toxic mode of action of silver nanoparticles using stress-specific bioluminescent bacteria. *Small* **2008**, *4*, 746–750.

(87)   Choi, O.; Deng, K. K.; Kim, N.-J.; Ross, L.; Surampalli, R. Y.; Hu, Z. The inhibitory effects of silver nanoparticles, silver ions, and silver chloride colloids on microbial growth. *Water Res.* **2008**, *42*, 3066–3074.

(88)   Navarro, E.; Wagner, B.; Marconi, F.; Kaegi, R.; Odzak, N.; Box, P. O.; Navarro, E.; Piccapietra, F.; Wagner, B.; Marconi, F.; et al. Toxicity of silver nanoparticles to

Chlamydomonas reinhardtii. *Environ. Sci. Technol.* **2008**, *42*, 8959–8964.

(89) Kittler, S.; Greulich, C.; Diendorf, J.; Köller, M.; Epple, M. Toxicity of Silver Nanoparticles Increases during Storage Because of Slow Dissolution under Release of Silver Ions. *Chem. Mater.* **2010**, *22*, 4548–4554.

(90) Greulich, C.; Braun, D.; Peetsch, A.; Diendorf, J.; Siebers, B.; Epple, M.; Köller, M. The toxic effect of silver ions and silver nanoparticles towards bacteria and human cells occurs in the same concentration range. *RSC Adv.* **2012**, *2*, 6981–6987.

(91) Das, P.; Xenopoulos, M. a.; Williams, C. J.; Hoque, M. E.; Metcalfe, C. D. Effects of silver nanoparticles on bacterial activity in natural waters. *Environ. Toxicol. Chem.* **2012**, *31*, 122–130.

(92) Yang, Y.; Wang, J.; Xiu, Z.; Alvarez, P. J. J. Impacts of silver nanoparticles on cellular and transcriptional activity of nitrogen-cycling bacteria. *Environ. Toxicol. Chem.* **2013**, *32*, 1488–1494.

(93) Yang, Y.; Quensen, J.; Mathieu, J.; Wang, Q.; Wang, J.; Li, M.; Tiedje, J. M.; Alvarez, P. J. J. Pyrosequencing reveals higher impact of silver nanoparticles than Ag+ on the microbial community structure of activated sludge. *Water Res.* **2014**, *48*, 317–325.

(94) Yoon, K.-Y.; Hoon Byeon, J.; Park, J.-H.; Hwang, J. Susceptibility constants of Escherichia coli and Bacillus subtilis to silver and copper nanoparticles. *Sci. Total Environ.* **2007**, *373*, 572–575.

(95) Dror-Ehre, A.; Mamane, H.; Belenkova, T.; Markovich, G.; Adin, A. Silver nanoparticle-E. coli colloidal interaction in water and effect on E. coli survival. *J. Colloid Interface Sci.* **2009**, *339*, 521–526.

(96) Fabrega, J.; Fawcett, S. R.; Renshaw, J. C.; Lead, J. R. Silver nanoparticle impact on bacterial growth: effect of pH, concentration, and organic matter. *Environ. Sci. Technol.* **2009**, *43*, 7285–7290.

(97) Fabrega, J.; Renshaw, J. C.; Lead, J. R. Interactions of silver nanoparticles with Pseudomonas putida biofilms. *Environ. Sci. Technol.* **2009**, *43*, 9004–9009.

(98) Fabrega, J.; Zhang, R.; Renshaw, J. C.; Liu, W.-T.; Lead, J. R. Impact of silver nanoparticles on natural marine biofilm bacteria. *Chemosphere* **2011**, *85*, 961–966.

(99)   Wirth, S. M.; Lowry, G. V; Tilton, R. D. Natural Organic Matter Alters Biofilm Tolerance to Silver Nanoparticles and Dissolved Silver. *Environ. Sci. Technol.* **2012**, *46*, 12687–12696.

(100)   Boenigk, J.; Beisser, D.; Zimmermann, S.; Bock, C.; Jakobi, J.; Grabner, D.; Groβmann, L.; Rahmann, S.; Barcikowski, S.; Sures, B. Effects of silver nitrate and silver nanoparticles on a planktonic community: general trends after short-term exposure. *PLoS One* **2014**, *9*, e95340.

(101)   Morones, J. R.; Elechiguerra, J. L.; Camacho, A.; Holt, K.; Kouri, J. B.; Ramírez, J. T.; Yacaman, M. J. The bactericidal effect of silver nanoparticles. *Nanotechnology* **2005**, *16*, 2346–2353.

(102)   Park, H.-J.; Kim, J. Y.; Kim, J.; Lee, J.-H.; Hahn, J.-S.; Gu, M. B.; Yoon, J. Silver-ion-mediated reactive oxygen species generation affecting bactericidal activity. *Water Res.* **2009**, *43*, 1027–1032.

(103)   Li, W.; Xie, X.; Shi, Q. Antibacterial activity and mechanism of silver nanoparticles on Escherichia coli. *Appl. Microb. Cell Physiol.* **2010**, *85*, 1115–1122.

(104)   Batchelor-mcauley, C.; Tschulik, K.; Neumann, C. C. M. Why are Silver Nanoparticles More Toxic Than Bulk Silver ? Towards Understanding the Dissolution and Toxicity of Silver Nanoparticles. *Int. J. Electrochem. Sci.* **2014**, *9*, 1132–1138.

(105)   Priester, J. H.; Singhal, A.; Wu, B.; Stucky, G. D.; Holden, P. A. Integrated approach to evaluating the toxicity of novel cysteine-capped silver nanoparticles to Escherichia coli and Pseudomonas aeruginosa. *Analyst* **2014**, *139*, 954–963.

(106)   Manshian, B. B.; Pfeiffer, C.; Garcia, B.; Heimerl, T.; Gallego, M.; Mo, M.; Pino, P.; Himmelreich, U.; Parak, W. J.; Soenen, S. J. High-Content Imaging and Gene Expression Approaches To Unravel the Effect of Surface Functionality on Cellular Interactions of Silver Nanoparticles. *ACS Nano* **2015**, *9*, 10431–10444.

(107)   Sudheer Khan, S.; Ghouse, S. S.; Chandran, P. Toxic effect of environmentally relevant concentration of silver nanoparticles on environmentally beneficial bacterium Pseudomonas putida. *Bioprocess Biosyst. Eng.* **2015**, *38*, 1243–1249.

(108)   Sheng, Z.; Liu, Y. Effects of silver nanoparticles on wastewater biofilms. *Water Res.* **2011**, *45*, 6039–6050.

(109) Akhavan, O.; Ghaderi, E. Self-accumulated Ag nanoparticles on mesoporous TiO2 thin film with high bactericidal activities. *Surf. Coatings Technol.* **2010**, *204*, 3676–3683.

(110) Flores, C. Y.; Diaz, C.; Rubert, A.; Benítez, G. a; Moreno, M. S.; Fernández Lorenzo de Mele, M. a; Salvarezza, R. C.; Schilardi, P. L.; Vericat, C. Spontaneous adsorption of silver nanoparticles on Ti/TiO2 surfaces. Antibacterial effect on Pseudomonas aeruginosa. *J. Colloid Interface Sci.* **2010**, *350*, 402–408.

(111) Kalishwaralal, K.; BarathManiKanth, S.; Pandian, S. R. K.; Deepak, V.; Gurunathan, S. Silver nanoparticles impede the biofilm formation by Pseudomonas aeruginosa and Staphylococcus epidermidis. *Colloids Surf. B. Biointerfaces* **2010**, *79*, 340–344.

(112) Flores, C. Y.; Min, A. G.; Grillo, C. A.; Salvarezza, R. C.; Vericat, C.; Schilardi, P. L. Citrate-Capped Silver Nanoparticles Showing Good Bactericidal Effect against Both Planktonic and Sessile Bacteria and a Low Cytotoxicity to Osteoblastic Cells. *Appl. Mater. Interfaces* **2013**, *5*, 3149–3159.

(113) Radzig, M. A.; Nadtochenko, V. A.; Koksharova, O. A.; Kiwi, J.; Lipasova, V. A.; Khmel, I. A. Antibacterial effects of silver nanoparticles on gram-negative bacteria: influence on the growth and biofilms formation, mechanisms of action. *Colloids Surf. B. Biointerfaces* **2013**, *102*, 300–306.

(114) Taglietti, A.; Arciola, C. R.; D'Agostino, A.; Dacarro, G.; Montanaro, L.; Campoccia, D.; Cucca, L.; Vercellino, M.; Poggi, A.; Pallavicini, P.; et al. Antibiofilm activity of a monolayer of silver nanoparticles anchored to an amino-silanized glass surface. *Biomaterials* **2014**, *35*, 1779–1788.

(115) Palanisamy, N. K.; Ferina, N.; Amirulhusni, A. N.; Mohd-Zain, Z.; Hussaini, J.; Ping, L. J.; Durairaj, R. Antibiofilm properties of chemically synthesized silver nanoparticles found against Pseudomonas aeruginosa. *J. Nanobiotechnology* **2014**, *12*, 2.

(116) Wirth, S. M.; Bertuccio, A. J.; Cao, F.; Lowry, G. V; Tilton, R. D. Inhibition of bacterial surface colonization by immobilized silver nanoparticles depends critically on the planktonic bacterial concentration. *J. Colloid Interface Sci.* **2016**, *467*, 17–27.

(117) Calder, A. J.; Dimkpa, C. O.; McLean, J. E.; Britt, D. W.; Johnson, W.; Anderson, A. J. Soil components mitigate the antimicrobial effects of silver nanoparticles towards a beneficial soil bacterium, Pseudomonas chlororaphis O6. *Sci. Total Environ.* **2012**, *429*, 215–222.

(118) Gunsolus, I. L.; Mousavi, M. P. S.; Hussein, K.; Bühlmann, P.; Haynes, C. L. Effects of Humic and Fulvic Acids on Silver Nanoparticle Stability, Dissolution, and Toxicity. *Environ. Sci. Technol.* **2015**, *49*, 8078–8086.

(119) Flemming, C. A.; Trevors, J. T. Copper toxicity and chemistry in the environment: a review. *Water. Air. Soil Pollut.* **1989**, *44*, 143–158.

(120) Kiaune, L.; Singhasemanon, N. *Pesticidal copper(I) oxide: environmental fate and aquatic toxicity. In Reviews of Environmental Contamination and Toxicology Volume 213*; 2011.

(121) Gajjar, P.; Pettee, B.; Britt, D. W.; Huang, W.; Johnson, W. P.; Anderson, A. J. Antimicrobial activities of commercial nanoparticles against an environmental soil microbe , Pseudomonas putida KT2440. *J. Biol. Eng.* **2009**, *13*, 1–13.

(122) Menkissoglu, O.; Lindow, S. E. Relationship of free ionic copper and toxicity of bacteria in solutions of organic compounds.pdf. *Dis. Control Pest Manag.* **1991**, *81*, 1258–1263.

(123) Rubilar, O.; Rai, M.; Tortella, G.; Diez, M. C.; Seabra, A. B.; Durán, N. Biogenic nanoparticles: Copper, copper oxides, copper sulphides, complex copper nanostructures and their applications. *Biotechnol. Lett.* **2013**, *35*, 1365–1375.

(124) Zhao, J.; Wang, Z.; Dai, Y.; Xing, B. Mitigation of CuO nanoparticle-induced bacterial membrane damage by dissolved organic matter. *Water Res.* **2013**, *47*, 4169–4178.

(125) Xu, C.; Peng, C.; Sun, L.; Zhang, S.; Huang, H.; Chen, Y.; Shi, J. Distinctive effects of TiO 2 and CuO nanoparticles on soil microbes and their community structures in fl ooded paddy soil. *Soil Biol. Biochem.* **2015**, *86*, 24–33.

(126) Bertuccio, A. J.; Tilton, R. D. Silver Sink Effect of Humic Acid on Bacterial Surface Colonization in the Presence of Silver Ions and Nanoparticles. *Environemntal Sci. Technol.* **2017**, *51*, 1754–1763.

(127) Pradhan, A.; Geraldes, P.; Seena, S.; Pascoal, C.; C??ssio, F. Humic acid can mitigate the toxicity of small copper oxide nanoparticles to microbial decomposers and leaf decomposition in streams. *Freshw. Biol.* **2016**, *61*, 2197–2210.

(128) Shah, V.; Jones, J.; Dickman, J.; Greenman, S. Response of soil bacterial community to metal nanoparticles in biosolids. *J. Hazard. Mater.* **2014**, *274*, 399–403.

(129) Brandt, K. K.; Holm, P. E.; Nybroe, O. Evidence for Bioavailable Copper - Dissolved Organic Matter Complexes and Transiently Increased Copper Bioavailability in Manure-Amended Soils as Determined by Bioluminescent Bacterial Biosensors. *Environemntal Sci. Technol.* **2008**, *42*, 3102–3108.

(130) Franklin, N. M.; Stauber, J. L.; Apte, S. C.; Lim, R. P. Effect of Initial Cell Density on the Bioavailability and Toxicity of Copper in Microalgal Bioassays. *Environ. Toxicol. Chem.* **2002**, *21*, 742–751.

(131) Macomber, L.; Imlay, J. A. The iron-sulfur clusters of dehydratases are primary intracellular targets of copper toxicity. *Proc. Natl. Acad. Sci. U. S. A.* **2009**, *106*, 8344–8349.

(132) Kaweeteerawat, C.; Chang, C. H.; Roy, K. R.; Liu, R.; Li, R.; Toso, D.; Fischer, H.; Ivask, A.; Ji, Z.; Zink, J. I.; et al. Cu Nanoparticles Have Different Impacts in Escherichia coli and Lactobacillus brevis than Their Microsized and Ionic Analogues. *ACS Nano* **2015**, *9*, 7215–7225.

(133) Johnson, M. D. L.; Kehl-Fie, T. E.; Rosch, J. W. Copper intoxication inhibits aerobic nucleotide synthesis in Streptococcus pneumoniae. *Metallomics* **2015**, *7*, 786–794.

(134) Gu, M.; Imlay, J. A. Superoxide poisons mononuclear iron enzymes by causing mismetallation. **2013**, *89*, 123–134.

(135) Imlay, J. A. The molecular mechanisms and physiological consequences of oxidative stress : lessons from a model bacterium. *Nat. Reivew Microbiol.* **2014**, *11*, 443–454.

(136) Honsa, E. S.; Johnson, M. D. L.; Rosch, J. W. The roles of transition metals in the physiology and pathogenesis of Streptococcus pneumoniae. **2013**, *3*, 1–15.

(137) Gunther, M. R.; Hanna, P. M.; Mason, R. P.; Cohen, M. S. Hydroxyl Radical Formation from Cuprous Ion and Hydrogen Peroxide A Spin Trapping Study.pdf. *Arch. Biochem. Biophys.* **1995**, *316*, 515–522.

(138) Macomber, L.; Rensing, C.; Imlay, J. A. Intracellular copper does not catalyze the formation of oxidative DNA damage in Escherichia coli. *J. Bacteriol.* **2007**, *189*, 1616–1626.

(139) Solioz, M.; Abicht, H. K.; Mermod, M.; Mancini, S. Response of Gram-positive bacteria

to copper stress. *J. Biol. Inorg. Chem.* **2010**, *15*, 3–14.

(140) Baker, J.; Sitthisak, S.; Sengupta, M.; Johnson, M.; Jayaswal, R. K.; Morrissey, J. A. Copper stress induces a global stress response in staphylococcus aureus and represses sae and agr expression and biofilm formations. *Appl. Environ. Microbiol.* **2010**, *76*, 150–160.

(141) Kershaw, C. J.; Brown, N. L.; Constantinidou, C.; Patel, M. D.; Hobman, J. L. The expression profile of Escherichia coli K-12 in response to minimal, optimal and excess copper concentrations. *Microbiology* **2005**, *151*, 1187–1198.

(142) Yamamoto, K.; Ishihama, A. Transcriptional response of Escherichia coli to external copper. *Mol. Microbiol.* **2005**, *56*, 215–227.

(143) Moore, J. D.; Avellan, A.; Noack, C. W.; Guo, Y. (Alex); Lowry, G. V; Gregory, K. B. Time-dependent bacterial transcriptional response to CuO nanomaterials differs from that of Cu2+ and provides insights into CuO nanomaterial toxicity mechanisms. *Environ. Sci. Nano* **2017**, *Submitted*.

(144) Rensing, C.; Fan, B.; Sharma, R.; Mitra, B.; Rosen, B. P. CopA: An Escherichia coli Cu(I)-translocating P-type ATPase. *Proc. Natl. Acad. Sci. U. S. A.* **2000**, *97*, 652–656.

(145) Grass, G.; Rensing, C. CueO Is a Multi-copper Oxidase That Confers Copper Tolerance in Escherichia coli. *Biochem. Biophys. Res. Commun.* **2001**, *286*, 902–908.

(146) Franke, S.; Grass, G.; Rensing, C.; Nies, D. H. Molecular Analysis of the Copper-Transporting Efflux System CusCFBA of Escherichia coli Molecular Analysis of the Copper-Transporting Efflux System CusCFBA of Escherichia coli. **2003**, *185*, 3804–3812.

(147) Outten, F. W.; Huffman, D. L.; Hale, J. A.; O'Halloran, T. V. The Independent cue and cus Systems Confer Copper Tolerance during Aerobic and Anaerobic Growth in Escherichia coli. *J. Biol. Chem.* **2001**, *276*, 30670–30677.

(148) Price, N. L.; Raivio, T. L. Characterization of the Cpx regulon in Escherichia coli strain MC4100. *J. Bacteriol.* **2009**, *191*, 1798–1815.

(149) Campo, P.; Venosa, A. D.; Suidan, M. T. Biodegradability of Corexit 9500 and Dispersed South Louisiana Crude Oil at 5 and 25 °C. *Environ. Sci. Technol.* **2013**, *47*, 1960–1967.

(150) Hamdan, L. J.; Fulmer, P. A. Effects of COREXIT EC9500A on bacteria from a beach oiled by the Deepwater Horizon spill. *Aquat. Microb. Ecol.* **2011**, *63*, 101–109.

(151) King, G. M.; Kostka, J. E.; Hazen, T. C.; Sobecky, P. A. Microbial Responses to the Deepwater Horizon Oil Spill : From Coastal Wetlands to the Deep Sea. *Annu. Revies Mar. Sci.* **2015**, *7*, 377–401.

(152) Dombrowski, N.; Donaho, J. A.; Gutierrez, T.; Seitz, K. W.; Teske, A. P.; Baker, B. J. Reconstructing metabolic pathways of hydrocarbon-degrading bacteria from the Deepwater Horizon oil spill Reconstructing metabolic pathways of hydrocarbon-degrading bacteria from the Deepwater Horizon oil spill. *Nat. Microbiol.* **2016**, *1*, 16057.

(153) Chakraborty, R.; Borglin, S. E.; Dubinsky, E. A.; Andersen, G. L.; Hazen, T. C. Microbial response to the MC-252 oil and Corexit 9500 in the Gulf of Mexico. *Front. Microbiol.* **2012**, *3*, 1–6.

(154) Aruguete, D. M.; Hochella, M. F. Bacteria-Nanoparticle Interactions and their Environmental Implications. *Environ. Chem.* **2010**, *7*, 3–9.

(155) Ma, R.; Levard, C.; Marinakos, S. M.; Cheng, Y.; Liu, J.; Michel, F. M.; Brown, G. E.; Lowry, G. V. Size-controlled dissolution of organic-coated silver nanoparticles. *Environ. Sci. Technol.* **2011**, *46*, 752–759.

(156) Barth, H. G. *Modern methods of particle size analysis*.

(157) Technology, W. Understanding dynamic light scattering http://www.wyatt.com/library/theory/dynamic-light-scattering-theory.html.

(158) Instruments, M. *Dynamic light scattering common terms defind*; 2011.

(159) Instruments, M. Dynamic Light Scattering Common Terms Defined http://www.biophysics.bioc.cam.ac.uk/wp-content/uploads/2011/02/DLS_Terms_defined_Malvern.pdf (accessed Nov 7, 2017).

(160) Barnett, C. E. Some applications of Wave-Length Turbidimetry in the Infrared. *J. Phys. Chem.* **1942**, *46*, 69–75.

(161) Malvern. Refractive Index - Gold NanoParticles http://www.materials-

talks.com/blog/2014/08/05/faq-how-important-are-refractive-index-absorption-for-nanoparticles/.

(162) Zalyubovskiy, S. J.; Bogdanova, M.; Deinega, A.; Lozovik, Y.; Pris, A. D.; An, K. H.; Hall, W. P.; Potyrailo, R. a. Theoretical limit of localized surface plasmon resonance sensitivity to local refractive index change and its comparison to conventional surface plasmon resonance sensor. *J. Opt. Soc. Am. A. Opt. Image Sci. Vis.* **2012**, *29*, 994–1002.

(163) Petryayeva, E.; Krull, U. J. Localized surface plasmon resonance: nanostructures, bioassays and biosensing--a review. *Anal. Chim. Acta* **2011**, *706*, 8–24.

(164) Burda, C.; Chen, X.; Narayanan, R.; El-Sayed, M. A. Chemistry and Properties of Nanocrystals of Different Shapes. *Chem. Rev.* **2005**, *105*, 1025–1102.

(165) Xia, Y.; Halas, N. J. Shape-Controlled Surface Plasmonic Nanostructures. *MRS Bull.* **2005**, *30*, 338–348.

(166) Chambers, W.; Fellers, T. J.; Davidson, M. W. Darkfield Illumination https://www.microscopyu.com/techniques/stereomicroscopy/darkfield-illumination.

(167) Detective, M. Bringing light to the dark field microscope http://www.microscope-detective.com/dark-field-microscope.html#sthash.7qChbzN2.lwi14P4u.dpbs.

(168) Fan, X.; Zheng, W.; Singh, D. J. Light scattering and surface plasmons on small spherical particles. *Light Sci. Appl.* **2014**, *3*, 1–14.

(169) Jain, P. K.; Huang, X.; El-sayed, I. H.; El-sayed, M. A. Noble Metals on the Nanoscale : Optical and Photothermal Properties and Some Applications in Imaging , Sensing , Biology , and Medicine. *Acc. Chem. Res.* **2008**, *41*, 7–9.

(170) Schindelin, J.; Arganda-carreras, I.; Frise, E.; Kaynig, V.; Longair, M.; Pietzsch, T.; Preibisch, S.; Rueden, C.; Saalfeld, S.; Schmid, B.; et al. Fiji : an open-source platform for biological-image analysis. *Nat. Methods* **2012**, *9*, 676–682.

(171) Gaines, P. Acid Digestions for Inorganic Samples https://www.inorganicventures.com/acid-digestions-inorganic-samples.

(172) Berghof. *Theory of Sample Preparation Using Acid Digestion , Pressure Digestion and*

Microwave Digestion (Microwave Decomposition); 2000.

(173) Zhang, C. (Carl). *Fundamentals of Environmental Sampling and Analysis*; 2007.

(174) Pettit, R. E. *Organic matter, humus, humate, humic acid, fulvic acid and humin: their importance in soil fertility and plant health*.

(175) Thurman, E. M. *Organic Geochemistry of Natural Waters*; Springer Netherlands: Dordrecht, 1985.

(176) International Humic Substances Society http://humic-substances.org/elemental-compositions-and-stable-isotopic-ratios-of-ihss-samples/.

(177) Company, G. E. *Summary of oxidation reactions in the Sievers Innovox TOC Analyzer*; 2015.

(178) Technologies, I. L. NDIR gas sensor light sources https://www.intl-lighttech.com/applications/light-sources/ndir-gas-sensor-lamps.

(179) Baum, M. M.; Kainovic, A.; Keeffe, T. O.; Pandita, R.; Mcdonald, K.; Wu, S.; Webster, P. Characterization of structures in biofilms formed by a Pseudomonas fluorescens isolated from soil. *BMC Microbiol.* **2009**, *13*, 1–13.

(180) Li, X. Z.; Hauer, B.; Rosche, B. Single-species microbial biofilm screening for industrial applications. *Biotechnol. Prod. Process Eng.* **2007**, *76*, 1255–1262.

(181) Hubalek, Z. Protectants used in the cryopreservation of microorganisms. *Cryobiology* **2003**, *46*, 205–229.

(182) Paoli, P. De. Biobanking in microbiology : From sample collection to epidemiology , diagnosis and research. *FEMS Microbiol. Rev.* **2005**, *29*, 897–910.

(183) Einarsson, H.; Snygg, B. G.; Eriksson, C. Inhibition of Bacterial Growth by Maillard Reaction Products. *J. Agric. Food Chem.* **1983**, *31*, 1043–1047.

(184) Plank, J. Doesn't play well with others- the chemistry of the autoclave http://bitesizebio.com/6128/doesn't-play-well-with-others-the-chemistry-of-the-autoclave/.

(185) Widdel, F. Theory and Measurement of Bacterial Growth. *Di dalam Grundpraktikum Mikrobiol.* **2007**, *4*, 1–11.

(186) Breed, R. S.; Dotterrer, W. D. The number of colonies allowable on satisfactory agar plates. *J. Bacteriol.* **1916**, *1*, 321–331.

(187) Bigelow National Center for Marine Algae and Microbiota. *NCMA Medium 7 : Mineral Solution*.

(188) Bigelow National Center for Marine Algae and Microbiota. *NCMA Medium 6 : Wolfe ' s Vitamin Solution*.

(189) Bassler, B. L. Small Talk : Cell-to-Cell Communication in Bacteria. *Cell* **2002**, *109*, 421–424.

(190) Karlsson, H. L.; Cronholm, P.; Gustafsson, J.; Möller, L. Copper oxide nanoparticles are highly toxic: A comparison between metal oxide nanoparticles and carbon nanotubes. *Chem. Res. Toxicol.* **2008**, *21*, 1726–1732.

(191) Fahmy, B.; Cormier, S. A. Toxicology in Vitro Copper oxide nanoparticles induce oxidative stress and cytotoxicity in airway epithelial cells. *Toxicol. Vitr.* **2009**, *23*, 1365–1371.

(192) Sudhandiran, G.; Shaha, C. Antimonial-induced Increase in Intracellular Ca2+ through Non-selective Cation Channels in the Host and the Parasite Is Responsible for Apoptosis of Intracellular Leishmania donovani Amastigotes. *J. Biol. Chem.* **2003**, *278*, 25120–25132.

(193) Lin, D.; Ji, J.; Long, Z.; Yang, K.; Wu, F. The influence of dissolved and surface-bound humic acid on the toxicity of TiO_2 nanoparticles to Chlorella sp. *Water Res.* **2012**, *46*, 4477–4487.

(194) Taglietti, A.; Diaz Fernandez, Y. a; Amato, E.; Cucca, L.; Dacarro, G.; Grisoli, P.; Necchi, V.; Pallavicini, P.; Pasotti, L.; Patrini, M. Antibacterial activity of glutathione-coated silver nanoparticles against Gram positive and Gram negative bacteria. *Langmuir* **2012**, *28*, 8140–8148.

(195) Amato, E.; Diaz-Fernandez, Y. a; Taglietti, A.; Pallavicini, P.; Pasotti, L.; Cucca, L.; Milanese, C.; Grisoli, P.; Dacarro, C.; Fernandez-Hechavarria, J. M.; et al. Synthesis,

characterization and antibacterial activity against Gram positive and Gram negative bacteria of biomimetically coated silver nanoparticles. *Langmuir* **2011**, *27*, 9165–9173.

(196) Feng, Q. L.; Wu, J.; Chen, G. Q.; Cui, F. Z.; Kim, T. N.; Kim, J. O. A mechanistic study of the antibacterial effect of silver ions on Escherichia coli and Staphylococcus aureus. *J. Biomedial Mater. Res.* **2000**, *52*, 662–668.

(197) Guo, Z.; Xue, J.; Liu, T.; Song, X.; Shen, Y.; Wu, H. Antibacterial mechanisms of silica/polydopamine/silver nanoparticles against gram positive and gram negative bacteria. *Micro Nano Lett.* **2014**, *9*, 210–214.

(198) Meyer, J.-M.; Geoffroy, V. A.; Baida, N.; Gardan, L.; Izard, D.; Lemanceau, P.; Achouak, W.; Palleroni, N. J. Siderophore Typing , a Powerful Tool for the Identification of Fluorescent and Nonfluorescent Pseudomonads. *Appl. Environ. Microbiol.* **2002**, *68*, 2745–2753.

(199) Lambert, R. J. W.; Johnston, M. D. Disinfection kinetics : a new hypothesis and model for the tailing of log-survivor / time curves. *J. Appl. Microbiol.* **2000**, 907–913.

(200) Firsov, A. A.; Vostrov, S. N.; Kononenko, O. V; Zinner, S. H.; Portnoy, Y. A. Prediction of the Effects of Inoculum Size on the Antimicrobial Action of Trovafloxacin and Ciprofloxacin against Staphylococcus aureus and Escherichia coli in an In Vitro Dynamic Model. *Antimicrob. Agents Chemother.* **1999**, *43*, 498–502.

(201) Santos, A. L.; Oliveira, V.; Baptista, I.; Henriques, I.; Gomes, N. C. M.; Almeida, A.; Correia, A.; Cunha, A. Wavelength dependence of biological damage induced by UV radiation on bacteria. *Arch. Microbiol.* **2013**, *195*, 63–74.

(202) Valappil, S. P.; Pickup, D. M.; Carroll, D. L.; Hope, C. K.; Pratten, J.; Newport, R. J.; Smith, M. E.; Wilson, M.; Knowles, J. C. Effect of Silver Content on the Structure and Antibacterial Activity of Silver-Doped Phosphate-Based Glasses. *Antimicrob. Agents Chemother.* **2007**, *51*, 4453–4461.

(203) Yang, Y.; Alvarez, P. J. J. Sublethal Concentrations of Silver Nanoparticles Stimulate Biofilm Development. *Environ. Sci. Technol. Lett.* **2015**, 150709100554007.

(204) Sutherland, I. W. Exopolysaccharides in biofilms, flocs and related structures. *Water Sci. Technol.* **2001**, *43*, 77–86.

(205) *Standard Test Method for Determining the Activity of Incorporated Antimicrobial Agent (s) In Polymeric or Hydrophobic Materials*; West Conshohocken, 2017; Vol. 8.

(206) Xiu, Z.; Ma, J.; Alvarez, P. J. J. Differential Effect of Common Ligands and Molecular Oxygen on Antimicrobial Activity of Silver Nanoparticles versus Silver Ions. *Environ. Sci. Technol.* **2011**, *45*, 9003–9008.

(207) Reinsch, B. C.; Levard, C.; Li, Z.; Wise, A.; Gregory, K. B.; Brown, G. E.; Lowry, G. V. Sulfidation of Silver Nanoparticles Decreases Escherichia coli Growth Inhibition. *Environ. Sci. Technol.* **2012**, *46*, 6992–7000.

(208) Teughels, W.; Van Assche, N.; Sliepen, I.; Quirynen, M. Effect of material characteristics and/or surface topography on biofilm development. *Clin. Oral Implants Res.* **2006**, *17*, 68–81.

(209) Morgan, T. D.; Wilson, M. The effects of surface roughness and type of denture acrylic on biofilm formation by Streptococcus oralis in a constant depth film fermentor. *J. Appl. Microbiol.* **2001**, *91*, 47–53.

(210) Mitik-Dineva, N.; Wang, J.; Truong, V. K.; Stoddart, P.; Malherbe, F.; Crawford, R. J.; Ivanova, E. P. Escherichia coli , Pseudomonas aeruginosa , and Staphylococcus aureus Attachment Patterns on Glass Surfaces with Nanoscale Roughness. *Curr. Microbiol.* **2009**, *58*, 268–273.

(211) De Prijck, K.; Nelis, H.; Coenye, T. Efficacy of silver-releasing rubber for the prevention of Pseuodomans aeruginosa biofilm formation in water. *Biofouling* **2007**, *23*, 405–411.

(212) Voinova, M. V.; Rodahl, M.; Jonson, M.; Kasemo, B. Viscoelastic Acoustic Response of Layered Polymer Films at Fluid-Solid Interfaces: Continuum Mechanics Approach. *Phys. Scr.* **1999**, *59*, 391–396.

(213) Helsel, D. R.; Hirsch, R. M. Statistical Methods in Water Resources, Techniques of Water Resources Investigations 04-A3. *U.S. Geol. Surv.* **2002**, *4-A3*, 523.

(214) Sirk, K. M.; Saleh, N. B.; Phenrat, T.; Kim, H.; Dufour, B.; Golas, P. L.; Matyjaszewski, K.; Lowry, G. V; Tilton, R. D. Effect of Adsorbed Polyelectrolytes on Nanoscale Zero Valent Iron Particle Attachment to Soil Surface Models Effect of Adsorbed Polyelectrolytes on Nanoscale Zero Valent Iron Particle Attachment to Soil Surface Models. *Environemntal Sci. Technol.* **2009**, *43*, 3803–3808.

(215) Miao, A. J.; Schwehr, K. A.; Xu, C.; Zhang, S. J.; Luo, Z.; Quigg, A.; Santschi, P. H. The algal toxicity of silver engineered nanoparticles and detoxification by exopolymeric substances. *Environ. Pollut.* **2009**, *157*, 3034–3041.

(216) Peng, S.; Stephan, R.; Hummerjohann, J.; Tasara, T. Evaluation of three reference genes of Escherichia coli for mRNA expression level normalization in view of salt and organic acid stress exposure in food. *FEMS Microbiol. Lett.* **2014**, *355*, 78–82.

(217) Livak, K. J.; Schmittgen, T. D. Analysis of Relative Gene Expression Data Using Real-Time Quantitative PCR and the 2- $\bar{X}$ ◌◌ C T Method. *Methods* **2001**, *25*, 402–408.

(218) Hayase, K.; Tsubota, H. Sedimentary humic acid and fulvic acid as fluorescent organic materials. *Geochim. Cosmochim. Acta* **1985**, *49*, 159–163.

(219) Mobed, J. J.; Hemmingsen, S. L.; Autry, J. L.; Mcgown, L. B. Fluorescence Characterization of IHSS Humic Substances : Total Luminescence Spectra with Absorbance Correction. *Environemntal Sci. Technol.* **1996**, *30*, 3061–3065.

(220) Changela, A.; Chen, K.; Xue, Y.; Holschen, J.; Outten, C. E.; O'Halloran, T. V; Mondragon, A. Molecular Basis of Metal-Ion Selectivity and Zeptomolar Sensitivity by CueR. *Science (80).* **2003**, *301*, 1383–1388.

(221) Ladomersky, E.; Petris, M. J. Copper tolerance and virulence in bacteria. *Metallomics* **2015**, *7*, 957–964.

(222) Ron, E. Z.; Rosenberg, E. Biosurfactants and oil bioremediation. *Curr. Opin. Biotechnol.* **2002**, *13*, 249–252.

(223) Atlas, R. M.; Hazen, T. C. Oil Biodegradation and Bioremediation : A Tale of the Two Worst Spills in U.S. History. *Environemntal Sci. Technol.* **2011**, *45*, 6709–6715.

(224) Mahmoudi, N.; Porter, T. M.; Zimmerman, A. R.; Fulthorpe, R. R.; Kasozi, G. N.; Silliman, B. R.; Slater, G. F. Rapid Degradation of Deepwater Horizon Spilled Oil by Indigenous Microbial Communities in Louisiana Saltmarsh Sediments. *Environ. Sci. Technol.* **2013**, *47*, 13303–13312.

(225) Ochsner, U. A.; Reiser, J. Autoinducer-mediated regulation of rhamnolipid biosurfactant synthesis in Pseudomonas aeruginosa. *Proc. Natl. Acad. Sci. U. S. A.* **1995**, *92*, 6424–6428.

(226) Zhang, Y.; Miller, R. M. Effect of a Pseudomonas Rhamnolipid Biosurfactant on Cell Hydrophobicity and Biodegradation of Octadecane. *Appl. Environ. Microbiol.* **1994**, *60*, 2101–2106.

(227) Bassler, B. L.; Greenberg, E. P.; Stevens, A. N. N. M. Cross-Species Induction of Luminescence in the Quorum- Sensing Bacterium Vibrio harveyi. **1997**, *179*, 4043–4045.

(228) Vilchez, R.; Lemme, A.; Thiel, V.; Schulz, S.; Sztajer, H.; Wagner-Döbler, I. Analysing traces of autoinducer-2 requires standardization of the Vibrio harveyi bioassay. *Anal. Bioanal. Chem.* **2007**, *387*, 489–496.

(229) Louie, S. M.; Gorham, J. M.; Mcgivney, E. A.; Liu, J.; Gregory, K. B.; Hackley, V. A. Photochemical transformations of thiolated polyethylene glycol coatings on gold. *Environ. Sci. Nano* **2016**, *3*, 1090–1102.

(230) Sigma Aldrich. *Tween 80 Product Information*; 1990.

(231) Fisher, H.; H, H. The isolation of nuclei from animal cells in culture. *Proc. R. Soc. London B Biol. Sci.* **1962**, *156*, 521–523.

(232) Salter, I.; Zubkov, M. V; Warwick, P. E.; Burkill, P. H. Marine bacterioplankton can increase evaporation and gas transfer by metabolizing insoluble surfactants from the air - seawater interface. *FEMS Microb. Lett.* **2009**, *294*, 225–231.

(233) Stewart, P. S.; William Costerton, J. Antibiotic resistance of bacteria in biofilms. *Lancet* **2001**, *358*, 135–138.

(234) Roberto, D.; Fernando, L.; Satie, A.; Ruvollo-filho, A. C.; Rodrigues, E.; Camargo, D.; Barros, D. International Journal of Antimicrobial Agents The growing importance of materials that prevent microbial adhesion : antimicrobial effect of medical devices containing silver. *Int. J. Antimicrob. Agents* **2009**, *34*, 103–110.

(235) Bazaka, K.; Jacob, M. V; Crawford, R. J.; Ivanova, E. P. Efficient surface modification of biomaterial to prevent biofilm formation and the attachment of microorganisms. *Appl. Microbiol. Biotechnol.* **2012**, 299–311.

(236) Chen, C. W.; Hsu, C. Y.; Lai, S. M.; Syu, W. J.; Wang, T. Y.; Lai, P. S. Metal nanobullets for multidrug resistant bacteria and biofilms. *Adv. Drug Deliv. Rev.* **2014**, *78*, 88–104.

(237) Noyce, J. O.; Michels, H.; Keevil, C. W. Potential use of copper surfaces to reduce survival of epidemic meticillin-resistant Staphylococcus aureus in the healthcare environment. *J. Hosp. Infect.* **2006**, *63*, 289–297.

(238) Poon, V. K. M.; Burd, A. In vitro cytotoxity of silver : implication for clinical wound care. *Burns* **2004**, *30*, 140–147.

(239) Klueh, U.; Wagner, V.; Kelly, S.; Johnson, A.; Bryers, J. D. Efficacy of Silver-Coated Fabric to Prevent Bacterial Colonization and Subsequent Device-Based Biofilm Formation. **2000**, 621–631.

(240) Benjamin, M. M. *Water Chemistry: Second Edition*; Waveland Press, 2014.

(241) Dusane, D. H.; Zinjarde, S. S.; Venugopalan, V. P.; Mclean, R. J.; Weber, M. M.; Rahman, P. K. S. M. Quorum sensing : implications on Rhamnolipid biosurfactant production. *Biotechnol. Genet. Eng. Rev.* **2010**, *27*, 159–184.

(242) Milo, R.; Phillips, R. *Cell Biology by the Numbers*; Scholl, S.; Wolfe, N.; Murdzek, J., Eds.; Garland Science, Taylor & Francis Group: Abingdon, 2015.

(243) Heldal, M.; Norland, S.; Tumyr, O. L. E. X-Ray Microanalytic Method for Measurement of Dry Matter and Elemental Content of Individual Bacteria. *Appl. Environ. Microbiol.* **1985**, *50*, 1251–1257.

Appendix

Table A1. Salts at their appropriate concentrations in VDMD, the media used to grow *E. coli* for copper toxicity studies, were modeled in Visual MINTEQ Version 3.0 to determine salt concentrations when 570 ppb Cu^{2+}, the solubility limit of Cu^{2+} estimated by Visual MINTEQ was added. The estimated molar concentrations of salts added and formed in VDMD from Visual MINTEQ are presented below.

	Concentration	Activity	Log activity
Al(OH)2+	8.1169E-10	6.5522E-10	-9.184
Al(OH)3 (aq)	8.1733E-10	8.2934E-10	-9.081
Al(OH)4-	1.5925E-09	1.2855E-09	-8.891
Al(SO4)2-	5.2154E-12	4.21E-12	-11.376
Al+3	8.8867E-12	1.2933E-12	-11.888
Al2(OH)2+4	1.0379E-17	3.3734E-19	-18.472
Al2PO4+3	4.3956E-13	6.3968E-14	-13.194
Al3(OH)4+5	5.883E-22	2.7826E-24	-23.556
AlCl+2	1.725E-16	7.3241E-17	-16.135
AlHPO4+	2.0763E-07	1.676E-07	-6.776
AlMo6O21-3	1.8739E-36	2.727E-37	-36.564
AlOH+2	9.6841E-11	4.1118E-11	-10.386
AlSO4+	3.2433E-11	2.6181E-11	-10.582
Cl-1	0.00017222	0.00013902	-3.857
Co(NH3)+2	2.9645E-09	1.2587E-09	-8.9
Co(NH3)2+2	1.8404E-12	7.8144E-13	-12.107
Co(NH3)3+2	3.372E-16	1.4317E-16	-15.844
Co(NH3)4+2	3.0963E-20	1.3147E-20	-19.881
Co(NH3)5+2	7.6527E-25	3.2493E-25	-24.488
Co(NO3)2 (aq)	5.206E-17	5.2824E-17	-16.277
Co(OH)2 (aq)	8.6163E-13	8.7429E-13	-12.058
Co(OH)3-	6.8709E-19	5.5463E-19	-18.256
Co+2	1.2852E-06	5.4571E-07	-6.263
Co4(OH)4+4	8.8171E-29	2.8657E-30	-29.543
CoCl+	4.1979E-11	3.3887E-11	-10.47
CoHPO4 (aq)	1.8332E-06	1.8602E-06	-5.73
CoNO3+	5.8601E-12	4.7304E-12	-11.325
CoOH+	4.2886E-10	3.4619E-10	-9.461
CoSO4 (aq)	0.000000314	3.1861E-07	-6.497
Cu(NH3)2+2	5.523E-09	2.345E-09	-8.63
Cu(NH3)3+2	7.5013E-11	3.185E-11	-10.497
Cu(NH3)4+2	1.9866E-13	8.4349E-14	-13.074
Cu(NO3)2 (aq)	2.4197E-18	2.4552E-18	-17.61

Cu(OH)2 (aq)	1.1928E-10	1.2104E-10	-9.917
Cu(OH)3-	1.8419E-14	1.4868E-14	-13.828
Cu(OH)4-2	8.9874E-21	3.816E-21	-20.418
Cu+2	4.8556E-07	2.0617E-07	-6.686
Cu2(OH)2+2	3.2E-11	1.3587E-11	-10.867
Cu2OH+3	1.7982E-13	2.6169E-14	-13.582
Cu3(OH)4+2	3.3425E-15	1.4192E-15	-14.848
CuCl+	7.0842E-11	5.7186E-11	-10.243
CuCl2 (aq)	2.1579E-15	2.1896E-15	-14.66
CuCl3-	3.5191E-21	2.8407E-21	-20.547
CuCl4-2 1	4.6614E-27	1.9792E-27	-26.704
CuHPO4 (aq)	8.1372E-06	8.2567E-06	-5.083
CuHSO4+	5.1704E-14	4.1737E-14	-13.379
CuNH3+2	1.0945E-07	4.6471E-08	-7.333
CuNO3+	4.4173E-12	3.5658E-12	-11.448
CuOH+	2.5679E-08	2.0728E-08	-7.683
CuSO4 (aq)	1.362E-07	1.382E-07	-6.859
Fe(NH3)2+2	2.8245E-14	1.1993E-14	-13.921
Fe(NH3)3+2	1.6365E-18	6.9485E-19	-18.158
Fe(NH3)4+2	4.0446E-23	1.7173E-23	-22.765
Fe(OH)2 (aq)	4.6919E-15	4.7609E-15	-14.322
Fe(OH)3-	5.9298E-19	4.7867E-19	-18.32
Fe+2	3.5076E-07	1.4893E-07	-6.827
FeCl+	1.6183E-11	1.3063E-11	-10.884
FeH2PO4+	1.3854E-06	1.1184E-06	-5.951
FeHPO4 (aq)	1.7549E-06	1.7807E-06	-5.749
FeNH3+2	1.8966E-10	8.053E-11	-10.094
FeOH+	2.3353E-10	1.8851E-10	-9.725
FeSO4 (aq)	1.0543E-07	1.0698E-07	-6.971
H+1	3.9175E-07	3.1623E-07	-6.5
H2Mo6O21-4	9.7632E-41	3.1732E-42	-41.499
H2PO4-	0.018561	0.014983	-1.824
H2W12O42-10	7.2496E-66	3.6285E-75	-74.44
H2W6O22-6	1.8942E-35	8.496E-39	-38.071
H3Mo8O28-5	2.1902E-54	1.0359E-56	-55.985
H3PO4	6.5653E-07	6.6618E-07	-6.176
HMo7O24-5	9.0969E-46	4.3027E-48	-47.366
HMoO4-	1.134E-09	9.1536E-10	-9.038
HPO4-2	0.0070731	0.0030032	-2.522
HSO4-	1.1202E-07	9.0427E-08	-7.044
HW7O24-5	4.8267E-41	2.283E-43	-42.641
HWO4-	1.9998E-11	1.6143E-11	-10.792
K+1	0.034213	0.027617	-1.559

K2HPO4 (aq)	0.000030103	0.000030545	-4.515
K2PO4-	6.8858E-10	5.5584E-10	-9.255
KCl (aq)	1.8963E-06	1.9242E-06	-5.716
KH2PO4 (aq)	0.00081364	0.00082559	-3.083
KHPO4-	0.00077942	0.00062917	-3.201
KNO3 (aq)	9.6113E-08	9.7525E-08	-7.011
KOH (aq)	1.5038E-09	1.5259E-09	-8.816
KPO4-2	7.0112E-09	2.9769E-09	-8.526
KSO4-	0.00070873	0.00057211	-3.243
Mg(NH3)2+2	1.8774E-13	7.9713E-14	-13.098
Mg+2	0.00026159	0.00011107	-3.954
MgCl+	7.615E-08	6.147E-08	-7.211
MgHPO4 (aq)	0.00020742	0.00021047	-3.677
MgMoO4(aq)	1.9537E-08	1.9824E-08	-7.703
MgOH+	1.6632E-09	1.3426E-09	-8.872
MgPO4-	2.4842E-08	2.0053E-08	-7.698
MgSO4 (aq)	0.000058286	0.000059142	-4.228
MgWO4(aq)	1.4363E-09	1.4574E-09	-8.836
Mn(NH3)2+2	3.1851E-14	1.3524E-14	-13.869
Mn(NH3)3+2	9.249E-19	3.9271E-19	-18.406
Mn(NH3)4+2	1.4095E-23	5.9846E-24	-23.223
Mn(NO3)2 (aq)	1.9711E-16	2.0001E-16	-15.699
Mn(OH)4-2	2.0258E-28	8.6013E-29	-28.065
Mn+2	3.9554E-06	1.6795E-06	-5.775
Mn2(OH)3+	1.4138E-16	1.1413E-16	-15.943
Mn2OH+3	1.5479E-15	2.2526E-16	-15.647
MnCl+	2.8923E-10	2.3348E-10	-9.632
MnCl2 (aq)	5.6882E-14	5.7718E-14	-13.239
MnCl3-	2.7377E-18	2.2099E-18	-17.656
MnHPO4 (aq)	0.000013226	0.00001342	-4.872
MnNH3+2	5.8906E-10	2.5011E-10	-9.602
MnNO3+	1.8035E-11	1.4558E-11	-10.837
MnOH+	1.6616E-10	1.3413E-10	-9.872
MnSO4 (aq)	8.6127E-07	8.7392E-07	-6.059
Mo7O24-6	5.7804E-44	2.5926E-47	-46.586
Mo8O26-4	4.4129E-57	1.4343E-58	-57.843
MoO3(H2O)3(aq)	2.8527E-12	2.8946E-12	-11.538
MoO4-2	3.923E-07	1.6657E-07	-6.778
Na+1	0.00015994	0.00012911	-3.889
Na2HPO4 (aq)	4.3467E-10	4.4106E-10	-9.356
Na2PO4-	3.2174E-14	2.5971E-14	-13.586
NaCl (aq)	8.8652E-09	8.9954E-09	-8.046
NaH2PO4 (aq)	3.8037E-06	3.8596E-06	-5.413

NaHPO4-	5.6435E-06	4.5556E-06	-5.341
NaNO3 (aq)	1.9614E-10	1.9902E-10	-9.701
NaOH (aq)	5.0929E-12	5.1677E-12	-11.287
NaPO4-2	3.2777E-11	1.3917E-11	-10.856
NaSO4-	2.5719E-06	2.0761E-06	-5.683
NH3 (aq)	0.00002102	0.000021329	-4.671
NH4+1	0.014655	0.011829	-1.927
NH4SO4-	0.00045948	0.00037091	-3.431
Ni(NH3)2+2	2.1584E-11	9.1645E-12	-11.038
Ni(NH3)3+2	2.1237E-14	9.0173E-15	-14.045
Ni(NH3)4+2	6.0265E-18	2.5588E-18	-17.592
Ni(NH3)5+2	5.9297E-22	2.5177E-22	-21.599
Ni(NH3)6+2	1.1641E-26	4.9428E-27	-26.306
Ni(OH)2 (aq)	2.6579E-13	2.697E-13	-12.569
Ni(OH)3-	1.0623E-17	8.5748E-18	-17.067
Ni(SO4)2-2	3.5547E-11	1.5093E-11	-10.821
Ni+2	6.2835E-07	2.668E-07	-6.574
NiCl+	1.7071E-11	1.378E-11	-10.861
NiCl2 (aq)	6.5461E-17	6.6423E-17	-16.178
NiH2PO4+	4.1857E-08	3.3788E-08	-7.471
NiHPO4 (aq)	7.1192E-07	7.2238E-07	-6.141
NiNH3+2	7.0985E-09	3.014E-09	-8.521
NiNO3+	4.5407E-12	3.6653E-12	-11.436
NiOH+	1.3229E-10	1.0679E-10	-9.971
NiSO4 (aq)	1.5351E-07	1.5577E-07	-6.808
NO3-1	6.7755E-06	5.4694E-06	-5.262
OH-	3.9387E-08	3.1794E-08	-7.498
PO4-3	2.752E-08	4.0049E-09	-8.397
SO4-2	0.0068916	0.0029262	-2.534
W7O24-6	1.4346E-39	6.4344E-43	-42.191
WO3(H2O)3(aq)	6.0485E-13	6.1374E-13	-12.212
WO4-2	2.8841E-08	1.2246E-08	-7.912
Zn(NH3)2+2	2.2814E-11	9.6867E-12	-11.014
Zn(NH3)3+2	1.125E-13	4.7769E-14	-13.321
Zn(NH3)4+2	2.5359E-16	1.0767E-16	-15.968
Zn(NO3)2 (aq)	9.995E-18	1.0142E-17	-16.994
Zn(OH)2 (aq)	8.4841E-11	8.6088E-11	-10.065
Zn(OH)3-	1.0722E-15	8.6554E-16	-15.063
Zn(OH)4-2	1.0272E-21	4.3615E-22	-21.36
Zn(SO4)2-2	2.5994E-08	1.1037E-08	-7.957
Zn+2	1.5932E-06	6.7646E-07	-6.17
Zn2OH+3	9.9975E-15	1.4549E-15	-14.837
ZnCl+	3.3599E-10	2.7122E-10	-9.567

ZnCl2 (aq)	3.6312E-14	3.6845E-14	-13.434
ZnCl3-	7.1196E-18	5.7472E-18	-17.241
ZnCl4-2	9.4307E-22	4.0043E-22	-21.397
ZnHPO4 (aq)	4.1352E-06	0.000004196	-5.377
ZnNH3+2	5.562E-09	2.3616E-09	-8.627
ZnNO3+	1.1513E-11	9.2936E-12	-11.032
ZnOH+	2.6644E-09	2.1508E-09	-8.667
ZnSO4 (aq)	4.2679E-07	4.3306E-07	-6.363

Table A2. Estimated ion activity products (IAP, also known as activity quotients) and saturation indices for salt complexes in VDMD with 570 ppb Cu^{2+} from Visual MINTEQ version 3.0 are reported in this table. The saturation index is the difference between $\log(IAP) - \log K$.[240] When the saturation index is positive there is a thermodynamic driving force for precipitates to form, negative values indicate that the salt will be dissolved and a value of 0 indicates the solution is saturated. 570 ppb Cu^{2+} in VDMD forms $Cu_3(PO_4)_2$ which has a saturation index of -0.002. This value is near the saturation limit for $Cu_3(PO_4)_2$. Copper salts are identified in the bold font.

Mineral	log IAP	Sat. index
Al(OH)3 (am)	7.61	-3.19
Al(OH)3 (Soil)	7.61	-0.68
Al2(MoO4)3(s)	-44.112	-46.479
Al2O3(s)	15.221	-4.431
Al4(OH)10SO4(s)	14.907	-7.793
AlOHSO4(s)	-7.923	-4.693
AlPO4x1.5H2O	-20.287	0.173
Alunite	-3.295	-1.895
Antlerite	3.406	-5.382
Atacamite	2.27	-5.121
Bianchite	-8.707	-6.942
Boehmite	7.61	-0.968
Brochantite	9.719	-5.503
Brucite	9.044	-8.056
Chalcanthite	-9.223	-6.583
Co(OH)2 (am)	6.736	-6.358
Co(OH)2 (c)	6.736	-5.554
Co3(PO4)2(s)	-35.584	-0.896
CoCl2(s)	-13.977	-22.244
CoCl2:6H2O(s)	-13.981	-16.517
CoHPO4(s)	-21.16	-2.1
CoMoO4(s)	-13.041	-5.281
CoO(s)	6.736	-6.85

CoSO4(s)	-8.797	-11.599
CoSO4:6H2O(s)	-8.801	-6.328
Cu(OH)2(s)	**6.313**	**-2.977**
Cu2(OH)3NO3(s)	**0.864**	**-8.387**
Cu3(PO4)2(s)	**-36.852**	**-0.002**
Cu3(PO4)2:3H2O(s)	**-36.854**	**-1.734**
CuMoO4(s)	**-13.464**	**-0.388**
CuOCuSO4(s)	**-2.906**	**-13.209**
CuSO4(s)	-9.219	-12.159
Diaspore	7.61	0.737
Epsomite	-6.493	-4.366
Fe(OH)2 (am)	6.172	-7.318
Fe(OH)2 (c)	6.172	-6.718
FeMoO4(s)	-13.605	-3.514
Gibbsite (C)	7.61	-0.13
Goslarite	-8.708	-6.697
H2MoO4(s)	-19.778	-6.902
H2WO4(s)	-20.912	-5.512
Halite	-7.746	-9.296
Hercynite	21.394	-1.499
K2MoO4(s)	-9.896	-13.158
K-Alum	-18.522	-13.352
KCl(s)	-5.416	-6.316
Langite	9.719	-7.77
Melanothallite	-14.4	-20.657
Melanterite	-9.365	-7.156
Mg(OH)2 (active)	9.044	-9.75
Mg2(OH)3Cl:4H2O(s)	7.73	-18.27
Mg3(PO4)2(s)	-28.658	-5.378
MgHPO4:3H2O(s)	-18.854	-0.679
MgMoO4(s)	-10.733	-8.883
Mirabilite	-10.318	-9.204
Mn3(PO4)2(s)	-34.119	-10.292
MnCl2:4H2O(s)	-13.491	-16.206
MnHPO4(s)	-20.672	4.728
MnSO4(s)	-8.309	-10.892
MoO3(s)	-19.778	-11.778
Morenosite	-9.112	-6.967
Na2Mo2O7(s)	-34.334	-17.738
Na2MoO4(s)	-14.557	-16.047
Na2MoO4:2H2O(s)	-14.558	-15.782
Ni(OH)2 (am)	6.425	-6.465
Ni(OH)2 (c)	6.425	-4.365

Ni3(PO4)2(s)	-36.516	-5.216
Ni4(OH)6SO4(s)	10.167	-21.833
NiMoO4(s)	-13.352	-2.21
Periclase	9.045	-12.539
Pyrochroite	7.224	-7.97
Retgersite	-9.111	-7.071
Spinel	24.266	-12.581
Struvite	-14.283	-1.023
Tenorite(am)	6.314	-2.176
Tenorite(c)	6.314	-1.326
Thenardite	-10.312	-10.633
Variscite	-20.287	1.783
Vivianite	-37.281	0.479
Zincite	6.83	-4.4
Zincosite	-8.703	-12.633
Zn(NO3)2:6H2O(s)	-16.698	-20.013
Zn(OH)2 (am)	6.829	-5.645
Zn(OH)2 (beta)	6.829	-4.925
Zn(OH)2 (delta)	6.829	-5.015
Zn(OH)2 (epsilon)	6.829	-4.705
Zn(OH)2 (gamma)	6.829	-4.905
Zn2(OH)2SO4(s)	-1.875	-9.375
Zn2(OH)3Cl(s)	3.302	-11.889
Zn3(PO4)2:4H2O(s)	-35.307	0.113
Zn3O(SO4)2(s)	-10.577	-29.491
Zn4(OH)6SO4(s)	11.783	-16.617
Zn5(OH)8Cl2(s)	13.432	-25.068
ZnCl2(s)	-13.884	-20.934
ZnMoO4(s)	-12.948	-2.823
ZnSO4:1H2O(s)	-8.704	-8.066

Table A3. Salts at their appropriate concentrations in VDMD and 60 mg C/L HA, modeled as DOC (Nica Donnan), were modeled in visual MINTEQ to determine salt concentrations when 3200 ppb Cu^{2+}, the solubility limit of Cu^2 based on the estimation from Visual MINTEQ was added. The estimated molar concentrations of salts output from Visual MINTEQ Version 3.0 are presented below.

	Concentration	Activity	Log activity
(6)Al(OH)2+D(aq)	1.1133E-16	1.1133E-16	-15.953
(6)Al+3D(aq)	1.6982E-15	1.6982E-15	-14.77
(6)AlOH+2D(aq)	4.959E-16	4.959E-16	-15.305
(6)AlSO4+D(aq)	4.4616E-18	4.4616E-18	-17.351
(6)Cl-1D(aq)	8.1886E-10	8.1886E-10	-9.087
(6)Co+2D(aq)	2.7321E-07	2.7321E-07	-6.564
(6)CoNO3+D(aq)	3.338E-14	3.338E-14	-13.477
(6)Cu+2D(aq)	1.2016E-07	1.2016E-07	-6.92
(6)Fe+2D(aq)	5.3472E-11	5.3472E-11	-10.272
(6)H+1D(aq)	2.5979E-09	2.5979E-09	-8.585
(6)K+1D(aq)	0.00022551	0.00022551	-3.647
(6)Mg+2D(aq)	0.000055814	0.000055814	-4.253
(6)Mn+2D(aq)	8.0034E-07	8.0034E-07	-6.097
(6)Na+1D(aq)	1.0542E-06	1.0542E-06	-5.977
(6)NH4+1D(aq)	0.000096577	0.000096577	-4.015
(6)Ni+2D(aq)	9.4251E-08	9.4251E-08	-7.026
(6)NiCl+D(aq)	6.8617E-14	6.8617E-14	-13.164
(6)NiNO3+D(aq)	1.8251E-14	1.8251E-14	-13.739
(6)NO3-1D(aq)	3.2215E-11	3.2215E-11	-10.492
(6)OH-D(aq)	1.872E-13	1.872E-13	-12.728
(6)SO4-2D(aq)	8.7883E-10	8.7883E-10	-9.056
(6)Zn+2D(aq)	3.6649E-07	3.6649E-07	-6.436
Al(OH)2+	1.6785E-14	1.3552E-14	-13.868
Al(OH)3 (aq)	1.6904E-14	1.7151E-14	-13.766
Al(OH)4-	3.2925E-14	2.6583E-14	-13.575
Al(SO4)2-	1.0846E-16	8.7567E-17	-16.058
Al+3	1.835E-16	2.6754E-17	-16.573
Al2(OH)2+4	4.4265E-27	1.4434E-28	-27.841
Al2PO4+3	1.8815E-22	2.7431E-23	-22.562
Al3(OH)4+5	5.1799E-36	2.4625E-38	-37.609
AlCl+2	3.5668E-21	1.5157E-21	-20.819
AlHPO4+	4.303E-12	3.4742E-12	-11.459
AlMo6O21-3	4.0464E-41	5.8994E-42	-41.229
AlOH+2	2.0015E-15	8.5053E-16	-15.07
AlSO4+	6.7264E-16	5.4308E-16	-15.265
Cl-1	0.00017224	0.00013906	-3.857

Co(NH3)+2	2.5276E-09	1.0741E-09	-8.969
Co(NH3)2+2	1.5594E-12	6.6265E-13	-12.179
Co(NH3)3+2	2.8393E-16	1.2065E-16	-15.918
Co(NH3)4+2	2.5909E-20	1.101E-20	-19.958
Co(NH3)5+2	6.3635E-25	2.7041E-25	-24.568
Co(NO3)2 (aq)	4.4731E-17	4.5387E-17	-16.343
Co(OH)2 (aq)	7.3975E-13	7.5059E-13	-12.125
Co(OH)3-	5.8969E-19	4.7611E-19	-18.322
Co+2	1.1027E-06	4.6859E-07	-6.329
Co4(OH)4+4	4.7761E-29	1.5574E-30	-29.808
CoCl+	3.6052E-11	2.9108E-11	-10.536
CoHPO4 (aq)	1.5774E-06	1.6005E-06	-5.796
CoNO3+	5.0324E-12	4.0631E-12	-11.391
CoOH+	3.6814E-10	2.9723E-10	-9.527
CoSO4 (aq)	2.7037E-07	2.7433E-07	-6.562
Cu(NH3)2+2	5.4478E-09	2.315E-09	-8.635
Cu(NH3)3+2	7.353E-11	3.1246E-11	-10.505
Cu(NH3)4+2	1.9351E-13	8.2232E-14	-13.085
Cu(NO3)2 (aq)	2.4203E-18	2.4558E-18	-17.61
Cu(OH)2 (aq)	1.1922E-10	1.2097E-10	-9.917
Cu(OH)3-	1.8403E-14	1.4858E-14	-13.828
Cu(OH)4-2	8.9732E-21	3.8131E-21	-20.419
Cu+2	4.8498E-07	2.0609E-07	-6.686
Cu2(OH)2+2	3.1944E-11	1.3574E-11	-10.867
Cu2OH+3	1.7934E-13	2.6147E-14	-13.583
Cu3(OH)4+2	3.3347E-15	1.4171E-15	-14.849
CuCl+	7.0826E-11	5.7184E-11	-10.243
CuCl2 (aq)	2.1586E-15	2.1902E-15	-14.66
CuCl3-	3.5207E-21	2.8426E-21	-20.546
CuCl4-2 1	4.6623E-27	1.9812E-27	-26.703
CuHPO4 (aq)	0.000008151	8.2704E-06	-5.082
CuHSO4+	5.1814E-14	4.1834E-14	-13.378
CuNH3+2	1.0864E-07	4.6164E-08	-7.336
CuNO3+	4.4161E-12	3.5655E-12	-11.448
CuOH+	2.5661E-08	2.0719E-08	-7.684
CuSO4 (aq)	1.3653E-07	1.3853E-07	-6.858
DOC (NICA-Donnan)	0.005	0.005	-2.301
FA1-Al(6)(aq)	4.0721E-10	4.0721E-10	-9.39
FA1-Co(6)(aq)	2.0923E-07	2.0923E-07	-6.679
FA1-Cu(6)(aq)	0.000033349	0.000033349	-4.477
FA1-Fe(II)(6)(aq)	3.5947E-06	3.5947E-06	-5.444
FA1-H(6)(aq)	0.000032653	0.000032653	-4.486

FA1-Mg(6)(aq)	0.000016725	0.000016725	-4.777
FA1-Mn(6)(aq)	0.000002472	0.000002472	-5.607
FA1-Ni(6)(aq)	4.781E-07	4.781E-07	-6.32
FA1-Zn(6)(aq)	6.2376E-08	6.2376E-08	-7.205
FA2-Al(6)(aq)	2.1061E-07	2.1061E-07	-6.677
FA2-Co(6)(aq)	1.0631E-10	1.0631E-10	-9.973
FA2-Cu(6)(aq)	7.3682E-06	7.3682E-06	-5.133
FA2-Fe(II)(6)(aq)	1.9918E-11	1.9918E-11	-10.701
FA2-H(6)(aq)	0.00016631	0.00016631	-3.779
FA2-Mg(6)(aq)	3.442E-09	3.442E-09	-8.463
FA2-Mn(6)(aq)	1.981E-09	1.981E-09	-8.703
FA2-Ni(6)(aq)	3.4906E-08	3.4906E-08	-7.457
FA2-Zn(6)(aq)	1.5153E-09	1.5153E-09	-8.819
Fe(NH3)2+2	1.7163E-17	7.2933E-18	-17.137
Fe(NH3)3+2	9.8819E-22	4.1992E-22	-21.377
Fe(NH3)4+2	2.4271E-26	1.0314E-26	-25.987
Fe(OH)2 (aq)	2.8888E-18	2.9312E-18	-17.533
Fe(OH)3-	3.6497E-22	2.9468E-22	-21.531
Fe+2	2.1582E-10	9.1713E-11	-10.038
FeCl+	9.967E-15	8.0472E-15	-14.094
FeH2PO4+	8.5471E-10	6.9008E-10	-9.161
FeHPO4 (aq)	1.0829E-09	1.0988E-09	-8.959
FeNH3+2	1.1597E-13	4.9281E-14	-13.307
FeOH+	1.4376E-13	1.1607E-13	-12.935
FeSO4 (aq)	6.5102E-11	6.6055E-11	-10.18
H+1	3.9167E-07	3.1623E-07	-6.5
H2Mo6O21-4	1.0177E-40	3.3183E-42	-41.479
H2PO4-	0.018595	0.015013	-1.824
H2W12O42-10	7.7701E-66	3.9688E-75	-74.401
H2W6O22-6	1.9664E-35	8.8845E-39	-38.051
H3Mo8O28-5	2.313E-54	1.0996E-56	-55.959
H3PO4	6.579E-07	6.6753E-07	-6.176
HFA1-(6)(aq)	0.00049258	0.00049258	-3.308
HFA2-(6)(aq)	0.000010219	0.000010219	-4.991
HMo7O24-5	9.536E-46	4.5334E-48	-47.344
HMoO4-	1.1422E-09	9.2216E-10	-9.035
HPO4-2	0.0070818	0.0030093	-2.522
HSO4-	1.123E-07	9.0673E-08	-7.043
HW7O24-5	5.0602E-41	2.4056E-43	-42.619
HWO4-	2.0143E-11	1.6263E-11	-10.789
K+1	0.033997	0.027449	-1.561
K2HPO4 (aq)	0.0000298	0.000030236	-4.519
K2PO4-	6.8147E-10	5.5021E-10	-9.259

KCl (aq)	1.8855E-06	1.9131E-06	-5.718
KH2PO4 (aq)	0.00081037	0.00082224	-3.085
KHPO4-	0.0007761	0.00062661	-3.203
KNO3 (aq)	9.5561E-08	9.6961E-08	-7.013
KOH (aq)	1.4946E-09	1.5165E-09	-8.819
KPO4-2	6.977E-09	2.9648E-09	-8.528
KSO4-	0.00070619	0.00057017	-3.244
Mg(NH3)2+2	1.5966E-13	6.7847E-14	-13.168
Mg+2	0.00022527	0.000095728	-4.019
MgCl+	6.5641E-08	5.2998E-08	-7.276
MgHPO4 (aq)	0.00017914	0.00018177	-3.74
MgMoO4(aq)	1.6964E-08	1.7213E-08	-7.764
MgOH+	1.4331E-09	1.157E-09	-8.937
MgPO4-	2.145E-08	1.7319E-08	-7.761
MgSO4 (aq)	0.000050374	0.000051111	-4.291
MgWO4(aq)	1.2472E-09	1.2655E-09	-8.898
Mn(NH3)2+2	2.5689E-14	1.0916E-14	-13.962
Mn(NH3)3+2	7.4129E-19	3.15E-19	-18.502
Mn(NH3)4+2	1.1226E-23	4.7705E-24	-23.321
Mn(NO3)2 (aq)	1.6121E-16	1.6357E-16	-15.786
Mn(OH)4-2	1.6537E-28	7.0274E-29	-28.153
Mn+2	3.2303E-06	1.3727E-06	-5.862
Mn2(OH)3+	9.4402E-17	7.6219E-17	-16.118
Mn2OH+3	1.0321E-15	1.5047E-16	-15.823
MnCl+	2.3643E-10	1.9089E-10	-9.719
MnCl2 (aq)	4.6526E-14	4.7207E-14	-13.326
MnCl3-	2.2395E-18	1.8081E-18	-17.743
MnHPO4 (aq)	0.000010833	0.000010991	-4.959
MnNH3+2	4.7807E-10	2.0315E-10	-9.692
MnNO3+	1.4742E-11	1.1903E-11	-10.924
MnOH+	1.3577E-10	1.0962E-10	-9.96
MnSO4 (aq)	7.0589E-07	7.1623E-07	-6.145
Mo7O24-6	6.0459E-44	2.7316E-47	-46.564
Mo8O26-4	4.6698E-57	1.5227E-58	-57.817
MoO3(H2O)3(aq)	2.874E-12	2.9161E-12	-11.535
MoO4-2	3.9489E-07	1.6781E-07	-6.775
Na+1	0.00015894	0.00012832	-3.892
Na2HPO4 (aq)	4.3031E-10	4.3661E-10	-9.36
Na2PO4-	3.1843E-14	2.5709E-14	-13.59
NaCl (aq)	8.8148E-09	8.9439E-09	-8.048
NaH2PO4 (aq)	3.7885E-06	0.000003844	-5.415
NaHPO4-	5.6195E-06	4.5371E-06	-5.343
NaNO3 (aq)	1.9501E-10	1.9787E-10	-9.704

NaOH (aq)	5.0617E-12	5.1359E-12	-11.289
NaPO4-2	3.2618E-11	1.3861E-11	-10.858
NaSO4-	2.5627E-06	2.0691E-06	-5.684
NH3 (aq)	0.00002089	0.000021196	-4.674
NH4+1	0.01456	0.011756	-1.93
NH4SO4-	0.00045776	0.00036959	-3.432
Ni(NH3)2+2	1.2905E-11	5.4838E-12	-11.261
Ni(NH3)3+2	1.2618E-14	5.362E-15	-14.271
Ni(NH3)4+2	3.5583E-18	1.5121E-18	-17.82
Ni(NH3)5+2	3.4793E-22	1.4785E-22	-21.83
Ni(NH3)6+2	6.7879E-27	2.8845E-27	-26.54
Ni(OH)2 (aq)	1.6102E-13	1.6338E-13	-12.787
Ni(OH)3-	6.4331E-18	5.194E-18	-17.284
Ni(SO4)2-2	2.1638E-11	9.1948E-12	-11.036
Ni+2	3.8041E-07	1.6165E-07	-6.791
NiCl+	1.0345E-11	8.3522E-12	-11.078
NiCl2 (aq)	3.9692E-17	4.0274E-17	-16.395
NiH2PO4+	2.5408E-08	2.0514E-08	-7.688
NiHPO4 (aq)	4.3226E-07	4.3859E-07	-6.358
NiNH3+2	4.2707E-09	1.8148E-09	-8.741
NiNO3+	2.7515E-12	2.2215E-12	-11.653
NiOH+	8.0132E-11	6.4698E-11	-10.189
NiSO4 (aq)	9.3271E-08	9.4638E-08	-7.024
NO3-1	6.7762E-06	0.000005471	-5.262
OH-	3.9375E-08	3.1791E-08	-7.498
PO4-3	2.7525E-08	4.013E-09	-8.397
SO4-2	0.0069048	0.0029341	-2.533
W7O24-6	1.5006E-39	6.78E-43	-42.169
WO3(H2O)3(aq)	6.0938E-13	6.1831E-13	-12.209
WO4-2	2.9032E-08	1.2337E-08	-7.909
Z-(6)(aq)	-0.00043807	-0.00043807	0
Zn(NH3)2+2	2.0918E-11	8.8889E-12	-11.051
Zn(NH3)3+2	1.0251E-13	4.3561E-14	-13.361
Zn(NH3)4+2	2.2962E-16	9.7576E-17	-16.011
Zn(NO3)2 (aq)	9.2934E-18	9.4295E-18	-17.026
Zn(OH)2 (aq)	7.8823E-11	7.9977E-11	-10.097
Zn(OH)3-	9.9584E-16	8.0403E-16	-15.095
Zn(OH)4-2	9.5334E-22	4.0511E-22	-21.392
Zn(SO4)2-2	2.4265E-08	1.0311E-08	-7.987
Zn+2	1.4792E-06	6.2857E-07	-6.202
Zn2OH+3	8.6155E-15	1.2561E-15	-14.901
ZnCl+	3.1224E-10	2.521E-10	-9.598
ZnCl2 (aq)	3.3766E-14	3.426E-14	-13.465

ZnCl3-	6.6211E-18	5.3458E-18	-17.272
ZnCl4-2	8.768E-22	3.7259E-22	-21.429
ZnHPO4 (aq)	3.8505E-06	3.9069E-06	-5.408
ZnNH3+2	5.1319E-09	2.1807E-09	-8.661
ZnNO3+	1.0699E-11	8.6382E-12	-11.064
ZnOH+	2.475E-09	1.9983E-09	-8.699
ZnSO4 (aq)	3.9767E-07	4.0349E-07	-6.394

Table A4. Estimated ion activity products (IAP, also known as activity quotients) and saturation indices for salt complexes in VDMD with 3200 ppb Cu^{2+} and 60 mg C/L HA, modeled as DOC (Nica Donnan), from Visual MINTEQ version 3.0 are reported in this table. The saturation index is the difference between $\log(IAP) - \log K$. When the saturation index is positive there is a thermodynamic driving force for precipitates to form, negative values indicate that the salt will be dissolved and a value of 0 indicates the solution is saturated. 3200 ppb Cu^{2+} in VDMD with 60 mg C/L HA forms $Cu_3(PO_4)_2$ which has a saturation index of -0.001. This value is near the saturation limit for $Cu_3(PO_4)_2$. Copper salts are identified in the bold font.

Mineral	log IAP	Sat. index
Al(OH)3 (am)	2.925	-7.875
Al(OH)3 (Soil)	2.925	-5.365
Al2(MoO4)3(s)	-53.471	-55.838
Al2O3(s)	5.853	-13.8
Al4(OH)10SO4(s)	-3.83	-26.53
AlOHSO4(s)	-12.606	-9.376
AlPO4x1.5H2O	-24.97	-4.51
Alunite	-17.349	-15.949
Antlerite	3.407	-5.381
Atacamite	2.269	-5.122
Bianchite	-8.738	-6.973
Boehmite	2.926	-5.652
Brochantite	9.72	-5.502
Brucite	8.98	-8.12
Chalcanthite	-9.222	-6.582
Co(OH)2 (am)	6.669	-6.425
Co(OH)2 (c)	6.669	-5.621
Co3(PO4)2(s)	-35.781	-1.093
CoCl2(s)	-14.043	-22.31
CoCl2:6H2O(s)	-14.047	-16.583
CoHPO4(s)	-21.226	-2.165
CoMoO4(s)	-13.104	-5.343
CoO(s)	6.67	-6.916

CoSO4(s)	-8.862	-11.664
CoSO4:6H2O(s)	-8.866	-6.393
Cu(OH)2(s)	**6.313**	**-2.977**
Cu2(OH)3NO3(s)	**0.864**	**-8.387**
Cu3(PO4)2(s)	**-36.851**	**-0.001**
Cu3(PO4)2:3H2O(s)	**-36.853**	**-1.733**
CuMoO4(s)	**-13.461**	**-0.385**
CuOCuSO4(s)	**-2.905**	**-13.208**
CuSO4(s)	**-9.218**	**-12.158**
Diaspore	2.926	-3.947
Epsomite	-6.556	-4.43
Fe(OH)2 (am)	2.961	-10.529
Fe(OH)2 (c)	2.961	-9.929
FeMoO4(s)	-16.813	-6.722
Gibbsite (C)	2.925	-4.815
Goslarite	-8.739	-6.728
H2MoO4(s)	-19.775	-6.899
H2WO4(s)	-20.909	-5.509
Halite	-7.748	-9.298
Hercynite	8.814	-14.079
K2MoO4(s)	-9.898	-13.16
K-Alum	-23.207	-18.037
KCl(s)	-5.418	-6.318
Langite	9.719	-7.77
Melanothallite	-14.4	-20.657
Melanterite	-12.575	-10.366
Mg(OH)2 (active)	8.98	-9.814
Mg2(OH)3Cl:4H2O(s)	7.6	-18.4
Mg3(PO4)2(s)	-28.85	-5.57
MgHPO4:3H2O(s)	-18.918	-0.743
MgMoO4(s)	-10.794	-8.944
Mirabilite	-10.323	-9.209
Mn3(PO4)2(s)	-34.38	-10.553
MnCl2:4H2O(s)	-13.579	-16.294
MnHPO4(s)	-20.759	4.641
MnSO4(s)	-8.395	-10.978
MoO3(s)	-19.774	-11.774
Morenosite	-9.329	-7.184
Na2Mo2O7(s)	-34.333	-17.736
Na2MoO4(s)	-14.559	-16.049
Na2MoO4:2H2O(s)	-14.56	-15.784
Ni(OH)2 (am)	6.207	-6.683
Ni(OH)2 (c)	6.207	-4.583

Ni3(PO4)2(s)	-37.167	-5.867
Ni4(OH)6SO4(s)	9.298	-22.702
NiMoO4(s)	-13.567	-2.425
Periclase	8.98	-12.604
Pyrochroite	7.136	-8.058
Retgersite	-9.328	-7.288
Spinel	14.833	-22.015
Struvite	-14.349	-1.089
Tenorite(am)	6.313	-2.177
Tenorite(c)	6.313	-1.327
Thenardite	-10.316	-10.638
Variscite	-24.971	-2.901
Vivianite	-46.911	-9.151
Zincite	6.798	-4.432
Zincosite	-8.734	-12.664
Zn(NO3)2:6H2O(s)	-16.73	-20.045
Zn(OH)2 (am)	6.797	-5.677
Zn(OH)2 (beta)	6.797	-4.957
Zn(OH)2 (delta)	6.797	-5.047
Zn(OH)2 (epsilon)	6.797	-4.737
Zn(OH)2 (gamma)	6.797	-4.937
Zn2(OH)2SO4(s)	-1.937	-9.437
Zn2(OH)3Cl(s)	3.238	-11.953
Zn3(PO4)2:4H2O(s)	-35.401	0.019
Zn3O(SO4)2(s)	-10.671	-29.584
Zn4(OH)6SO4(s)	11.657	-16.743
Zn5(OH)8Cl2(s)	13.273	-25.227
ZnCl2(s)	-13.915	-20.965
ZnMoO4(s)	-12.977	-2.851
ZnSO4:1H2O(s)	-8.735	-8.097